Radiation Induced Degradation Pathways for Poly (Methyl Methacrylate) and Polystyrene Polymers as Models for Polymer Behavior in Space Environments.

by

Kenneth Henry Heffner

A dissertation submitted in partial fulfillment
Of the requirements of the degree of
Doctor of Philosophy
Department of Chemistry
College of Arts and Sciences
University of South Florida

Major Professor: Julie P. Harmon, Ph.D.
Edward Turos, Ph.D.
Kirpal S. Bisht, Ph.D.
Phillip F. Plantz, Ph.D.

Date of Approval:
November 17, 2003

Keywords: Free Volume, Gamma, Molecular Weight, Scission, Crosslinking

Acknowledgements

It is with deepest gratitude that I recognize Dr. Julie P. Harmon for her guidance and the professionalism she has displayed as my major professor. Her energy and commitment to science and academic excellence is inspiring. Her leadership and patient mentoring has helped me achieve a personal goal in my own passion for scientific research and learning. I am also very appreciative of my committee members: Dr. Kirpal Bisht, Dr. Phillip Plantz, and Dr. Edward Turos.

I am most grateful to my wife Kim, and to my daughters Meri and Katie, who have patiently and devotedly supported my pursuit of learning, and, in turn, have displayed their own passion for learning that I continue to find refreshing each day. I also thank my parents Hank and Twilia, my brother, Keith and my sister, Margaret for being the kind of family that encourages one another in working toward our goals.

I wish to recognize Aerospace Electronics Systems Division of Honeywell International, Inc. in Clearwater, FL for sponsoring my education, and for providing the analytical instrumentation and radiation simulators in support to my research at USF. I also wish to recognize the generosity of the Thermo-Electron Corporation of Waltham, MA for providing the ATR accessories to this research.

My thanks goes out to my fellow graduate students and Post-Doctoral students (Timofey Gerasimov, Yang Liu, Kadine Mohomed, LaNetra Clayton, Patti Dare, Hang Gao and Shayla Emran) from Dr Harmon's Research Group for their unselfish support and friendship.

Table of Contents

List of Tables

List of Figures

List of Abbreviations

PMMA:	Poly (Methyl methacrylate)
PS:	Polystyrene
G(s):	Radiation Yield for main-chain scission events per 100 eV per gram
G(c)-G(x):	Radiation Yield for crosslinking events per 100 eV per gram.
$G(H_2)$:	Radiation Yield for hydrogen gas events per 100 eV per gram.
$G(COOCH_3)$:	Radiation Yield for PMMA decarboxylation events per 100 eV per gram.
^{60}Co:	Atomic symbol for the cobalt-60 nuclide.
FTIR:	Fourier Transform Infrared
GPC:	Gel Permeation Chromatography
SEC:	Size Exclusion Chromatography
DSC:	Differential Scanning Calorimetry
NMR:	Nuclear Magnetic Resonance
Mw:	Weight Average Molecular Weight
Mw_0:	Original Weight Average Molecular Weight
Mn:	Number Average Molecular Weight
Mn':	Number Average Molecular Weight following irradiation.
PD:	Polydispersity.
H:	Peak Height (or Area) of a component partition of the molecular weight distribution
NASA:	National Aeronautics and Space Administration
SPENVIS:	Space Environment Information System
SRIM:	Stopping and Range of Ions in Matter
CASINO:	Monte Carlo Simulation of Electrons in Solids
AP8:	NASA's Space Proton Modeling Software
AE8:	NASA's Space Electron Modeling Software
ICP:	Inherently Conductive Polymer
EOP:	Electro-optic Polymer
POF:	Polymer Optical Fiber
PE:	Polyethylene
PP:	Polypropylene
TFE:	Tetrafluoroethylene
PTFE:	Poly (tetrafluoroethylene)
ETFE:	Ethylene tetrafluoroethylene
LEO:	Low Earth Orbit
HEO:	Highly Elliptical Orbit
AO:	Atomic Oxygen
UV:	Ultraviolet
eV:	electron volt
KeV:	Kiloelectron volt
MeV:	Megaelectron volt
D:	Absorbed dose
Tg:	Glass Transition Temperature
Tg_∞:	Glass Transition Temperature for Mn approaching an infinite value
K:	Dimensionless constant for the Fox Flory function.
w:	Monomer molecular weight
p_0	Number of scissions per monomer segment

r:	Unit dose
Ne:	Expected number of particles striking a defined surface area.
a:	The area of the target under exposure to radiation.
t:	Time
T:	Temperature.
K:	Degrees in Kelvin
C:	Degrees in Centigrade
P:	Atomic nucleus.
δ:	Distance of transient particle or photon from the atomic nucleus.
F:	Columbic force where momentum and energy are transferred to the electron.
h	Planck's constant.
ν:	Frequency
γ:	gamma radiation
LET:	Linear energy transfer
LINAC:	Linear electron accelerator
TLD:	Thermoluminescence detector
ATR:	Attenuated Total Reflectance
SB-ATR:	Single Bounce - Attenuated Total Reflectance
CTE:	Coefficient of Thermal Expansion
CT:	Count of chains in a Partition Band.
X:	Number of molecules per gram of target polymer
m_{Ir}:	Remaining concentration of chains at Partition I.
m_I:	Pre-Exposure concentration of chains at Partition I.
M_I:	Molecular weight of chains at Partition I.
N_A:	Avagadro's number.
k:	Rate constant for the radiation event under study (e.g. k_s = rate constant for main-chain scission)
WLF:	William-Landis-Ferry
H_a:	Activation energy for molecular motion (relaxation of the polymer chains at Tg). Also referred to as E_a.
C_1:	Universal constant for the WLF expression (-17.44)
C_2:	Universal constant for the WLF expression (51.6^o K)
f_g:	Fractional free volume.
R:	Gas Constant
α:	Coefficient of thermal expansion.
B:	Unity (A term used in the determination of f_g.
m_{max}:	Pre-exposure concentration of highest partition in the Mw distribution of polymer.
P:	Partition of a molecular weight distribution.
MALDI-MS:	Matrix-Assisted Laser Desorption Ionization - Mass Spectrometry

Radiation Induced Degradation Pathways for Poly (Methyl Methacrylate) and Polystyrene Polymers as Models for Polymer Behavior in Space Environments.

Kenneth Henry Heffner

ABSTRACT

Modeling methods are required for predicting the chemical stability of macromolecular materials used in critical spacecraft components of satellites orbiting in the high-energy radiation environment of near earth and deep space planetary magnetic belts. Methods for establishing degradation mechanisms and predicting and simulating the total absorbed dose and ionization for long term space missions are presented herein. This investigation evaluates cross-linking, main-chain scission and elimination products in a linear series of narrowly dispersed poly(methyl methacrylate) (PMMA) and polystyrene (PS) polymers. A comparison is made of the scission radiation yield (G_s) and crosslinking (G_x) predicted for the simulated ionization data to the results of degradation in a ground-based simulation of the space radiation environment using a ^{60}Co source. The influence of molecular weight on the stability of post-irradiated polymer is evident in the degree of change observed for each molecular weight series with respect to the degradation products produced by exposure to gamma radiation. The analysis of the specific polymer degradation products and changes in the average molecular weight (M_w) were performed using chemical analysis (FTIR and GPC) and thermal analysis (DSC). The analytical results for PMMA and polystyrene radiation-induced degradation products demonstrate that, depending on Mw, the amount and types of degradation products will vary with respect to crosslinking, chain scission and other oxidative pathways. The results support the preference for end group loss with free volume properties driving the observed differences in the G(s) and (G_x) values. The cross-linking observed for polystyrene is controlled by molecular weight as well wherein the lowest molecular weight molecules display greater resistance to cross-linking. This research investigation employs proven tools of analysis (NASA AP8 and AE8) that accurately predict the amount of energy applied to spacecraft materials during a typical near-earth, aggressive mission environment . Another model (SPENVIS) is applied to determine the amount of total

energy absorbed by the spacecraft materials from proton, electron and Brehmsstralung radiation throughout the mission life. Another set of models (SRIM and CASINO) are used to asses the range of penetration of particles into the materials and the extent of ionization caused by the particle spectrum and fluence. The absorption coefficients for the PS and PMMA structure are determined to ensure good correlation between ground simulation and the true space environment. The total dose values are used to establish the total dose that is to be deposited during the ground simulation experiments. A ^{60}Co irradiator was used as the ground simulation source. Dosimetry was used to determine the exposure time needed to deposit an equivalent amount of dose accumulation needed to simulate the total dose modeled for the space mission. Using gel permeation chromatography, previous studies have demonstrated that the characteristic Gaussian distribution of narrowly-dispersed PS and PMMA is perturbed by the accumulation of degradation products following irradiation. The change in distribution provides insight into the preferred path of degradation. The role of free volume in the glass transition temperature are reported with respect to Tg variation with molecular weight. Using differential scanning calorimetry. The role of free volume in the determination of the mechanism of radiation-induced degradation is a primary focus of this investigation when considering the ability of the main chain to recombine or undergo abstraction as opposed to crosslinking or scission where motion is restricted in the solid state. The subtle distinction of structural changes brought about by the loss of side groups, double bond formation and crosslinking have been characterized by infrared spectroscopy. The resultant spectra of irradiated polymers offer considerable information on verifying the extent of competing reactions that involve structural features of the molecule. These instrumental methods are the tools of research that will assess the affect of molecular structure on polymer radiation resistance, and will support the rationale explaining the preference for one degradation mechanism over another. This research investigation has yielded information on the affect of polymer molecular structure on radiation resistance. The work goes beyond previous studies that define empirical observations for a change in radiation resistance by virtue of a change in side group. The effect of free volume, stabilized intermediates and reactive intermediates are related to molecular weight and side group functionality. The understanding of the mechanistic rationale behind the effect of structural features on polymer radiation resistance are essential to the development of modeling systems for predicting polymer stability in space mission environments.

Chapter One

Introduction

Project Overview

This thesis involves a research investigation into the influence of molecular structure on polymer susceptibility to degradation in space radiation regimes for deep space and near-earth spacecraft flight missions. The radiation spectrum and fluence for spacecraft missions is an extreme environment that requires specialty materials with high radiation resistance. This research is concerned with the determination of chemical mechanisms of degradation that will be used as the foundation for the development of modeling methods to predict the radiation susceptibility of polymeric material in advance of use for spacecraft designs. The availability of knowledge-based modeling methods of analysis has considerable importance to the satellite and manned space industries as a tool for the selection of polymeric materials that are suitable for stable performance in the space radiation regime.

Molecular weight, tacticity and side groups are three structural factors selected for this research investigation since these are fundamental structural features used to manipulate the properties of polymeric materials. Polymethyl methacrylate (PMMA) and polystyrene (PS) where selected as the model compounds for the investigation in view of their respective, post-exposure, degradative pathways through main-chain scission and crosslinking as two common modes of radiation-induced polymer degradation. The PMMA and PS compounds were also selected for their availability as well-characterized, narrowly-dispersed, linear series standards. The two compounds have been studied extensively with respect to radiation-induced degradation using various sources of particle or electromagnetic radiation. Figure 1.1 describes the abstraction and scission products observed for PMMA following the formation of reactive intermediates during gamma irradiation. A similar description of the cross-linking degradation pathway for PS is presented in Figure 1.2.

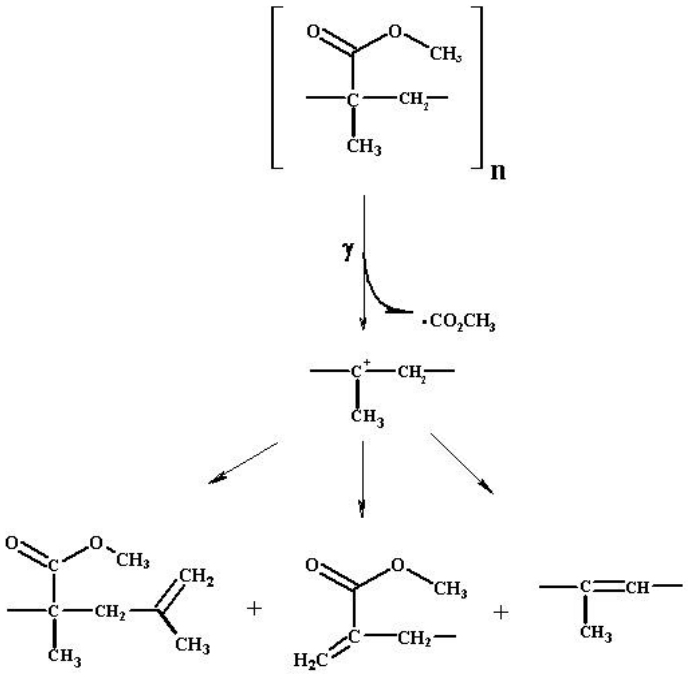

Figure 1. 1. Radiation-Induced Degradative Pathways for PMMA.

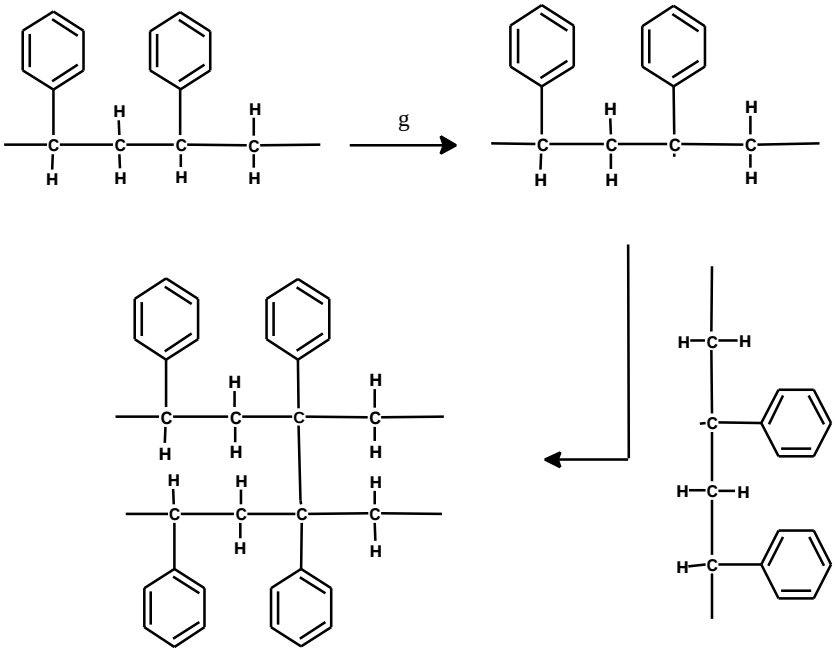

Figure 1. 2. Radiation-Induced Degradative Pathways for PS.

The influence of Mw and common, polymeric structural features, as displayed by PS and PMMA, are selected to limit the complexity of the degradation chemistry under study. Using a set of experiments that control the significant, interfering factors this investigation evaluates the polymers with a specific preference for scission or crosslinking which are the primary, mechanistic pathways for radiation-induced polymer degradation with respect to significant effects on the polymer properties.

This research investigation employs proven tools of analysis (NASA AP8 and AE8) that accurately predict the amount of energy applied to spacecraft materials in a typical near-earth, aggressive mission environment . Another model (SPENVIS) is applied to determine the amount of total energy absorbed by the spacecraft materials from proton, electron and Brehmsstralung radiation throughout the mission life. Another set of models (SRIM and CASINO) are used to assess the range of penetration of particles into the materials and the extent of ionization caused by the particle spectrum and fluence. The absorption coefficients for the PS and PMMA structure are determined to ensure good correlation between ground simulation and the true space environment. The total dose values are used to establish the total dose that is to be deposited during the ground simulation experiments. A ^{60}Co irradiator was used as the ground simulation source. Dosimetry was used to determine the exposure time needed to deposit an equivalent amount of dose accumulation needed to simulate the total dose modeled for the space mission.

Using gel permeation chromatography, previous studies have demonstrated that the characteristic Gaussian distribution of narrowly-dispersed chains of PS and PMMA is perturbed by the accumulation of degradation products following irradiation. The change in distribution provides insight into the preferred path of degradation. The role of free volume in second order phase transitions are reported with respect to Tg variation with molecular weight using differential scanning calorimetry. The role of free volume in the determination of the mechanism of radiation-induced degradation is a primary focus of this investigation when considering the ability of the main chain to recombine or undergo abstraction as opposed to crosslinking or scission where motion is restricted in the solid state. The subtle distinction of structural changes brought on about by the loss of side groups, double bond formation and crosslinking have been characterized by infrared spectroscopy. The resultant spectra of irradiated polymers offer information for verifying the extent of competing reactions that involve structural features of the molecule. These

instrumental methods are the tools of research that will assess the affect of molecular structure on polymer radiation resistance, and will support the rationale explaining the preference for one degradation mechanism over another.

Previous PMMA radiation studies report differences in the extent of scission and crosslinking when other factors are evaluated, such as: temperature, energy fluence, and the size of the acrylate side groups. The studies demonstrate that chemical structure does influence the extent of radiation-induced damage to the PMMA polymer molecule. The studies also demonstrate the need for controlled experimental simulation conditions used in the assessment of radiation damage on polymers. However, previous studies do not report on the effects of molecular weight, and molecular weight in conjunction with the effects of the side group, on polymer degradation. Such factors remain to be understood before being useful in modeling radiation damage.

The influence of the rigid phenyl groups in limiting segmental motion, along with the potential for resonance stabilization of the reactive intermediate, have previously helped to explain the preference for a cross-linking mechanism in polystyrene. The current investigation shows free volume working through end group effects related to Mw, plays a significant role in the extent of cross-linking.

The results of this investigation are designed to contribute to the knowledge of the molecular behavior of polymers and initiate the development of modeling rules for predicting polymer degradation, as a means of assessing the affect of polymer molecular structure on radiation resistance. The work goes beyond previous studies that define empirical observations for a change in radiation resistance by virtue of a change in side group. The results demonstrate the effect of free volume, stabilized intermediates and reactive intermediates are related to molecular weight in addition to side group functionality. Predicted random, main-chain scission and PS cross-linking are described to demonstrate the expected result of using a steady state environment, a controlled dose rate and the established radiation yield values in the determination of radiation-induced degradation products. This study demonstrates the use of the same predictive model in removing the effects of main-chain events and redefining the model based on preferred paths of degradation (e.g. end-group loss). The experimental results are examined to define the chemistry of the degradation products, and to assess which model best fits the experimental results. This approach

provides a strong case for the preferred influence of Mw, end group depolymerization and free volume effects.

Before applying the findings to an analytical model, this investigation has also considered the effects that might interfere with achieving an accurate assessment of the degradation process. Many of these effects are well studied and provide guidance in conducting the experimentation for this study. For example, the use of ambient (~25^{o}C) experimental temperature yielded a condition for the polymer that is well below the Tg for the PS and PMMA linear series used for this study, and prevented any premature annealing of the radical intermediates formed during irradiation.

All polymeric linear series compounds used for this study were equilibrated in air, then followed by irradiation in air in a single exposure regime at a high constant dose rate [>3 x 10^6 rads][1] to minimize oxygen diffusion effects. The use of steady state conditions with respect to temperature is designed to eliminate interference from temperature-driven dose rate effects. The free radical intermediates that persist long after the exposure period are susceptible to reactions with reactive gasses (mainly oxygen) that are present in the bulk polymer. Oxygen diffuses into the polymer and competes with other reactive, free-radical intermediates forming oxidation products (e.g. peroxides), and thereby suppresses the scission and cross-linking yields.[2,3] This investigation, therefore, performed GPC analysis within a few days after irradiation to minimize the post-irradiation oxidation of the experimental samples. The study included measures to apply experimental and sample conditions that would limit the influence of oxygen in assessing the mechanistic rationale behind the effect of structural features on polymer radiation resistance.

The PMMA and PS linear polymer standards used for this study displayed low polydispersity, and high purity to limit the effects of contaminants and monomer. The molecular weight range for each standard was selected to achieve sufficient definition of the molecular weight effects in the degradation of the polymer. Tacticity was defined by the manufacturer, and as part of the experimental plan for this study, using FTIR and NMR . The well-reported influence of tacticity on the segmental, conformational motion of the polymer main chain was important to completing the demonstration of the influence of free volume of the degradation behavior of polymers.

The PMMA results for this study demonstrated a significant difference in the Mw distribution of products as a function of the Mw of the polymer in the linear series. As expected, the loss of the carboxy-methyl side chain and scission products were readily observed, however, the distribution of scission products was different by GPC analysis for each PMMA polymer standard evaluated for this study. The pattern of degradation provided insight into the preferential reaction pathways for each molecular weight. Graphical and numerical analysis of the data yields a second-order rate equation that supports end-group analysis as the preferred degradation pathway for PMMA The rate constant is significantly higher for lower Mw linear PMMA polymer that is attributed to the high concentration of end-group moieties and the associated free volume.

The results of the analysis of isotactic PMMA support the observations for end-group contribution to the primary degradation pathway and the influence of the closer packing of the PMMA main-chain segments in isotactic polymers that limits conformational motion throughout the main-chain and near the chain end groups. The rate constant is considerably lower for the isotactic PMMA when compared to the atactic PMMA of similar Mw. The results provided the basis for a scission model based on end group free volume and segmental motion both of which are related to the polymer chain length and tacticity.

The PMMA data also suggests that although the loss of the carboxy-methyl side group is observed for all PMMA samples by FTIR, there is evidence for significant recombination in the main chain of longer oligomers since the GPC data does not show 100% efficiency for random chain scission. The second order reaction kinetics can be applied to the scission rate of PMMA as a function of the Mw of the polymer. The model also accounts for the effects of Mw as the data displays a critical Mw where the Tg begins to decrease rapidly with a decrease in Mw that is supported by the free volume effects described by the Fox-Flory equation.

The atactic polystyrene results demonstrate the effect of Mw on the cross-linking behavior of PS polymer that is explained by free volume as well. The higher Mw oligomers display a higher rate of cross-linking that is attributed to the lack of lateral segmental motion reported for polymers with stiff side groups. The reactive radical intermediate formed in the PS main-chain is held in close to the main-chain of a neighboring oligomer. The lower Mw PS samples display higher segmental motion due to the free volume

at the end groups. The kinetics display a first order rate equation. As with PMMA, the PS displays a critical Mw that is accounted for in the model.

The generalization of the models developed under this investigation to all polymeric materials will not be practical without further research into the effects of other molecular features that will alter the rate equations defined for these simpler models. The models are a starting point that demonstrate the importance of free volume in radiation chemistry of polymers, and that Mw effects on the rate of degradation are driven by the free volume differences associated with Mw.

Space Radiation Background

Technology Transfer: From Ground Applications to the Space Mission Environment

Before ground-based technology advancements are applied in space, any associated polymer technologies must be investigated with respect to chemical stability in the intended space-use environment. New polymer applications introduce new concerns for stable polymer performance and provide a challenge with respect to studying polymer behavior under irradiation conditions. Polymer degradation results from changes in the polymeric chemical structure initiated by the high-energy particles (e.g. electrons, protons and neutrons) and the electromagnetic photon spectrum that is expected for the space mission. The study of the chemistry of radiation effects on polymeric materials requires an understanding of radiation physics, dosimetry, chemical analysis and instrumental analysis as applied to modeling and simulation of the space radiation environment. In addressing the challenges for presented by the introduction of new roles for polymeric materials in space, there is a need to understand the influence of polymer structure on the vulnerability to radiation-induced degradation.

Aerospace design engineers employ numerous materials in the construction of spacecraft systems. The materials are selected based on specific properties that will ensure material performance in the rigorous mechanical and environmental conditions anticipated for spaceflight missions. The space-flight mission environment varies with respect to the duration and destination of the flight path for the spacecraft. The common Near-Earth mission environments impose severe thermal and mechanical stress on spacecraft materials. Temperature extremes for the external surface of the spacecraft with direct solar heating and non-illumination are about $^{-}200^{o}$ C to 100^{o} C and can cycle from one temperature extreme to the other within minutes.[4] The physical stress in spacecraft materials induced by the space environment becomes more significant when considering the concurrent environmental threat of material degradation caused by atomic oxygen, geomagnetically-trapped particle radiation, solar flare protons and the galactic cosmic radiation regimes comprising the Near-Earth mission environment.[5,6] The potential for molecular decomposition and chemical etching presented by the Near-Earth particle regime raises the risk for the alteration of the molecular structure of spacecraft materials. A change in the molecular structure of the spacecraft materials can lead to a deterioration of the mission performance of the spacecraft.[7]

Interplanetary missions can present greater challenges with respect to extreme radiation fluence and spacecraft material stability. As the exploration of space broadens to deep space, more is expected from the performance of spacecraft system materials to meet the demanding mission requirements. Further research into what can be learned about the Earth through the study of other planets (e.g. Mercury, Venus, Saturn and the Saturn moons) will require deep-space, exploratory spacecraft that will need to survive long enough to enable the spacecraft instruments to gather and transmit scientific data. Such future satellite missions are thereby driving greater demand for novel, radiation-hardened, performance polymers.

Role of Polymers in Space Mission Technology

To assist the polymer specialist in the development of materials that meet advancing spacecraft requirements, modern tools, such as, improvements in radiation simulation and advancements in instrumental analysis have developed with the sophistication needed to improve the knowledge of the energy flux in the spaceborne polymeric material. Through the use of such modeling tools, polymer improvements can be designed to enable advancement in ground-based communications, data processing, navigation, solar panels and composite structures. Figure 1.3 illustrates the broad range of space mission engineering functions and advanced space systems applications that apply polymer technology to achieve mission performance objectives.

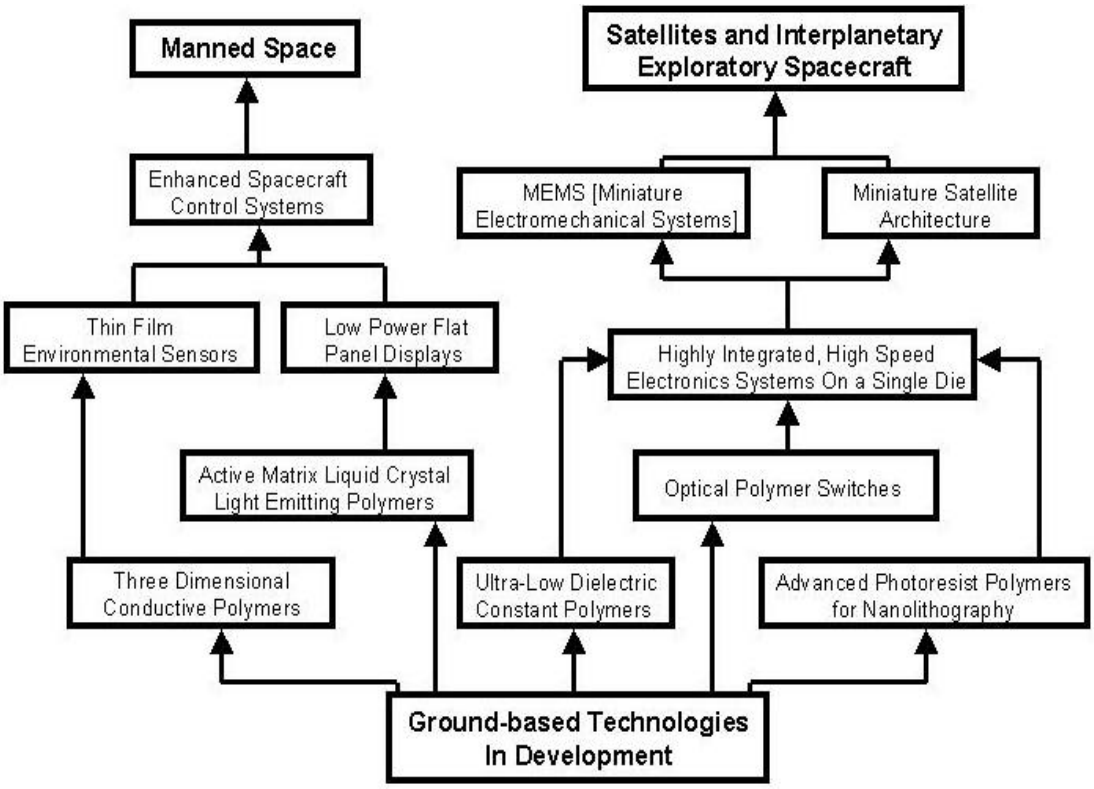

Figure 1. 3. Illustration of the Migration of Ground-Based Polymer Technologies into Space

Chemical Effects of Particle and Photon Radiation

Optical Polymers

The typical progression of polymer innovations into spacecraft designs is frequently an indirect path that begins with concepts that are first proven for applications in conventional ground-based industries. As an example, inherently conductive polymers (ICPs) and electro-optic polymers (EOPs) are evolving towards broad, ground-based, commercial applications in photonics and metal waveguide alternatives with numerous applications for industry. The EOP and ICP polymer base structure is typically a highly unsaturated chain. The integrity of the unsaturated chain structure is critical to maintaining the properties critical to polymer performance. The ICP or EOP unsaturated main-chain polymer developed for the ground-based systems may be unsuitable for use in space environments.[8]

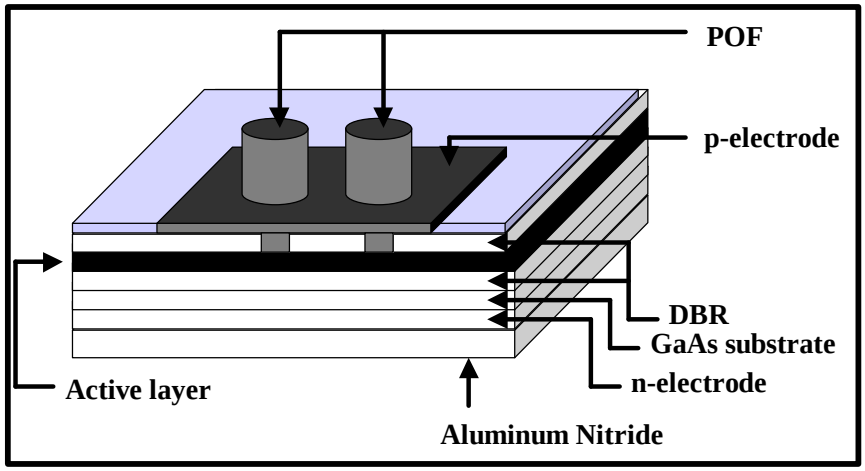

Figure 1.4. Illustration of the application of EOPs

As space missions are conducted at high cost, and opportunities are rare for on-orbit experimentation to understand the chemistry of polymer degradation in space. Therefore, radiation modeling, ground simulation and analytical methods are needed to accurately assess the amount of total

ionizing dose deposited in a polymeric material over the duration of the space flight mission and to assess the radiation-induced changes in the chemical structure. The prospect of a costly mission failure compels space programs to assess the risk of radiation susceptibility for the organic, polymeric materials comprising the space system. The polymer must be evaluated before use in a space system application through research in the area of radiation effects and space simulation and modeling. A growing use for polymers in space is photonics combining optical science with electronics thereby enabling new frontiers in space-based satellite communication, navigation and signal processing. The next generation of microprocessor technology is targeted at achieving clock rates of more than 1 GHz.[9] The current state of the art of conventional microcircuit metallized interconnects is constrained by powder dissipation and delay times that will remain a barrier to mid-distance (~60 cm) high-throughput (>1 Gb/s) point-to-point interconnects.[10] Optoelectronics interconnects such as vertical-cavity surface emitting layers (VCSELs) are coupled with highly-flexible PMMA polymer optical fiber (POF)[11] yielding low-cost interconnection modules with low power dissipation and multi-Gb/s transmission at high clock speeds. PMMA undergoes degradation following irradiation, presenting a risk of change in key physical properties. Survivability of optical fibers for data bus and for gyroscope applications is challenged in the natural space environment. The silicone-based core materials to the primary and secondary organic, buffer coatings of the fiber coil must be hardened against radiation-induced chemical changes that can affect key fiber properties such as refractive index properties or buffer separation resulting in a risk of signal attenuation and noise. Unlike the more straightforward resolution or TFE insulation applications or solar cell coatings, the resolution of radiation effects on fiber polymers is encumbered by the complexity of the multilayer design of the fiber, and the requirement for optical clarity for low signal loss. Optoelectronics are providing an example of the

increasing challenge of transferring technology breakthroughs in polymer science to space applications.[12,13,14]

PTFE Degradation

Polytetrafluoroethylene (PTFE) is a well-studied example of polymer susceptibility to degradation in natural space. The inert, low dielectric properties of PTFE held promise for a wide range of uses in spacecraft electronic systems based on its success as an insulator in numerous ground-based electronics interconnect applications (e.g. wiring bundles for circuit interconnection). However, the PTFE polymer is susceptible to radiation-induced main-chain scission that alters the electrical and mechanical properties of PTFE (e.g. dielectric constant, dissipation factor, loss factor and dc insulation resistance). The degradation mechanism includes the formation of reactive short-chain carbon radicals and fluorinated gasses such as SiF_4 (reaction of fluoride radicals with glass). These degradation products can induce further damage by re-deposition throughout the surrounding spacecraft surfaces adversely affecting the performance of highly sensitive components such as optical sensors or receivers.[15]

Limitations in the use of a polymeric material for space use are sometimes overcome through a straightforward alteration of the chemical structure. The radiation resistance of polyethylene is significantly higher than PTFE.[16] The radiation resistance of PTFE is improved when co-polymerized with polyethylene to form ethylene-tetrafuoroethylene (ETFE) (Figure 1.5).[16] The chemical rationale for the difference in chemical stability is in the reactive intermediate that readily undergoes scission in PTFE and crosslinking in the ETFE. The fluoro groups restrict the movement of the segments in the chain, and display steric effects that restrict crosslinking. The cross-linking process in ETFE degradation is a higher energy process than C-C-F scission.

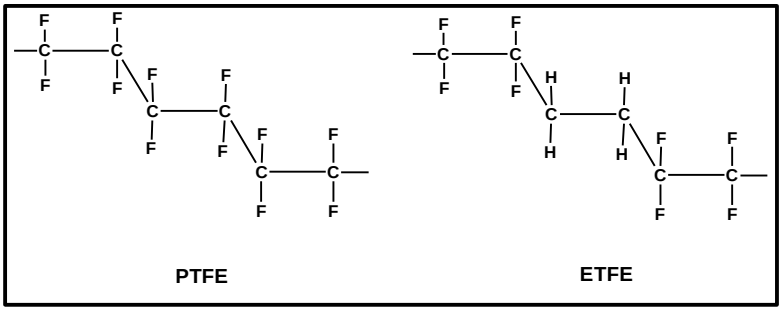

Figure 1.5 Illustration of the Structural Differences Between PTFE And ETFE.

The threshold dose for a 1% change in radiation hardness is improved by two orders of magnitude through the use of the resultant copolymer. The new copolymer does require a compromise in the loss of some of the chemical and mechanical properties of the coating. In most heritage space applications, this is an acceptable alternative.

New challenges for space use in polymer technology, however, are driving the need for performance materials that will display specialized, preferred properties while retaining chemical integrity in harsh radiation regimes that exist for space missions. There are many new space technology areas supporting the observation that polymers will play a critical role in advancing spacecraft technology. For example, to reduce the cost of satellite deployment and enable multiple payloads in a single flight, space system agencies, space missions now require designs that miniaturize and bring about substantial weight reductions in the spacecraft structure. Ground-based systems use advancements in polymer technologies that enable miniaturized electronics applications through the development of high-density microcircuits used for ground-based products. The transition of high density microelectronics to space applications is limited by the power dissipation that accompanies continuous operation and the high rates of information and signal processing required by satellite missions. Ground based applications use convection to dissipate

heat from the circuitry. The vacuum of space requires a conductive network to transfer heat to the exterior radiator of the spacecraft (Figure 1.6). Specialized, low-density, filled thermally conductive polymeric laminates are a critical segment of a conductive thermal dissipation path to the exterior spacecraft surfaces for dissipation into space. Retention of the thermal, electrical and mechanical properties of the laminate in the dynamic radiation regimes in space will be critical to maintaining the reliability of the electronics supporting the goal to miniaturize spacecraft designs.[17]

The growth in the use Low Earth Orbit (LEO) satellites for global commerce presents a challenge to many polymeric materials used for the exterior surfaces of the spacecraft architecture. The atomic oxygen (AO) present in the LEO orbit erodes organic polymeric compounds and rapidly degrades polymer performance.[18] Conventional ground-based systems for energy generation or imaging (e.g. solar-array substrates and second-surface mirrors) use polymeric materials that must be stabilized against the aggressive AO and UV radiation effects in the LEO orbit.[19]

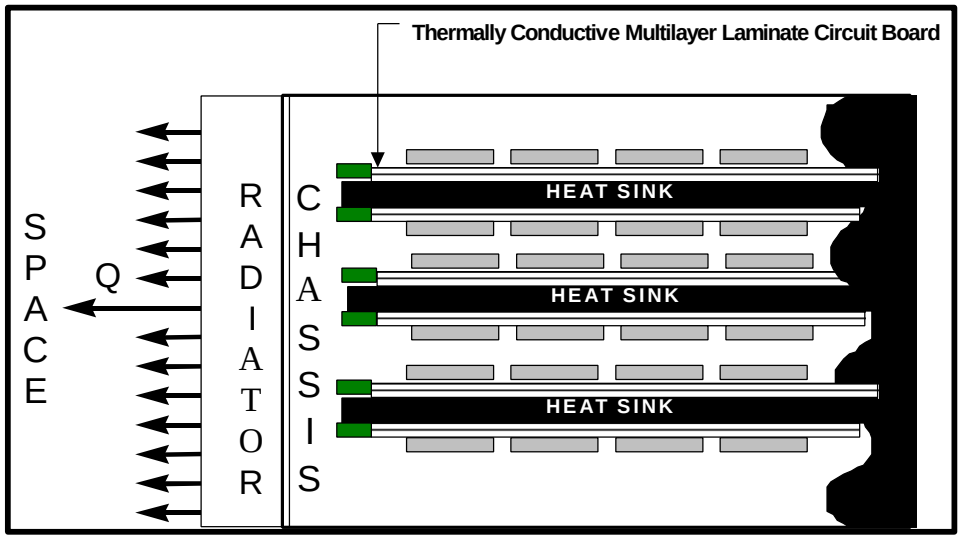

Figure 1.6. Thermal Path through Polymeric Substrate for Spacecraft Electronics (Not to Scale).

Interaction of Radiation with Polymer Material

Space Particle and Radiation Distribution

The particle spectrum of the space environment is comprised of high-energy electrons and atomic nuclei (primarily protons) within an energy spectrum that ranges from a few keV to more than 100 MeV and heavy ions (>10^{10} MeV).[20] The photon electromagnetic spectrum in space is comprised mainly of high-energy ultraviolet (1 keV) and gamma (to 10 MeV).[20] The radiation is distributed throughout deep space, and is concentrated in the magnetic fields as radiation belts that surround the planets. The Near-Earth distribution of particle flux is omnidirectional, and there is no preferred orientation for spacecraft within a radiation belt where the fluence for the spacecraft surface would be reduced.

Traditional flight paths for spacecraft will traverse in and out of the radiation belts at varying speed, and therefore the spacecraft will be exposed to varying dose rate and flux spectra over the life of the mission. Materials within the spacecraft will accumulate dose from the collective radiation regime of protons, electrons and secondary X-ray radiation (Bremmstralung).[21]

Particle Interaction with the Bulk Polymer

The radiation-induced change in the chemical structure of polymeric molecules occurs through ionic or free radical intermediates. The reactive intermediate is formed when an atom comprising the molecular structure absorbs energy imparted by the high-energy particle (or photon) when the transient particle passes near the atomic orbitals of the atom. Particle collisions with the nucleus or electrons of the atom can also result in the formation of reactive intermediates. High-energy ultraviolet photons usually only lead to electronically excited states. Each event leads to reactions that alter the molecular structure of

the polymer.[22] Table 1.1 summarizes the space radiation regime with respect to particle energy and the electromagnetic spectrum.

Particle or Photon	Energy Spectrum	Event
Protons and other heavy ions	1 MeV to >100 MeV	Ionization/Free Radical formation
Electrons	1 KeV to 10 MeV	Ionization/Free Radical formation
Gamma	10 MeV	Ionization/Free Radical formation
Ultraviolet	1 KeV	Electronic excited state

Table 1.1 Summary of Particle and Photon Energies Expected for the Space Environment.[20]

The reactive intermediates formed by ionizing radiation pursue several reaction pathways resulting in the loss of a side chain, chain scission, crosslinking or oxidation.[23,24] The preference for one reaction pathway over another is determined by the structural formula and the chemical formula along with the temperature and surrounding atmosphere of the radiation.

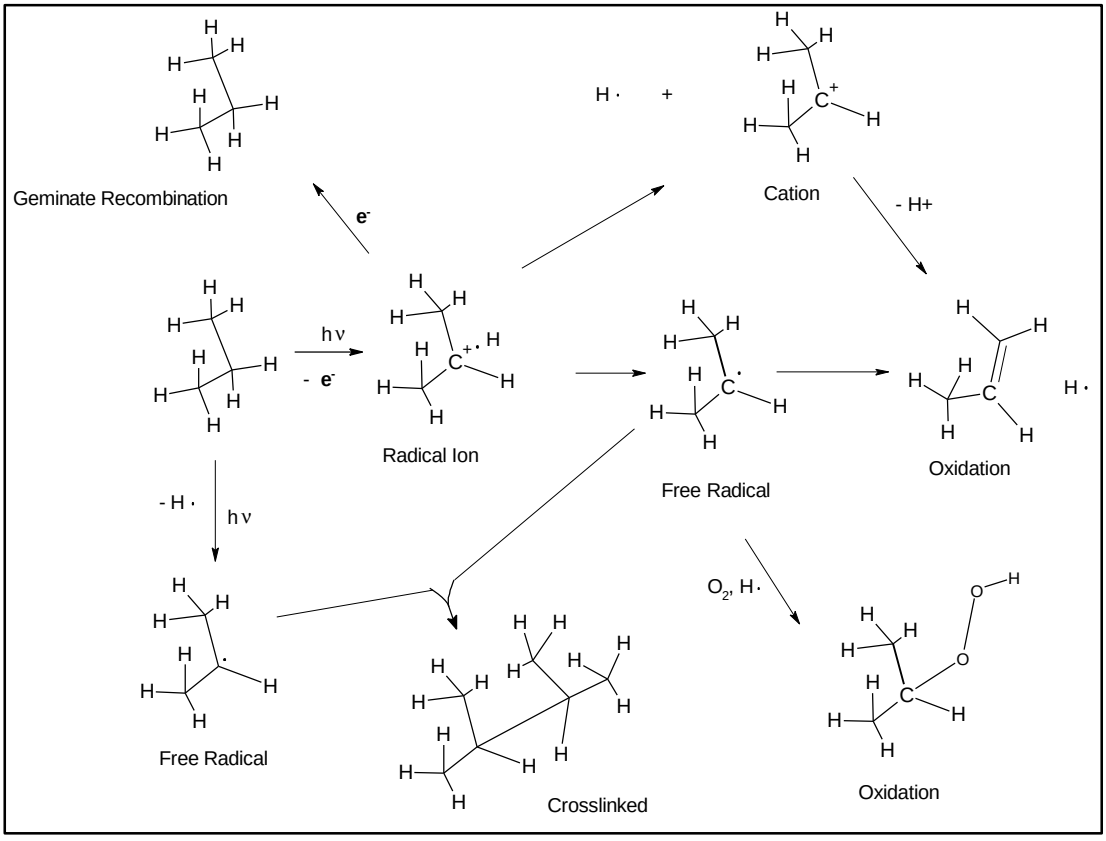

Figure 1.7. Decomposition Scheme for Irradiated Propane Molecules.

The ejected electron and the parent cation formed from the incipient ionization reaction can lead to the formation of a complex combination of reactive chemical intermediates. The multiple pathways illustrated in Figure 1.7 for the decomposition and recombination of a simple molecule like propane underscore the difficulty in predicting the chemical fate of a polymer network in an ionizing radiation environment.[25]

Absorbtivity and Damage Potential

The polymeric material may be viewed as a matrix of atoms. The structure of the matrix is comprised of elements in a proportion defined by the molecular formula. The molecular structure determines the bonding that will comprise the matrix, and the bondlength and tertiary structure provide the distance between the elements. As particle radiation enters the polymer, a proportion of the particles will penetrate the matrix, and impart energy to the elements as the particles track a path through the matrix. Two broad classes of events may take place. One is the radiochemical ionization and free radical production, and the other is atomic displacement collisions. The particle energy imparted to the atoms excites the electronic configuration resulting in the loss of an electron or a photon (X-ray) as the element tries to achieve a lower energy state.[26] This is described as the linear stopping power of the atoms and covalent bonds comprising the polymer and is used to quantify the absorbed dose as shown in Figure 1.8.

This dose energy drives the ionization process that results from electron loss and leads to radical formation. The resultant radical intermediate follows free radical propagation and termination reactions that can result in scission, cross-linking, abstraction or recombination as shown in Figure 1.7, and it is these reaction products that determine the extent of radiation induced damage in the polymer.[28]

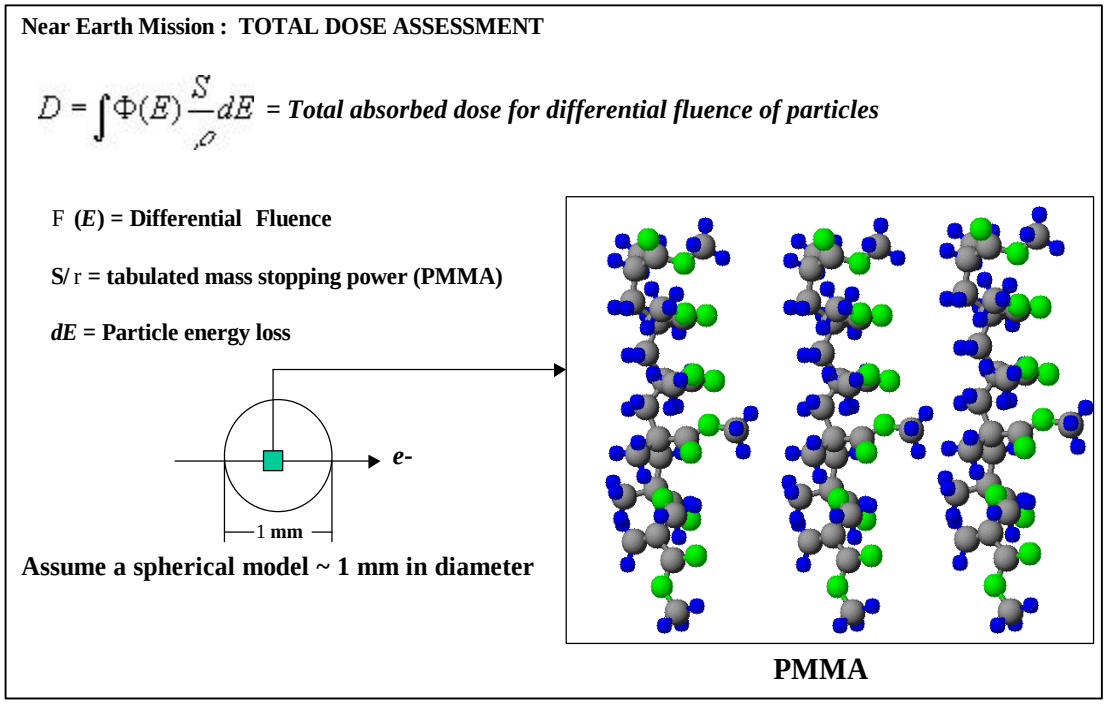

Figure 1.8. Illustration of the Stopping Power vs. Absorbed Dose.[27]

Application specific changes in the functional, physical properties induced by the collective effect of the radiation exposure are used to determine the extent of damage in the polymer in the space flight mission. The determination of the expected total dose for a space flight mission is needed to demonstrate polymer stability through ground simulation. The modeling and analytical processes used to determine the radiation damage expected for a defined flight path are presented in the next chapter along with the determination of total dose in ground simulation.

Polymer Composition and Intrinsic Radiation Hardness

The Polyethylene Baseline and Radiation Yield Values

For modeling methods for polymer degradation, polyethylene is a suitable baseline polymer structure that can be used to demonstrate the effects of substitution on the main-chain. Comparative data is presented in this section from a compilation of reports that demonstrate the varying degrees of change in the properties of polymers that differ from one another through the substitution of polyethylene hydrogens with side chains or other elements. The data also describes the known, preferred path of degradation for each polymer using the associated radiation yield or G value. The G value is a useful tool for associating the number of chemical events in a polymer structure with the amount of energy absorbed (total dose) by the polymer structure during a radiation event.

During the radiation event, the energy flux and spectrum of the particle or photon radiation regime provides a dose of ionizing radiation that yields a number of ionizations per unit area of polymeric material. As previously discussed, the atoms comprising the polymer display a specific stopping power for the energy spectrum of the incoming radiation flux. Not all ionizations result in the formation of products that can alter the performance of the polymer through degradative reactions such as scission or crosslinking reactions.

As expected for most chemical studies, the molecular formula and structure of the polymer determines the kinetics of degradation following ionization. The molecular formula of the polymer influences the amount of energy flux absorbed by the bulk polymer. Structural features of the polymer such as main-chain linkage, side groups and tacticity are structural features that determine the polymer degradation pathway. Therefore, in applying kinetics to specific reactions leading to the degradation of the polymer structure, some advanced knowledge of the polymer structural formula is required.

One method for applying kinetics to the study of radiation-induced polymer degradation is the radiation yield value which uses the products formed through polymer degradation as the baseline for describing the rate equation as a function of absorbed energy.[29] The radiation yield leading to the formation of specific products, like hydrogen, is called the "G value", which represents the number of molecules produced per 100 electron volts (eV) of energy absorbed by the target medium. The energy absorbed by a material is defined as total dose, and is expressed in "rad" units. One rad is equal to 6.25 x 10^{13} eV/gram of target material. By using polyethylene (G (H_2) value (*in vacuo*) = 3.7) and the equation in Figure 1.9, the radiation yield for hydrogen at a specific total dose (*D, with D = 10^6 rads*) can be determined.

D x G/100 = Molecules of hydrogen produced/gram of material

(6.25 x 10^{19} eV/gm) (3.7 molecules/100 eV) = 2.3 x 10^{18} molecules/gram of polyethylene

Figure 1.9. Formula for the Determination of the Radiation Yield of Hydrogen in Polyethylene.

Hydrogen abstraction is the preferred degradation path for irradiated polyethylene where the C-H bond is broken by the loss of a valence electron, and undergoes elimination of hydrogen gas (Figure 1.10).

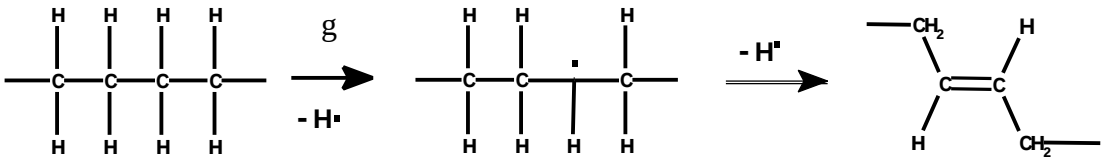

Figure 1.10. Hydrogen Abstraction in Polyethylene.[25]

The unpaired electron formed by breaking the polyethylene C-H bond in the polymer chain may react with an unpaired electron in a parallel chain leading to a cross-linked pair of polyethylene polymer chains. By cross-linking, the average molecular weight (M_w) of the polyethylene target can increase significantly. Polyethylene does not undergo significant scission reactions (Table 1.1).

The substitution of hydrogen with a methyl side group to the polyethylene main chain results in a change in the radiation degradative pathway. The G values described in Table 1 compare the degradation products formed by polymers with a common, linear, saturated, carbon-carbon chain that differ by the side group moieties. The polyethylene structure is provided as the baseline polymer where no side groups are present, and the degradation product yields are represented by G(x) for cross-linking bond formation, G(s) for cleavage of the main chain (or scission), and G(H_2) for hydrogen gas formation as a result of an elimination reaction along the main chain (or abstraction).[22]

Using G value data for linear polyethylene (PE), polypropylene (PP) and PMMA, the change in polymer radiation susceptibility with a change in polymeric structure can be demonstrated (Table 1.2).

POLYMER	G(x)	G(s)	G(abst)	G(CH4)	G(-COOCH3)
Polyethylene	1.00	0.20	3.70	-	-
Polypropylene	0.22	0.24	2.34 - 2.78	0.095	-
PMMA	0.12	1.20	0.40	-	1.00

Table 1.2 Radiation Yield Values (G) for Linear Polymers vs. Side Chain Modification.[22]

As side groups are added to the main chain, the formation of additional degradation products alters the yield values for G(X,S,H_2) while adding the formation of other products from decomposition of the side chain itself. For polypropylene, the formation of methane, G(CH_4), is accompanied by an increase in the G(S) value, a stable G(X) value and, as expected, a decrease in the G(H_2) value. The change in polymer degradation yield behavior is attributed to the stiff methyl side group that is reported to restrict lateral

segmental motion through steric hindrance, and to rotational barriers that prevent the close proximity needed for two radicals in neighboring chains to undergo cross-linking (Figure 1.11).

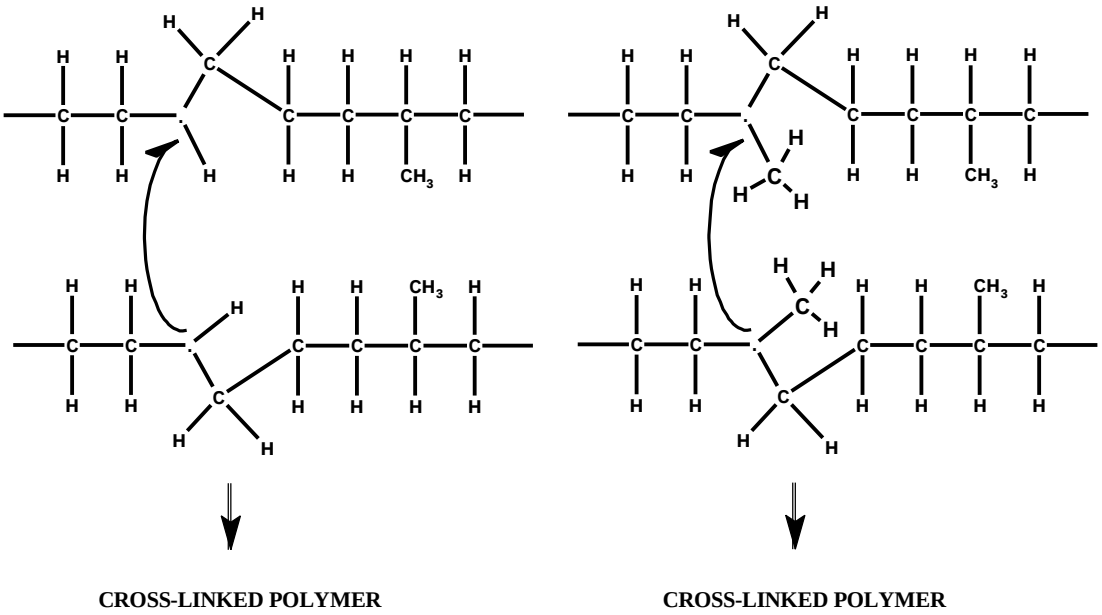

Figure 1.11. Illustration of the Steric Effects of Side Groups in Cross-linking [PE vs. PPE].

The degradation chemistry of polymers becomes more complex as a second geminal group is added to a main-chain carbon. The size, flexibility and dipole behavior of the additional side group affects the rotational and segmental motion of the polymer chains, and thereby influences the preference for scission or crosslinking. In polyalkyl methylmethacrylate (PAMA), the carboxy-alkyl side chain ($COOCH_3$) and the sterically hindered pathway of the resultant, tertiary free radical intermediate to a cross-linked product, are thought to influence the preference for a scission-based degradation over cross-linking, and $G(H_2)$ is insignificant by comparison to polyethylene. The ratios of gamma-induced, main chain scission to cross-linking (G(S)/G(X)) for polyethylene, polypropylene and PMMA are 0.2, 1.1, and 10.0 respectively, demonstrating the influence of the side groups in linear polymers.[22]

Previous studies have reported that the total dose (gamma radiation) required to achieve a significant change (25%) in the mechanical properties is 3 x 10^8 rads for polyethylene and 3 x 10^7 for polypropylene and about the same for PMMA.[16]

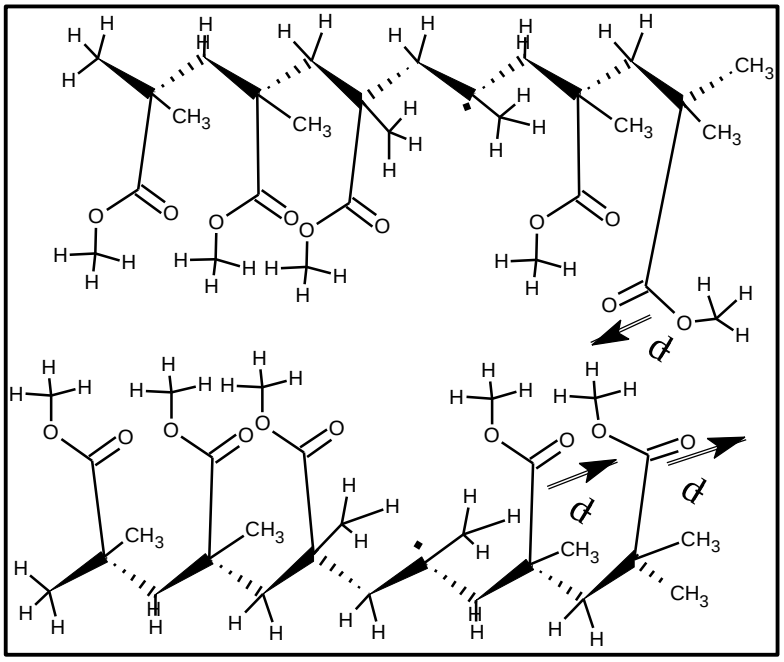

Figure 1.12. Illustration of the Intra- and Inter-chain Effect of Dipole Interactions

Dipole interactions of the PMMA side chains (Figure 1.12) also influence segmental mobility in the PMMA main-chain by restricting rotational and segmental motion of the polymer chain. This limitation in mobility influences recombination in the main-chain by retaining the main-chain radical intermediate in a stable state to permit recombination with a hydrogen radical, or if mid-chain, end group loss does occur, the dipole interactions influence the recombination of mid-chain radicals by the same mechanism. Isotactic PMMA is known to undergo recombination of the radical intermediates to yield a racemic product that alters the tacticity of the polymer chain (Figure 1.13).[30]

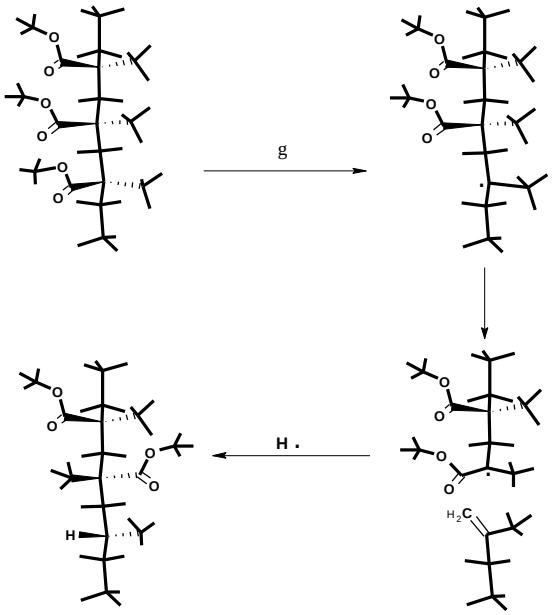

Figure 1.13. Illustration of the Change in Stereochemistry of PMMA through Recombination.

A study of the radiation behavior of other poly(alkyl methacrylates) showed that the length and composition of the side chain influenced the radiation yield for scission and cross-linking products. Branching in the side chain leads to a return to a preference for scission and side group loss. The data is summarized in Table 1.3.[31]

Side Group	Ratio (Scission/Ester Loss)	Scissions*	- COOR Loss*
Methyl acrylate	0.71	3.5	2.5
n-Butyl acrylate	0.27	2.7	10.0
iso-Butyl acrylate	0.35	3.9	11.0
sec-Butyl acrylate	0.75	5.3	7.1
tert-Butyl acrylate	0.71	9.6	13.6

* Events per 1,000 Monomeric Units

Table 1.3 Radiation Events for PMMA vs. Carboxy-Ester Side Group.

The literature also reports that G(x) remains small until the alkyl ester side chain is greater than four carbon units (Table 1.4)[32]. The resultant drop in G(s) is reported to be supplanted by an increase in G(x). The cross-linking is thought to be between the side group and another main-chain approaching a condition wherein the side group behaves as a copolymer of the PMMA chain.

Side Group	G(s)
Poly (methyl methacrylate)	1.30
Poly (*tert*-butyl methacrylate)	1.28
Poly (*n*-hexyl methacrylate)	0.38
Poly (cyclohexyl methacrylate)	0.44
Poly (benzyl methacrylate)	0.29

Table 1.4 G(s) Values for PMMA vs. Length of Carboxy-Alkyl Side Group.

The exception to this conclusion would be the benzyl ester. The benzyl moiety would impart less flexibility to the side chain. The stiffer side group restricts segmental motion (reptation) between chains, and the resonance stabilization for free radicals initiated in the ring would possess sufficient lifetime to promote cross-linking via the side group to the neighboring main-chain. The role of inflexible side groups, resonance stabilization and the availability of an α hydrogen are factors that also enable polystyrene to cross-link not only to the ring, but between to a neighboring main-chain as well with a G(x) value of 0.022 (Figure 1.14).[22]

In polystyrene, the resonance stabilization of the free radical generated at the α-carbon permitting time for preferred orientation with neighboring radical intermediate. The stabilized ionic (or free radical – Figure 1.14) intermediate is capable of undergoing crosslinking reactions leading to an increase in the average molecular weight of the polymer (Mw_{avg}) and a change in polydispersity. While cross-linking is the preferred degradative pathway for polystyrene, the G_x value is small (0.04). The chemical stability of polystyrene is also attributable to the resonance stabilized intermediate that permits time for self-annealing and recombination.[33]

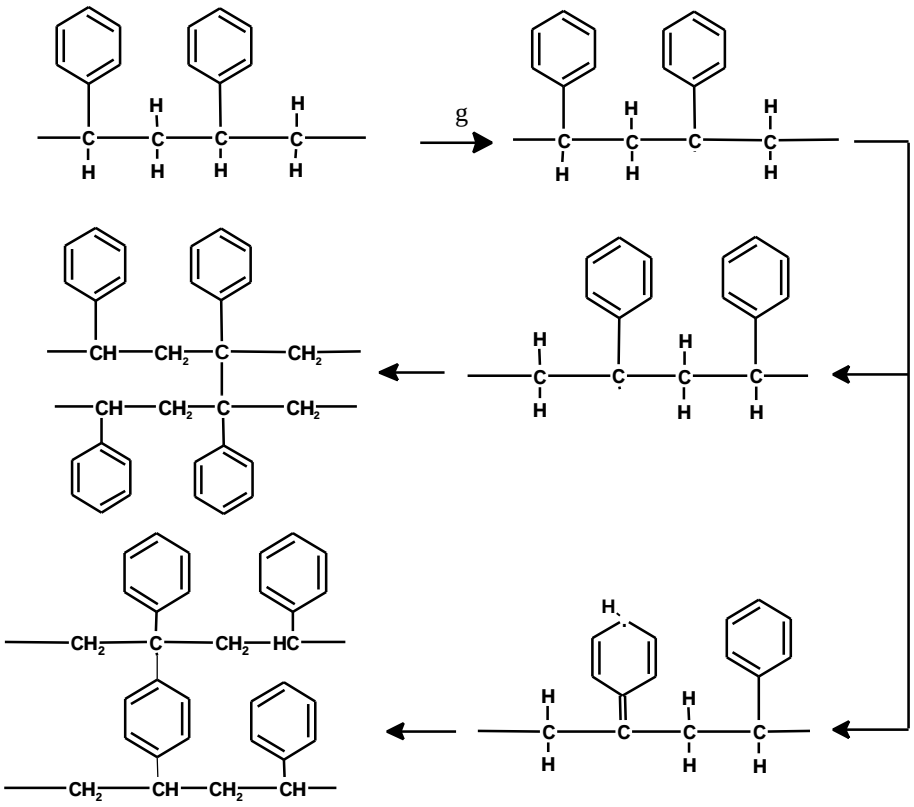

Figure 1.14 Alternate Cross-linking Mechanisms for Polystyrene

In polystyrene oligomers, the degree of crosslinking can be determined by using the relationship described in Figure 1.15 to determine crosslinking yield:

$$G_c = (n \times 10^5) / (D_g \times M_{w0})$$

Figure 1.15 Equation for the Determination of Crosslinking Yield for Polystyrene.[34]

where G_c is the crosslinking yield, D_g is the gel formation dose (Mrad), M_{wo} weight average molecular weight of the polymer. A range of G_c values for gamma irradiated polystyrene have been reported in the literature to be between 0.049 and 0.019.[22]

Scission results when the reactive intermediate results in a break in the chain bond of the polymer backbone. The G value for scission (G(s)) in polyethylene is about 5% of the G_c value. The G(s) value can be enhanced when polyethylene is irradiated in an oxygen environment. The peroxy-radical intermediates that form by reaction of oxygen with the carbon free radical of the polyethylene chain lead to chain insertion of a peroxy bridge that decomposes further to carbonyl-based products and chain scission.[35]

Irradiation of PTFE in air offers a good illustration of the role of oxygen in driving scission reactions. Substituting fluorine groups in place of hydrogen, as in the perfluorinated ethylenic compound in Figure 1.16 (polytetrafluoroethylene (PTFE)) can significantly diminish the radiation stability of the polymer. Unlike polyethylene that yields a volatile decomposition gas (hydrogen) following free radical formation in an oxygen atmosphere, PTFE does not undergo radiation-induced decomposition by the same mechanism to yield F_2, nor do fluorocarbons undergo disproportionation reactions. In the absence of oxygen, the initial cleavage of the CF bond, the resultant PTFE radical intermediate reacts with neighboring oxygen to yield a peroxy-radical that undergoes further decomposition in the radiation environment to yield scission products.[15] The high G values reported for the consumption of oxygen and the formation of CF_2O

support this mechanism along with the long stability of the PTFE free radical at high temperatures in a high-vacuum radiation environment.

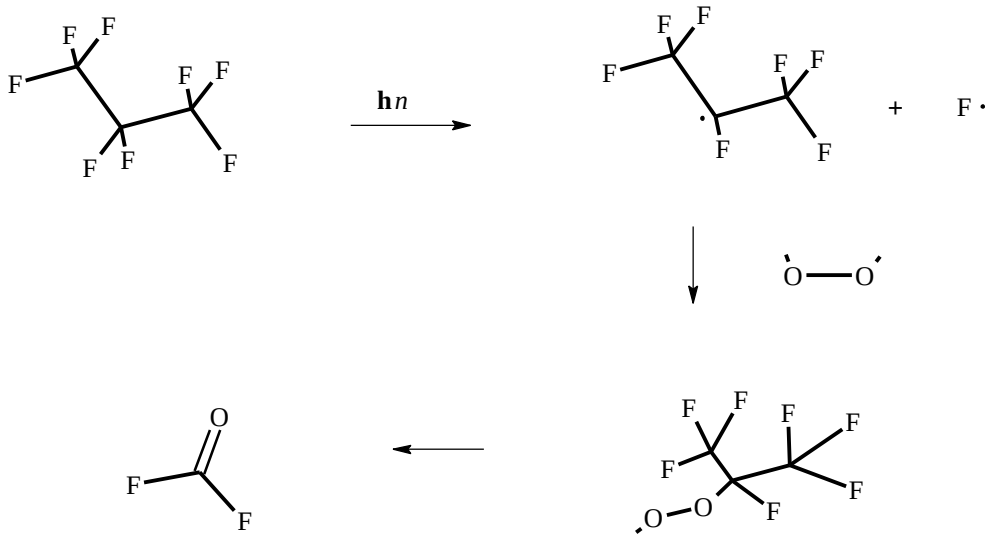

Figure 1.16 Oxygen-Assisted Decomposition of PTFE..

In polymethyl methacrylate (PMMA), the methyl carboxylate side group is introduced to the polyethylene backbone along with a methyl group at the α–carbon. The PMMA structure demonstrates that further complexity in the mechanism of radiation-induced degradation of polymers arises with greater structural complexity in the polymer. The PMMA structure introduces the use of highly polarized chemical bonds (e.g. carbonyl and carboxy moieties) that display a higher susceptibility to irradiation.[36] The most common degradation pathways for the PMMA polymer chain are illustrated in Figure 1.17. The scission reactions are so fast that cross-linking reactions are less observed (for PMMA G (S) >> 4 G (X)).

The free radical decay is promoted and quenched at a rate that suppresses the crosslinking activity in the irradiated polymer chain.

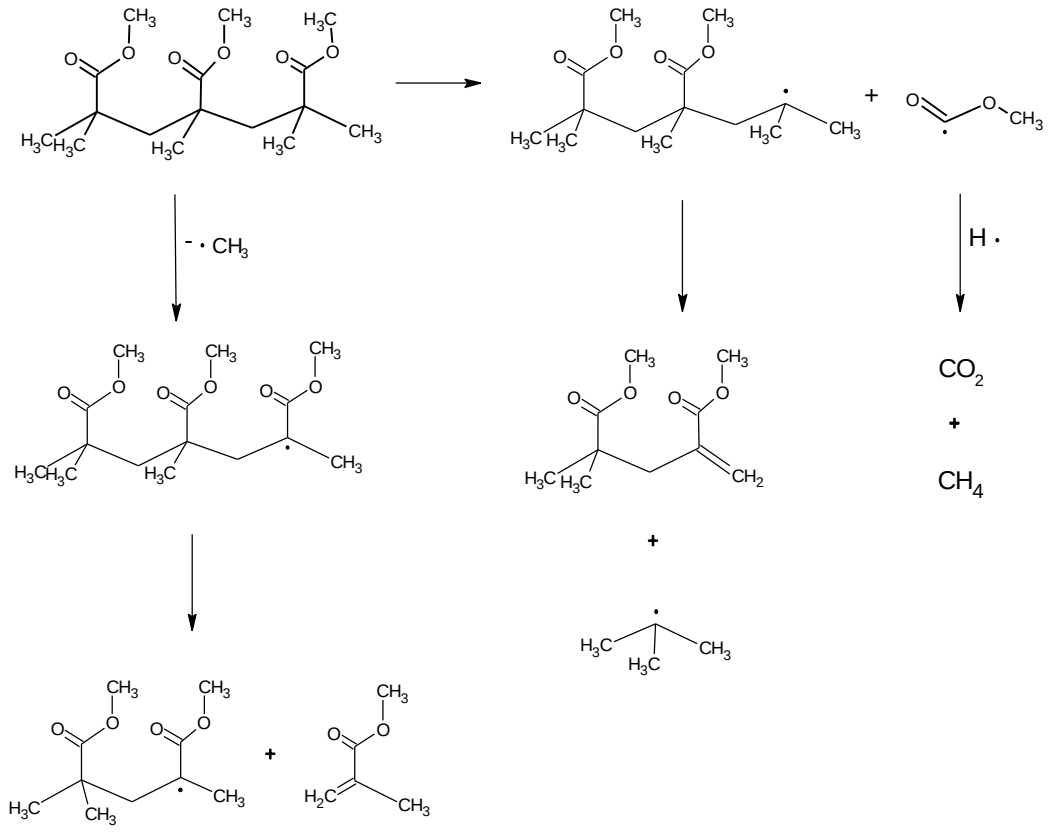

Figure 1.17 Free Radical Formation and Decay in PMMA.[37]

The examples of the influence of chemical structure and chemical formulation on susceptibility to radiation-induced degradation presented to this point are simple in comparison to the complex formulations of the polymeric materials used in spacecraft systems. Today's spacecraft materials do not typically use simple polymeric materials. To achieve specific performance features from space grade polymeric materials, chemists use complex acrylates, epoxies, polyimide and urethanes formulated with copolymers, crosslinking additives, flexibilizers and stabilizers that are incorporated into the final chemical structure of

the polymer network. A thorough study of the specific mechanisms of degradation in such complex polymeric materials is not a practical starting point in view of the numerous possibilities that exist for the degradation mechanism. Instead, the analyst can use simpler structural model polymer compounds to assess chemical changes and evaluating the physical properties (thermal, optical and electrical). Changes in the chemical and physical properties of polymers of simple chemical structure provide guidance in the approach to addressing vulnerability of chemical structure of more complex polymeric formulations to ionizing radiation.

Rationale for the Selection of Polymer Molecular Features

Molecular Weight and Free Volume

The common finding that substitution of the main chain can influence the probability of scission or crosslinking serves as the basis for selecting materials that permit a broader study of the influence of structure on specific degradation mechanisms. The preference for scission in the PMMA polymer is influenced by the flexibility in the carboxymethyl side group that is reported to enable lateral segmental motion. There is, however, the conflicting effect of dipole interaction between these side groups in neighboring chains that introduces rotational steric effects in the molecule. Where radiation-induced degradation is concerned, these effects may become more significant as the number of segments is varied in the polymer chain.

The effect of average molecular weight on the physical properties of polymers has been reported.[38] The length of the oligomeric chain influences segmental motion of the component atoms, and thereby alter the physical properties displayed by the polymer. Oligomeric chains of increasing length (higher molecular weight) influence the free volume of the polymer and will shift the glass transition temperature (Tg) to higher values.[39]

Previous work with respect to chain length attributes the decrease in Tg to the additional free volume that occurs at the end groups of the oligomers comprising the polymeric molecular structure.

Analysis of narrowly dispersed, PMMA standards shows that the Tg varies as a function of molecular weight. Lower molecular weight materials have considerably more end groups that implies more free volume as addressed in the Fox-Flory equation (Eq. 1). The Tg_{∞} refers to the glass transition temperature obtained by extrapolation of M_n to infinity and K is a dimensionless constant related to parameters describing free volume. K is independent of molecular weight (25×10^3). The predicted Fox-Flory T_g for the series of narrowly dispersed polystyrene standards is presented in Figure 1.18.

The prediction of a shift in the physical properties of polymers suggests that a polymer with a high G(s) value (e.g. PMMA) would display a decrease in Tg as random chain scission led to a decrease in the Mn. Combining the predictions of the Fox-Flory equation and the G-based predicted redistribution of chain lengths following scission, a post-exposure Mn could be pre-determined for PMMA of a known Mn and polydispersity. This approach would permit validation studies to experimentally demonstrate the predicted shift in physical properties based on the decrease in molecular weight.

The PMMA approach also provides an opportunity to study the role of polymer molecular weight, and, by implication, free volume in the radiation-induced degradation of polymers. The same free volume affects that drive a change in Tg also may influence the extent of specific degradation reactions in PMMA, and alter the resultant, apparent G-value of the polymer. Specifically, the free volume in the region of the end-groups is less subject to the influence of inter-chain dipole interactions or restricted segmental motion in the same manner as mid-chain segments of the oligomer. A free radical intermediate formed on the terminal segments of the main-chain by the incipient, radiation-induced ionization of the polymer can undergo a chain reaction leading to the loss of several segments by a reversed path of a free-radical polymerization of PMMA. Such events would not be the direct result of a radiation-induced scission reaction as the G-value would infer, but rather are a depropagation degradation mechanism that may perpetuate for some time in the PMMA solid sample before a termination reaction quenches the reactive radical intermediate. Conversely, at higher molecular weights, there are fewer end groups per molar quantity of polymer. The influence of chain entanglements and polymer alignment suggest that the resultant Mw distribution of exposed polymer would be expected to follow the distribution predicted on the basis of G-values.

$$T_g \sim T_{g\infty} - (K/M_n) \qquad (Eq.\ 1.1)$$

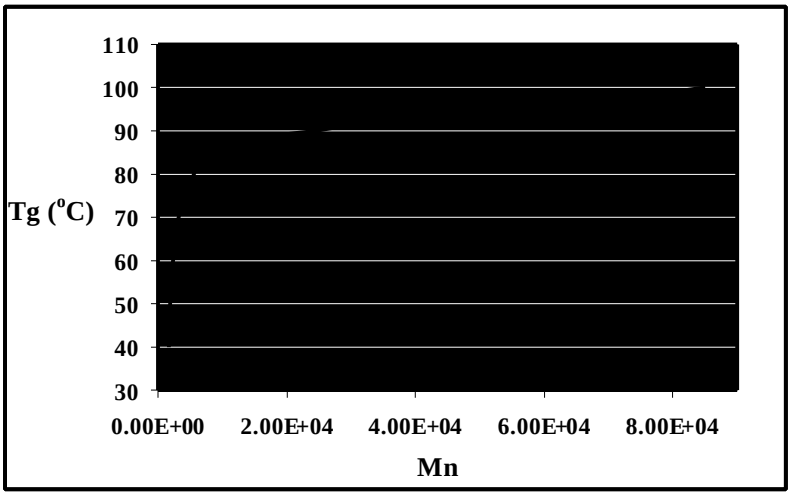

Figure 1.18 Predicted Fox Flory Tg Values vs. Polystyrene Mn.

Influence of Main Chain Tacticity

The affects of alignment between polymer chains has also been investigated to show that isotactic PMMA polymers display different G(s) values than the atactic PMMA. This is reported to be controlled by the more ordered packing between chains that further restricts rotational and segmental motion. suggesting free volume is at the center of this behavior.[40,41,42] Free volume is not defined as the unused spaces between molecules. The free volume is volume above and beyond the unused volume between molecules. For solids, free volume is created by the thermal motion of the atoms comprising the molecule. The amplitude of the oscillations is bounded by the proximity of neighboring atoms that form the cage for the oscillating atom. As the temperature increases in a solid, the thermal motion (or oscillations) increases, and main-chain segments begin to occupy new positions and permit new orientations.[43] The effects of a more ordered polymer network and closer packing between polymer chains has the strongest influence on the mid-chain molecules. The tighter packing could also affect free volume at the end groups and , thereby, diminish chain depropagation at the end groups.

The mid-chain scissions result in free-radical intermediates that are immobilized in a caged structure[44] that leads to recombination and, in some reports, an increase in crosslinked chains. For stereoregular polymers above the gel point, inversion would support the observed recombination. The effect of the isotactic structure on post-radiation PMMA end-group chemistry as a function of molecular weight remains to be studied.

Based on the numerous structural factors that influence the many degradative pathways of polymers, the study to isolate the specific effect of chain length requires consideration of four primary events: scission, crosslinking, side group loss and elimination reactions along the main chain (abstraction including end-group depropagation). Previous statistical modeling studies have yielded numerical and

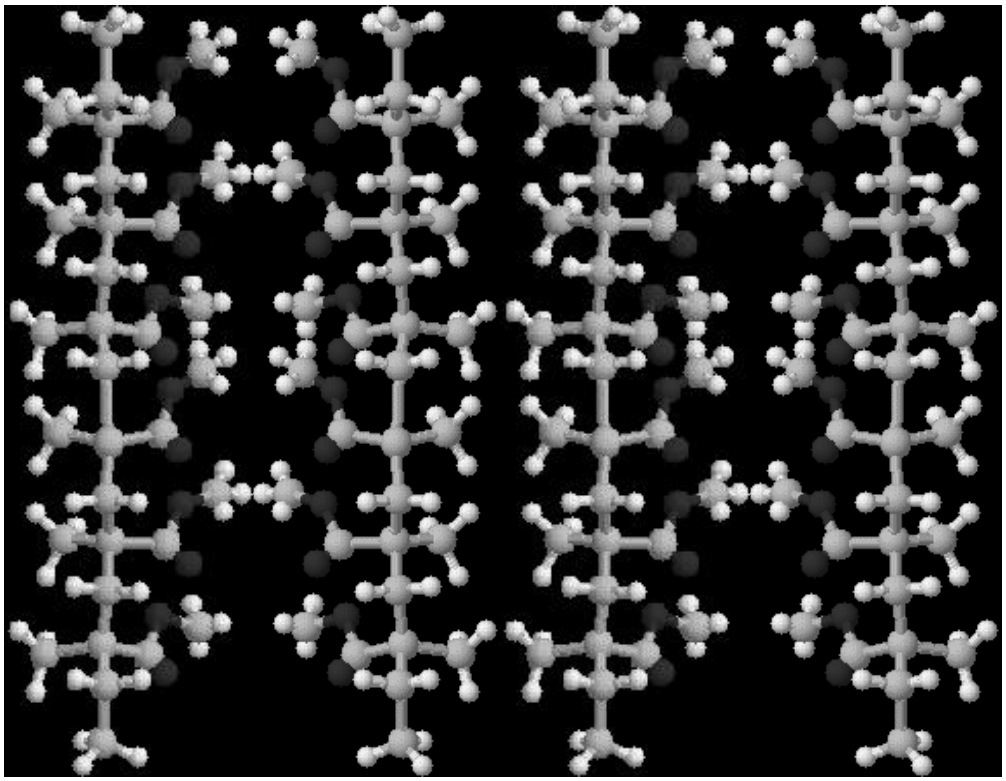

Figure 1.19. Illustration of the Enhanced Cage Effect for Isotactic PMMA.[42]

algebraic kinetic expressions for predicting the change in Mw distribution for solid state, linear series of oligomeric units as a result of scission events. [45,46,47,48,49,50] The modeling methods use assumptions in the Mw distribution and polydispersity of the polymer, and do not address contributions from cross-linking, recombination, end-group loss nor tertiary structure effects. The models also assume an equivalency in the probability of scission of each oligomer in the linear polymer series.

Approach to the Incorporation of Experimental Results into Model

Charlesby and Thomas[45] described the first rate equations for chain depolymerization leading to changes in molecular weight Their work also described PMMA main-chain scission to occur at random with a G value of about 1.6 at room temperature. Charlesby also associated decomposition of the PMMA carboxymethyl group with the chain scission event, and did not observe significant amounts of the methyl methacrylate polymer following exposure to high energy particles and photons.

Charlesby concluded that depolymerization of the main chain occurred at termination points, and at the newly-formed terminations at each scission point along the chain. This conclusion implies that there is a considerable amount of depolymerization driving the change in post-exposure Mn values. However, the extensive depolymerization is observed at higher temperatures (e.g. 125^{o}C), and is minimal by comparison at room temperature (Todd). Charlesby described the following expression to predict the post-exposure, number-average molecular weight (Mn') for PMMA (Equation 1.2) as a result of scission. Where Mn is the original number-average molecular weight, p_0 is the number of breaks/monomer, r is the unit dose, and w is the monomer weight.

$$\frac{1}{M_n'} = \frac{1}{M_n} + \frac{P_0 r}{w} \qquad \textit{(Eq. 1.2)}$$

Many of the studies performed by Charlesby and other investigators during the early development of the statistical models for polymer degradation used the gel point as the basis for model validation. The lack of separation methods like gel permeation chromatography led to the use of intrinsic viscosity as a method for assessing changes in the molecular weight distribution of polymers. This approach limited the evaluation of a linear series of solid polymers to solvated viscous blends and the connection of the modeling results to changes in the physical properties of solid polymers did not extend beyond the thermal working range of the solid polymer. Alongside Charlesby's initial work, and also based on liquid studies, Saito, et. al., developed an expression that predicted the resultant molecular size distribution for PMMA due to main-chain scission using an assumed Schulz-Zimm distribution.[46]

Work by Dole, et. al.,[52] recognized the limitations of evaluating polymers in the liquid region and developed expressions that predicted a significant drop in G values for solids. Dole also demonstrated another important finding in the non-linearity of the relationship between dose accumulation with time and the need for improved accuracy of the methods used to assess the initial molecular weight distribution. This was a recognition of Charlesby's early proposition[53] that incipient chain scission leads to long-lived reactive groups that, in turn, lead to secondary degradation pathways unrelated to direct radiolysis of a polymer segment. This is a significant concept in the development of models for structure-based correlation to polymer performance in space radiation environments and ground-based simulation studies. Later, O'Donnell, et. al., verified Saito's integrodifferential equation for chain scission, and incorporated an iterative series of calculations that improved include the contributions of simultaneous crosslinking, but, he too pointed out the restrictive applications of the models to the gel point region.[47]

As GPC methods began to provide Mw_{avg} data, kinetic modeling studies, such as those by Wolf, et. al.[48], began to examine random and full Gaussian probability of scission by fitting the model to experimental data. The work yielded a general expression for the chain scission process that provides individual rate constants per degree of polymerization. This was an important step in recognizing the differences in the probability of chain scission as a function of chain length. Later, Clegg reviewed the degradation kinetics of polymers and noted the work of Barry and Watson who demonstrated that the probability of chain scission was related to chain length.[54] The work provided insight into the significance

of chain length in the ultimate change in Polymer Mw_{avg}. The next step in the improvement of polymer degradation models requires a study to understand the impact of chain length and scission probability as it relates to the final Mw distribution.

In summary, the modeling work to date has demonstrated promise in accurately predicting the change in average molecular weight distribution for specific Mw ranges of linear polymer Mw. The area of uncertainty for the application of the modeling resides in the thermal region between gel point and T_{∞}.

By comparison, predictions can also be made using radiation yield values (G values) for specific changes in structural features that, in turn, are based on experimental observations from numerous studies in the literature. The G values are determined from the total dose deposited in a specific mass of the polymer and the change in Mw distribution for pre- and post-irradiated polymer. The G values for a polymer can represent specific chemical events in the free radical initiation or ionization process, and the subsequent formation of degradation products following ionization or free radical formation. the predicted radiation-induced degradation for a linear PMMA series can be modeled using the G values and total dose absorbed by one gram samples of the polymer.

It is the purpose of this study to advance the understanding of radiation-induced polymer degradation to improve modeling practices used to correlate polymer chemical structure to all aspects of the degradation process. This study will model and simulate the natural space radiation environment expected for a typical, worst-case space mission orbit. The radiation flux and spectrum will be used to determine changes in chemical structure and physical properties. The assumptions of random scission coupled with the use of experimentally observed G-values for multiple degradative pathways of polymer degradation will be used to model the change in Mw distribution based on a Gaussian distribution of each chain length in the polydispersed standards. A linear series of polymers will be used to prove that molecular weight will lead to a deviation from current model predictions as a function of molecular weight. The role of free volume and end group contribution will be studied to explain the deviations from the predicted Mw distribution of the exposed polymer, and to emphasize the importance of these deviations to the use of polymeric materials in the space environment.

References

1. Clegg, D. W. and Collyer, A. A.; *Irradiation Effects on Polymers*; Elsevier Applied Science, Oxford, 1991, p.195.

2. Ohnishi, S. and Nitta, I.; *Journal of Polymer Science*; 38, 1959, p. 451.

3. Parkinson, W. W. and Keyser, R. M.; *Radiation Chemistry of Macromolecules Volume 1*; Dole, M., Ed.; Academic Press, New York, 1972, p. 71.

4. Wong, H.; *Space Vehicle Mechanisms*; Conley, P. L., Ed..; John Wiley & Sons: New York, 1998, p. 621.

5. Hanks, C. L. and Hammon, D. J.; *The Effects of Radiation on Electrically Insulating Materials*; REIC Rep. 64, Battelle Memorial Institute, Columbus, OH, 1969.

6. *An Overview of the First Results on the Solar Array Materials Passive LDEF Experiment (SAMPLE), A0171*; Whitaker, A. F.; LDEF – 69 Month in Space-First Post Retrieval Symposium, NASA CP-3134 Parts 1-4, June 1991.

7. *Space Environmental Effects on Materials*; Swinghamer, R. J., NASA-TM-78306, Marshall Space Flight Center, Huntsville, AL, Aug. 1980.

8. Taylor, E. W.; *Inorganic and Polymer Photonic Sensor Technologies in Space Missions*; Proceedings of the IEEE Instrument and Measurement Technology Conference, Budapest Hungary, May 2001.

9. Wittmann, B.; et. al.; *IEEE Journal of Selected Topics in Quantum Electronics*; 5, 1999, p. 1243.

10. Kiamilev, P. et. al.; *Journal of Lightwave Technology*; 9, 1991, p. 1674.

11. Schnitzer, F., et. al., *Proc. Of the 8th International Plastic Optical Conference '99*; Chiba, Japan; 1999, pp. 209-212.

12. Harmon, J. P., et. al.; *American Chemical Society Symposium Series 620*; Clough, R. L. and Shalaby, S. W., Eds.; American Chemical Society, Washington, D.C., 1996, p. 302.

13. Taylor, E. W.; "Space and Enhanced Radiation Induced Effects in Key Photonics Technologies"; *IEEE Aerospace Conf. Proc.;* ISBN 0-7803-5427-3, Snowmass, CO, March 1999.

14. Taylor, E. W. et. al.; "Overview of Photonic Materials for Application in Space Environments"; *Proc. EOS/SPIE Europto 99 Symposium on Remote Sensing*; Vol. 3872. Florense, Italy, 20-24, Sept 1999.

15. Forsythe, J. L., et. al.; *Progress in Polymer Science*; 25, 2000, p. 101.

16. Hanks, C. L. and Hamman, D.; *The Effects of Radiation on Electrically Insulating Materials*; REIC Report 64, Battelle Memorial Institute, Columbus, OH, 1969.

17. Oktay, S., et.al.; *Mechanical Engineering 108*, 3, 1986, p. 36.

18. Dallimore, G. R.; *Space Vehicle Mechanisms*; Conley, P. L., Ed..; John Wiley & Sons: New York, 1998, p. 215.

19. Bourassa, R. J., et. al.; *Proceedings LDEF – 69 Month in Space-First Post Retrieval Symposium*, NASA CP-3134 Part 2, June 1991, p.643.

20. *Fundamentals of Space Systems*; Piscane, V. L. and Moore, R. C., Eds.; Oxford University Press: New York, 1994, p. 84.

21. Siedle, A. H. and Adams, L.; *Handbook of Radiation Effects*; Oxford University Press, New York, 1993.

22. Williams, F.; *Radiation Chemistry of Macromolecules Volume; I*Dole, M., Ed.; Academic Press, New York, 1972.

23. Charlesby, A.; *Proceedings of the Royal Society A, 215*, 1952, p. 187.

24. Lawton, E. J., et. al.; *Nature, London, 172*, 1953, p. 76.

25. Mandelkern, L.; *Radiation Chemistry of Macromolecules Volume; I*Dole, M., Ed.; Academic Press, New York, 1972 p. 287.

26. *Nuclear and Space Radiation Effects on Materials – NASA SP-8053*Coleman, T. L., Ed., 1970.

27. Anderson, H. H. and Ziegler, J. F.; *Hydrogen Stopping Powers and Ranges in All Elements*Vol 4 of Series: Stopping Ranges of Ions in Matter, Pergamon Press, New York, 1977.

28. Partridge, R. H.; *Radiation Chemistry of Macromolecules Volume; I*Dole, M., Ed.; Academic Press, New York, 1972.

29. Charlesby, A. and Pinner, S. H.; *Proceedings of the Royal Society A249*, 1959, p. 367.

30. Thompson, E. V.; *Polymer Letters*, *3*, 1965, p. 675.

31. Hill, D. J., et. al.; *Journal of Applied Polymer Science*, 1996, *59*, 589.

32. Lai, J. H. and Helbert, J. H.; *Macromolecules*, *11*, 3, 1978, p. 617.

33. Torikai, A.; *Die Angewandte Molekulare Chemie*, 1996, *216*, 225.

34. Clegg, D. W. and Collyer, A. A.; *Irradiation Effects on Polymers*; Elsevier Applied Science, Oxford, 1991, p.225.

35. Gunder, O. A., et. al..; *Radiochim*, 1969, *11*, p. 119.

36. Schneider, et. al., *Polymer Bulletin*, 1983, *9*, p. 495.

37. Clegg, D. W. and Collyer, A. A.; *Irradiation Effects on Polymers*; Elsevier Applied Science, Oxford, 1991, p.383.

38. Fox, T. G. and Flory, P. J.; *Journal of Applied Physics*, 1950, *21*, p.581.

39. Fox, T. G. and Flory, P. J.; *Journal of Polymer Science*, 1954, *14*, p.315.

40. Vacatello, M. and Flory, P.; *Macromolecules*, *19*, 1986, 405.

41. Sundararajan, P. R.; *Macromolecules*, *19*, 1986, 415.

42. Miller, K., et. al.; *Macromolecules*, *26*, 1993, 4945.

43. Gedde, U. W.; *Polymer Physics*, Chapman & Hall, London, 1995.

44. Manning, L. E.; *Macromolecules*, 1989, *22*, 4652.

45. Charlesby, A., et. al.; *Proceedings of the Royal Chemical Society of London, Series A, Mathematical and Physical Sciences*, 1954, *224*, 1156, p. 120.

46. Saito, O.; *Radiation Chemistry of Macromolecules Volume I*; Dole, M., Ed.; Academic Press, New York, 1972, p. 244.

47. O' Donnell, J. H., et. al.; *Macromolecules*, 1979, *12*, 113.

48. Wolf, B. A.; *Macromolecules*, 1981, *14*, 654.

49. Kashiwagi, T., Et. al.; *Macromolecules*, 1986, *19*, 2412.

50. Milne, K. A., et. al.; *American Chemical Society Symposium Series 620*; Clough, R. L. and Shalaby, S. W., Eds.; American Chemical Society, Washington, D.C., 1996, p. 130.

51. Charlesby, A. and Thomas, D. K.; *Proceedings of the Royal Chemical Society of London, Series A, Mathematical and Physical Sciences*, 1962, *269*, 1336, p. 104.

52. Dole, M.; *Radiation Chemistry of Macromolecules Volume I*; Dole, M., Ed.; Academic Press, New York, 1972, p 3.

53. Charlesby, A. and Thomas, D. K.; *Proceedings of the Royal Chemical Society of London, Series A, Mathematical and Physical Sciences*, 1954, *223*, 1154, p. 392.

54. Berry, J. P., et. al.; *Journal of Polymer Science*, 1953, *18*, 201.

Chapter Two

Radiation Modeling and Simulation

Overview

The extent of the interaction of polymeric, organic compounds with ionizing radiation is related to the energy absorbed during the period of exposure to photon or particle flux. Fluence energy is absorbed as the particles or photons transfer energy to the bulk mass of the polymer through collision events (Compton Effect) or by energy transfer from the coulombic field that accompanies the transient path of the particle or photon through the bulk material. Interaction of radiation with the polymer begins at the atomic level and the associated absorbtion coefficients. The polymeric molecular formula, therefore, also influences the susceptibility of the polymer to incipient ionization based on the ionization potential of the composite elements. [1,2]

The effect of the polymeric structural formula on degradation becomes important following the incipient ionization. Radiological studies of the bulk polymer provides insight into the chemistry of degradation and enables an improved understanding of the structural features that ensure radiation hardening. The test results thereby provide guidance in polymer application and in the synthetic design of novel polymers. An experimental study of radiation-induced polymer degradation requires a method for irradiating the polymer that also permits accurate representation of the application environment along with the ability to duplicate and verify the total absorbed energy deposited in the material. This is accomplished through simulation of the intended radiation regime using a calibrated dosimetry method and a source that generates a known field of flux energy. A stepwise approach used to determine the suitability of materials for a specific radiation environment consists of several elements.

The approach begins with an assessment of the proposed radiation environment followed by the selection of an ionizing source that will provide a total dose equivalent to the proposed environment. The stability of the flux generated by the ionizing source must also be characterized through an evaluation of the half-life of the source materials. Finally, the evaluation must include dosimetry to map and control the

dose rate of the specific coordinates within the radiation chamber thereby providing the means to accurately and meaningfully achieve the dose equivalence of the proposed radiation environment. Predicting the stability of polymeric materials in spacecraft applications is an example of an approach to radiation modeling and simulation.

Defining the Space Mission Environment

An assessment of the radiation environment for a polymeric material should provide information on the type of radiation, the flux density, the total dose and the period of exposure of the total dose. Other radiological factors such as secondary radiation, the constancy of the flux level and the mechanics of scattering effects should be considered as well. The space environment is a complex, dynamic radiation environment wherein a considerable amount of assessment experience exists. The prediction of survivability of the polymers comprising a spacecraft structure requires advanced knowledge of the environment where the craft will be deployed.

A spacecraft in earth orbit will be exposed to a broad range of the electromagnetic spectrum (e.g. radio waves through gamma rays) and energetic particle radiation (e.g. protons and electrons). The primary concerns for polymer stability are those components of the natural space total radiation spectrum that have sufficient energy to impart an ionizing field or ionization by electron impact while in transit in the polymer medium.[3-9] In natural space, the earth's magnetosphere is widely used for orbital earth missions. The trapped and transient electrons and protons, which are concentrated in the inner and outer belts of the magnetosphere, represent the main source of ionization energy that can lead to polymer degradation.[10-11] For example, assuming the spacecraft is in a geosynchronous earth orbit within the outer region of the magnetosphere, the type of radiation and the energy spectra needed for modeling can be defined based on limited satellite measurement data using onboard electron and proton detectors.[3] The particle energy spectrum for protons and electrons in the space environment extends to the GeV range. Simulation testing of spacecraft materials in advance of a flight mission must be done carefully to ensure consideration of many contributing factors to the total dose.

Fluence and Spectrum

Fluence defines the expected number of particles (N_e) striking the surface area of a component measured as the cross-sectional area of the sphere with the center as point P (Figure 2.1)[3]. Through a series of experimental measurements, a finite, non-stochastic expression of the ionizing energy deposited in the proximity of the target of an area (a) can be developed ($\Phi = ? \ dN_e/da$) and expressed as depositions per unit area (cm^{-2}). The fluence expression can be used to formulate an expression of the fluence rate (or flux density) by introducing a time variable into the fluence expression ($j = d/dt \ (dN_e/da)$).

The work to accurately map the electron and proton flux distribution is ongoing, but useful detailed maps do exist[10] and provide the flux density database for the software codes AE8 (Electrons) and AP8 (Protons). The AE8 and AP8 modeling softwares provide the most widely used estimation tools for electron and proton flux predictions of the space mission environment[10-11]. Using the length of mission and the orbital flight path of the mission (Figure 2.2), information necessary to perform the radiation assessment is nearly complete.

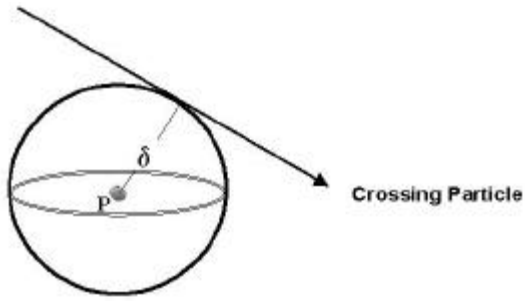

Figure 2.1. Spherical Description of the Fluence of Ionization Energy.

To complete the radiation assessment, factors that alter the established database for particle distribution must be accounted for in the model. Three main factors are discussed that require corrections for the database. The first deals with the continuity of the space radiation regime. The illustration in Figures 2.3 and 2.4 describe the omnidirectional proton and electron particle flux (> 1.0 MeV) distribution of the magnetosphere. The torroidal distribution of particle distribution is fairly uniform except in the

region of the South Atlantic Anomaly where the earth's magnetic field line (*B*) is low resulting in a higher particle flux. While the origin of the anomaly is not well understood, the database supporting the AE8 and AP8 models take the irregularity into account.

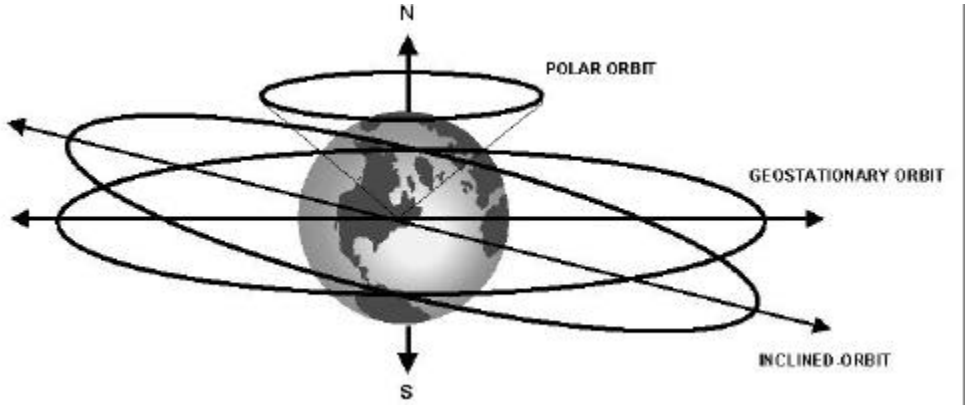

Figure 2.2. Illustration of Common Flight Paths for Spacecraft.

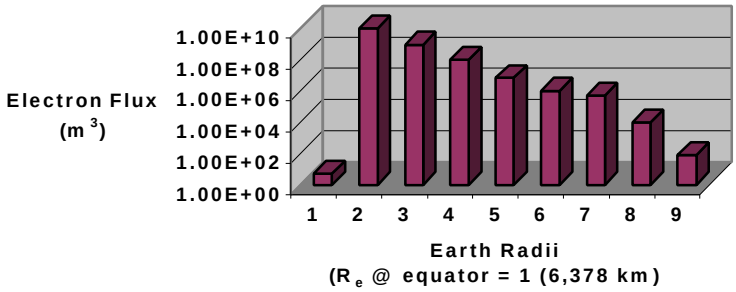

Figure 2.3. Geomagnetic Equatorial Electron Flux Levels (> 1 MeV) vs. Altitude (LEO)

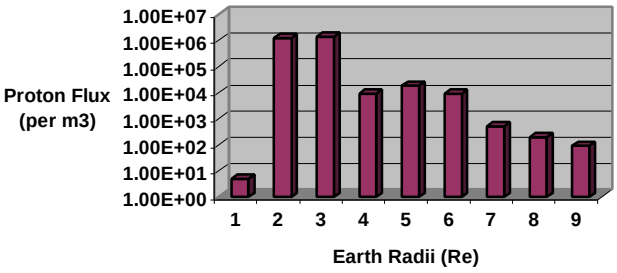

Figure 2.4. Proton Flux Distribution in the Magnetosphere (> 1.0 MeV)

The second factor to consider is the solar cycle and solar flare activity.[12] Each zone of flux in the magnetosphere is comprised of an electron energy spectrum that ranges from 1 KeV to 7 MeV and protons with energies up to 300 MeV.[13] The proton and electron energy levels (KeV and MeV) have been defined as a function of altitude (Lagranians or Earth Radii) are presented for the geomagnetic equator in Figures 2.3 and 2.4.[3] During periods of high solar activity, solar flares contribute protons and heavy ions to the radiation belts (Figure 2.5). The magnitude of a solar flare event is extremely variable and the resultant impact to the flux density distribution of the magnetosphere is difficult to predict. Instead, the space radiation analysts uses a conservative approach by assuming a worst-case (5X) enhancement to all mission environments (Figure 2.6).

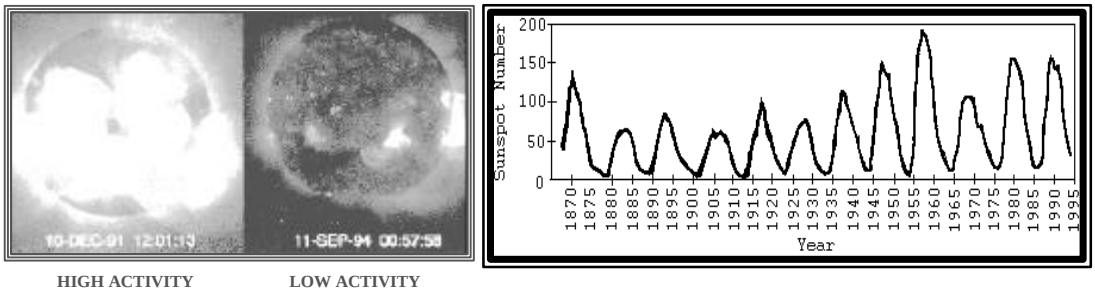

Figure 2.5. Illustration of the Periodicity and Flux Range for Solar Flare Events

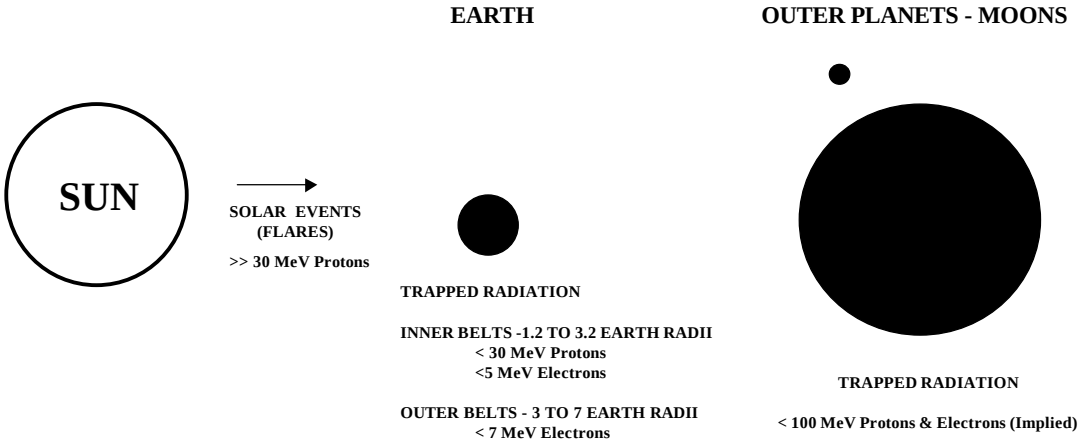

Figure 2.6. Composite Range and Type of Particle Energies for Space Missions.

Flightpath vs. Radiation Regime

Apart from the natural space environment there is the contribution of the spacecraft structure itself to the total dose through interaction with the space particle fluence. The particle radiation entering the surface of the craft interacts with the materials comprising the spacecraft structure surrounding the polymer under study. The effects of the interaction between the spacecraft structure and the space radiation environment can yield secondary radiation as photons or particles (electrons) that can alter the spectrum and enhance the total absorbed dose of the polymer.[14] The SPENVIS AE8 and AP8 software models account for this through the use of a spherical or box model that considers the material and determines the attenuation of the incoming particles and the yield of secondary radiation. An example of a typical approach to the assessment to the determination of a flight mission environment is provided in the following.

A new flight path for global positioning system satellite constellations, where close proximity to the earth, and wide area coverage is required, is the highly elliptical orbit (HEO).[15] In this current HEO example, the perigee is very narrow (500 km), and the apogee can extend to more than 10,000 km. The use of a five-hour orbit cycle and an inclined orbit (e.g. 35^{o}) relative to the equatorial plane of Earth results in what appears to be a convoluted flight path when taking the Earth's rotation into account (Figure 2.7).

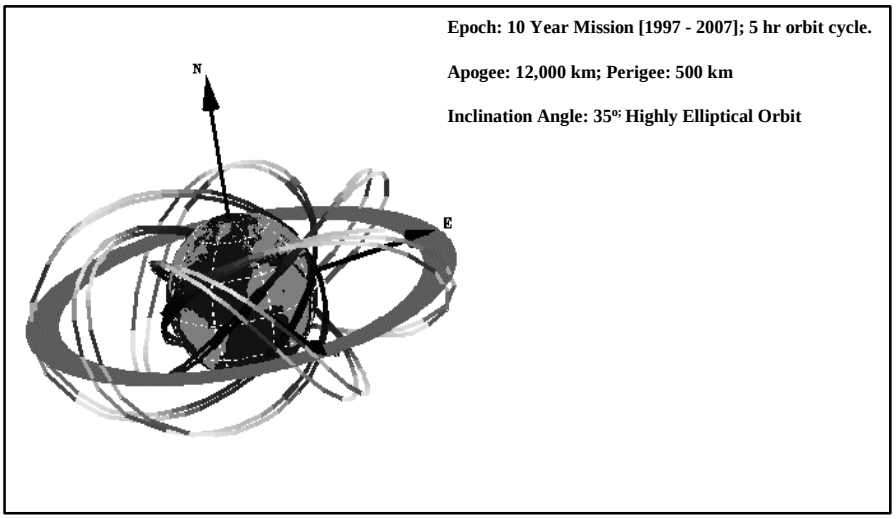

Figure 2.7. SPENVIS Near Earth Mission - Flight Path Definition - 2 Day Illustration

Using a ten-year mission (1997) mission epoch , a highly elliptical orbit was evaluated for particle flux over a two day period. The unshielded particle flux was estimated using NASA's AP-8 MAX and AE-8 MAX trapped particle models to estimate the particle flux ranges for the flight path environment. The specific energy range and types of particles selected for analysis are presented in Table 3. The spacecraft position is tracked through the orbital cycles as shown in Figure 2.8. The actual flight pattern as a function of altitude over the Earth's surface is illustrated in Figure 2.9. The two day flux measurements determined for the particles in Table 3 are presented in Figures 2.10 and 2.11. The average proton, electron and solar proton spectra are presented in Figures 2.12, 2.13 and 2.14. Contribution to the proton flux in periods of high solar activity during the on-orbit mission life was determined using the NASA JPL–91 model.[16]

Flux Range - HEO ORBIT	particles/cm-s
Two Day AE-8 MAX (> 1.0 MeV)	$1\,0 - 10^{7}$
Two Day AP-8 MAX (> 1.0 MeV)	$1\,0 - 10^{7}$
Two Day AE-8 MAX (> 7.0 MeV)	$1\,0 - 10^{5}$
Two Day AP-8 MAX (> 100 MeV)	$1\,0 - 10^{7}$

Table 2.1 Mission Particle Flux Environment

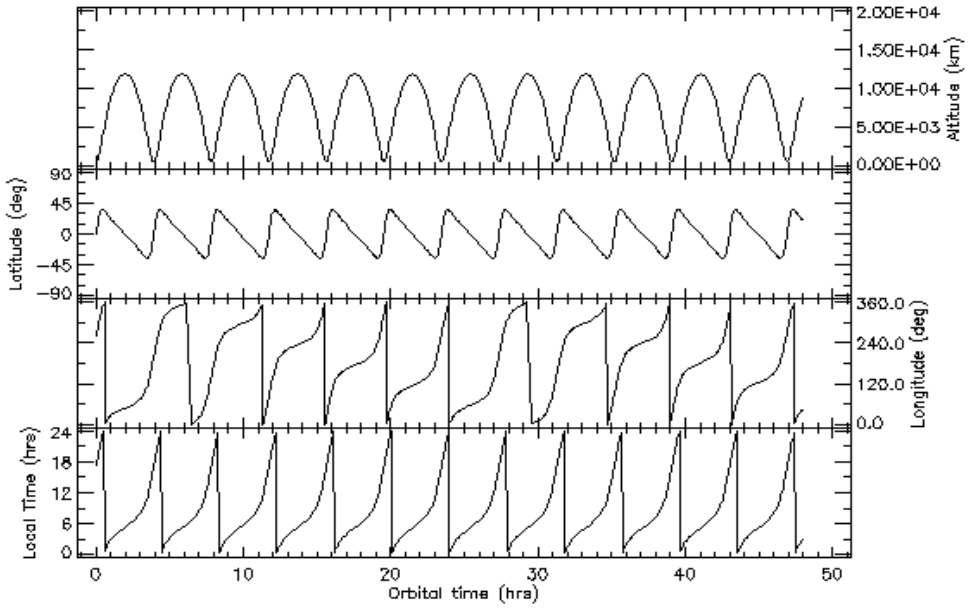

Figure 2.8. SPENVIS Near Earth Mission - Flight Path Definition - 2 Day Illustration.[16]

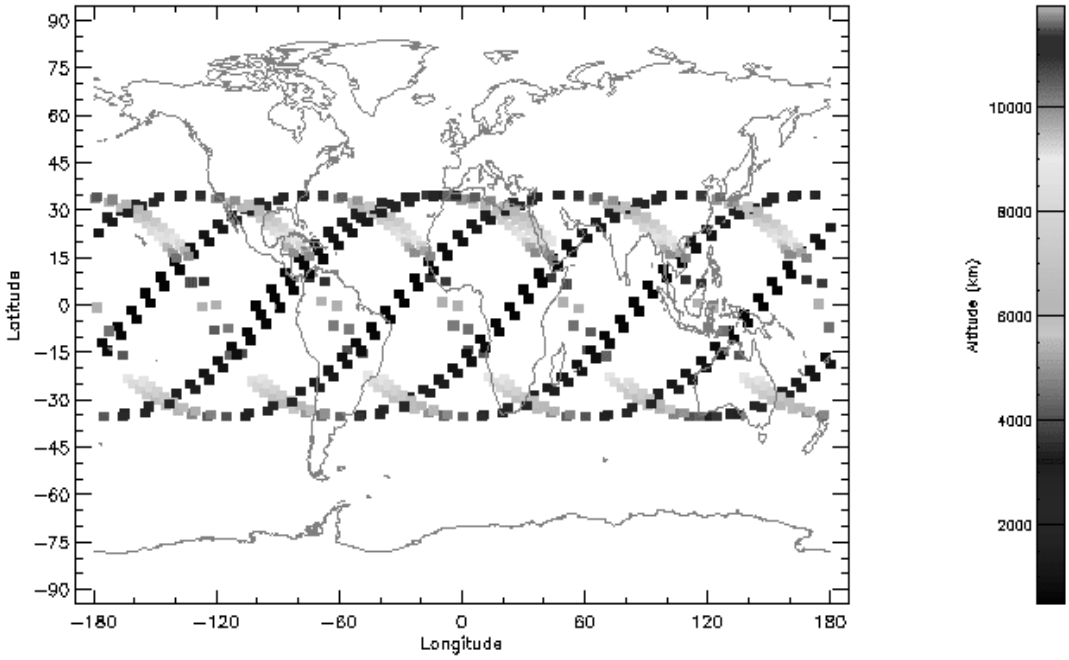

Figure 2.9. SPENVIS Near Earth Mission - Flight Path Tracking - 2 Day Illustration.[16]

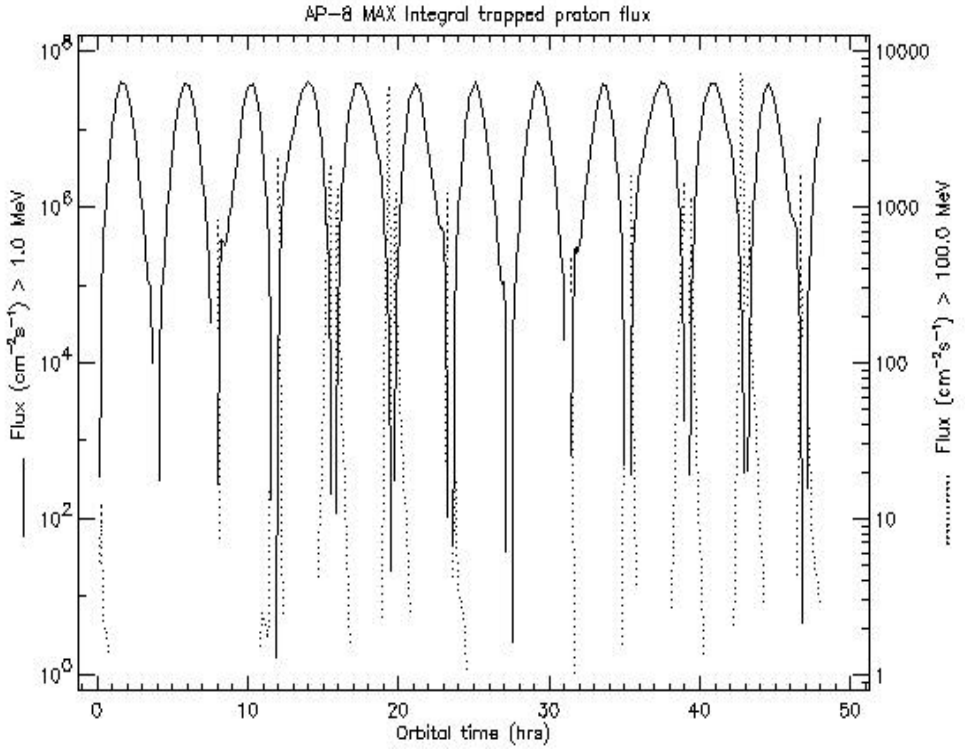

Figure 2.10. SPENVIS 2-Day Proton Flux Regime for HEO Flight Path.[16]

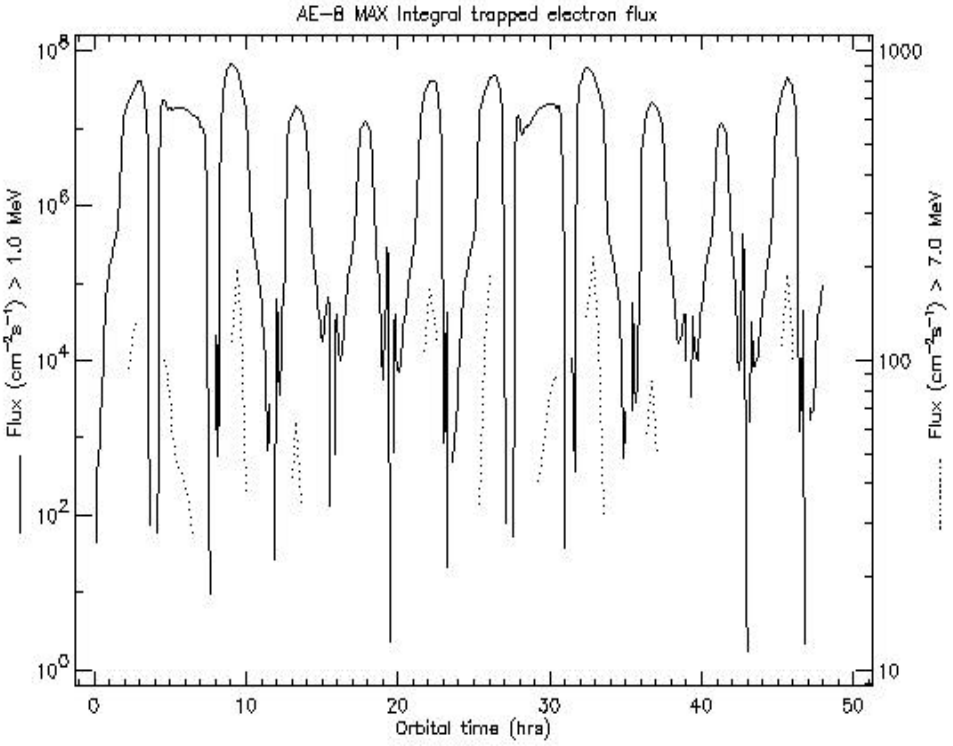

Figure 2.11. SPENVIS 2-Day Electron Flux Regime for the HEO Flight Path.[16]

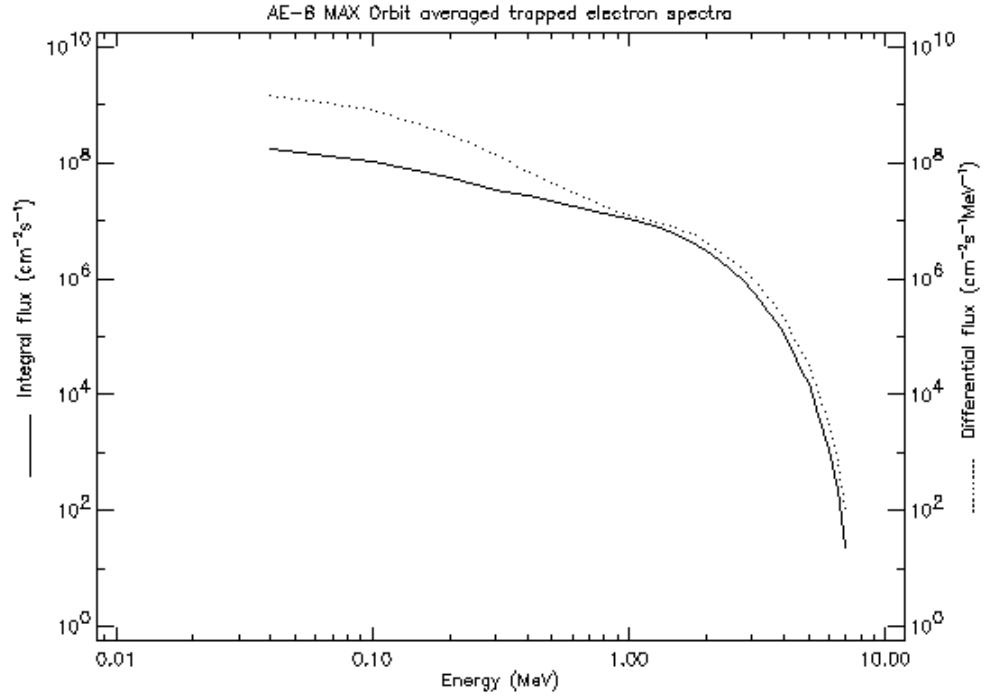

Figure 2.12. SPENVIS 2-Day Electron Flux Spectrum for the HEO Flight Path.[16]

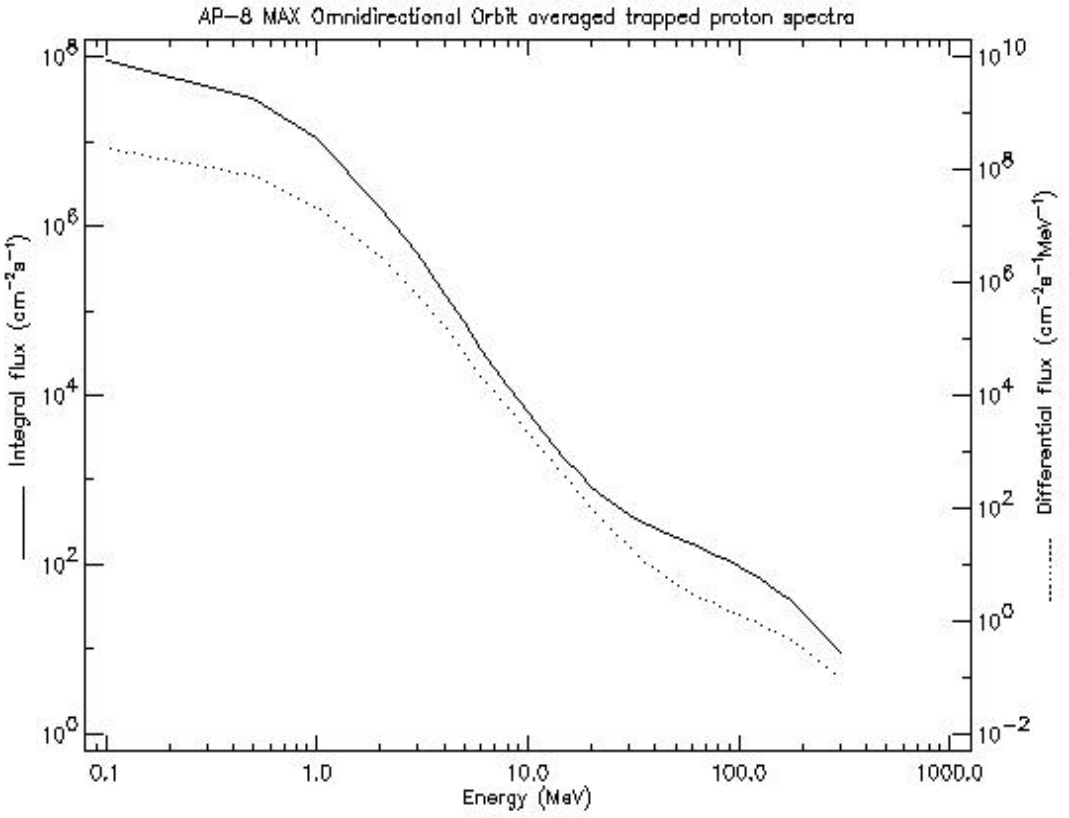

Figure 2.13. SPENVIS 2-Day Proton Flux Spectrum for the HEO Flight Path.[16]

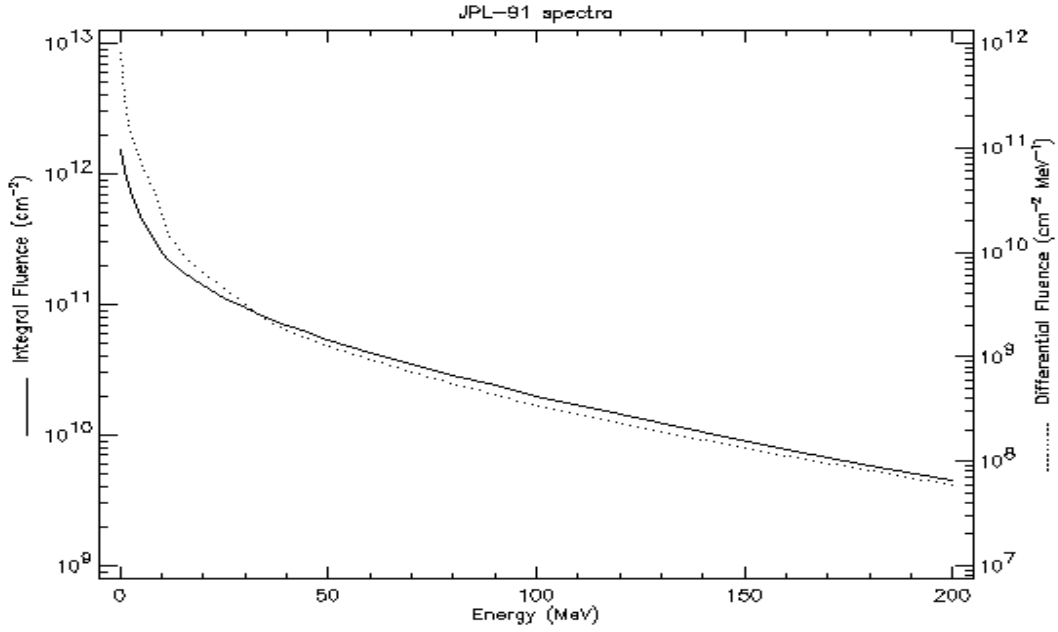

Figure 2.14. SPENVIS 2-Day Solar Proton Flux Spectrum for HEO Flight Path.[16]

The materials selected for this study are PMMA and PS. The total absorbed dose for the mission, including Bremsstrahlung (secondary X-ray) contribution was determined for graphite material using the NIST SHIELDOSE program (Figure 2.15). The unshielded spherical model for a small particle (1 mm diameter) to simulate the volume and form of the polymer sample material used in the estimation of total dose of ionizing radiation. As shown in Figures 2.16 and 2.17, graphite displays an adsorption coefficient similar to PMMA and polystyrene for electron and proton particle flux.

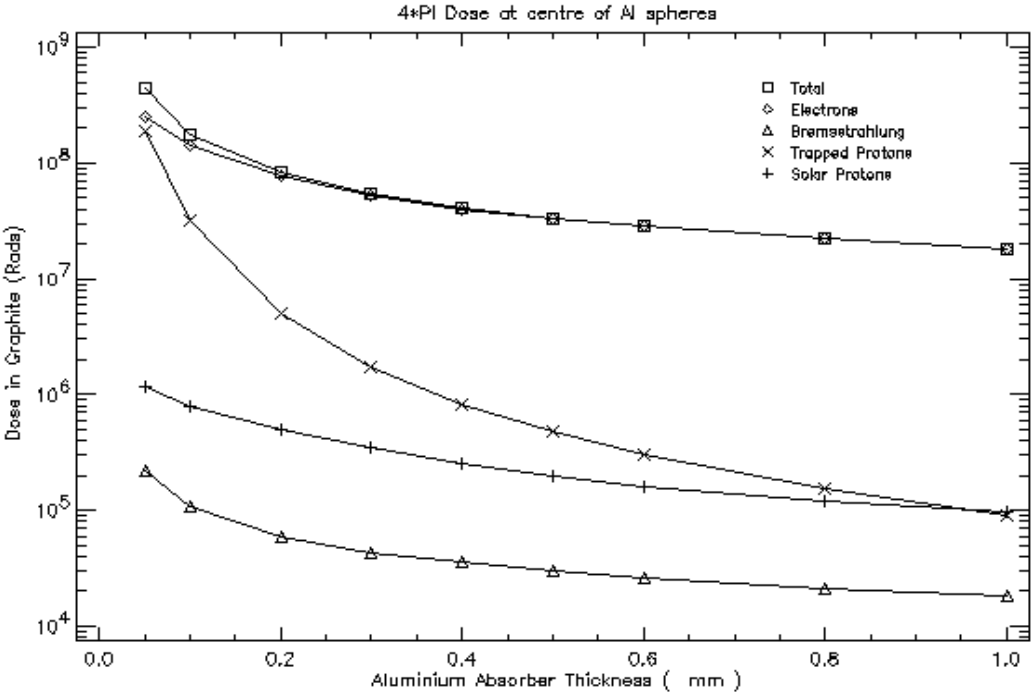

Figure 2.15. NIST - SHIELDOSE - Total Dose Estimation for HEO - Defined Flux Spectrum .[16]

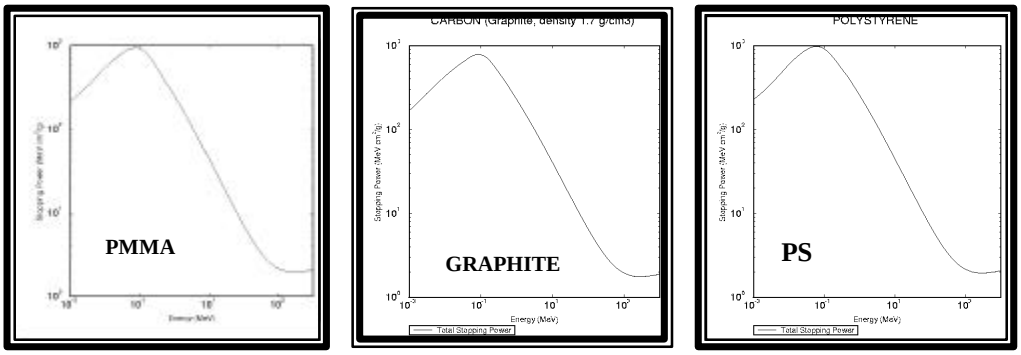

Figure 2.16. Demonstration of the Equivalency of Graphite Proton Stopping Power to PMMA and PS.

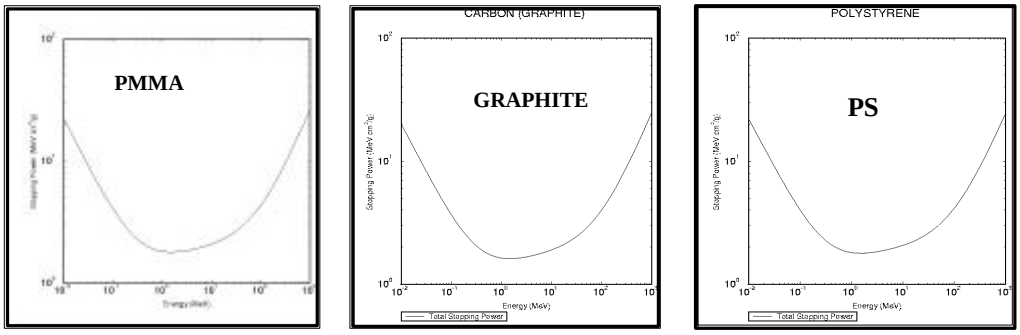

Figure 2.17. Equivalency of Graphite Electron Stopping Power to PMMA and PS.

The SHIELDOSE calculated total dose accumulated over the 10 year HEO mission approaches 400 Mrads for unshielded, 1 mm spheres of graphite.[16] This represents the composite dose is attributable to high energy electrons and protons along with a smaller contribution attributed to secondary radiation. The dose is sufficient to cause changes in the physical properties of many polymeric materials including the PMMA and to some extent polystyrene. The radiation efficiency of the total dose with respect to ionization can be determined using other modeling techniques (e.g. SRIM (TRIM) and CASINO). The simulation of the total dose energy for the space mission can be accomplished using a number of ground simulation techniques (Table 2.2).[17,18,19]

Method	Particle/Photon	Dose Rate	Energy
Linear Particle Accelerator	Electrons	10^{11} rads (Si)/s	1.7 to 3.3 MeV
Flash X-Ray	Photons	10^{12} rads (Si)/s	6.5 MeV
DC Beam Accelerator	Protons/ Electrons	1.0 Mrad (Si)/s	0.2 to 2.8 MeV
Gamma Cell	Photons	500 rads (Si)/s	1.39 MeV

Table 2.2 Summary of Methods Used to Simulate the Space Environment.

Linear Energy Transfer (LET) Assessment

In selecting a source for simulation of the space radiation environment, there is a first preference for a source with particle energy and mass similar to the space particle spectrum. However, a sustained, uniform flux of omnidirectional high energy particles is yet to be developed for ground testing. The problem is compounded by the desire to accumulate a total dose equivalent to a ten year exposure period in a matter of a few hours or days for practicality. Therefore, the equivalence of the linear energy transfer (LET) for ground simulation particles or photons to the LET properties of high-energy, space particle radiation, comes into question.[20]

The concern arises out of the cross-sectional area of energy distribution (i.e. spur) that is generated by the energy dissipated along the trajectory of the transient particle in the bulk material. The particle energy influences spur length and area. An example of the differences in the chemical mechanisms of incipient ionization of the polymer chain based on the ionizing particle are shown in Figure 2.18.[21] This suggests that the damage constants may not be the same.

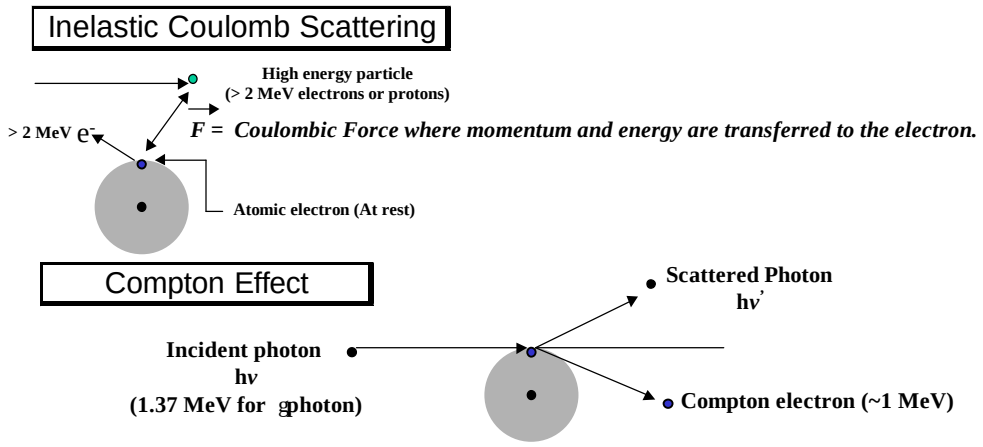

Table 2.18 Illustration of the Particle Energy Affect on the Mechanism of Ionization.

Investigations by Seguchi, et. al.,[22] reported that G(s) values for PMMA were constant up to LET values of 20-40 eV/nm. Graphical data charting the change in molecular weight for bulk solid polymers

exposed to gamma-rays, 30 MeV protons and 40 MeV protons showed good co-linearity. The lack of LET effect was attributed to the lack of overlapping spurs in the bulk polymer. An equation predicting the degree of overlap was developed by Seguchi (Eq. 3.1)[22] where r is the radius of a sphere-shaped spur, S is the LET value of the particle, and G_γ is the G value of the gamma radiation. The relationship is illustrated in Figure 2.19. The high LET values required to achieve overlapping spurs, and a resultant drop in G(s) values, can only be achieved by high-Z particles (galactic radiation – deep space mission environment). These particles are rare in the HEO environment, and may appear in the near Earth magnetic fields during periods of extreme solar activity.[3] Schnabel, et.al., reported a similar affect for cross-linking polymers.[23] The unchanged G(x) for polystyrene persisted for higher LET particles suggesting that more work is required to determine if and why polystyrene is unique.

$$\text{D. O.} = 2 - (3/2)[100/G_\gamma rS] + (1/8)[100/(G_\gamma rS)]^3 \qquad \textit{Eq. 3.1}$$

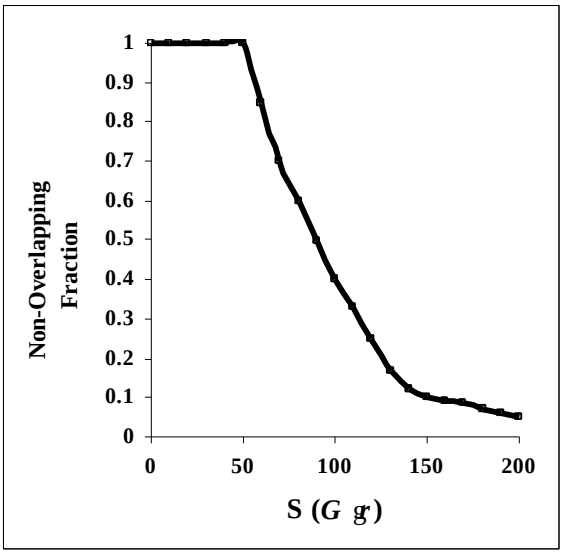

Table 2.19 Overlapping Fraction of Post-Exposure Spurs vs. LET Value (eV/nm).

Based on these findings, the approach to the simulation of the space environment for this study will assume that gamma radiation can deposit a total dose equivalent to the space proton and electron

radiation regime. The overall incipient ionization efficiency is thereby assumed to be equivalent, thereby validating the ground simulation model for the study of space radiation effects on polymers.

Ground Simulation

With the total dose and LET defined, a suitable test chamber must be selected. Polymers can require considerable dose (Mrads) to initiate a significant amount of change to the polymer structure. To duplicate radiation-induced chemical changes in the space environment, the logical radiation source would be one that produces high-energy ionizing radiation of sufficient energy and dose rate. The most common sources used to assess radiation hardness of materials are flash X-Ray generators, linear electron accelerators, and nuclides that produce high-energy γ rays (e.g. ^{60}Co and Cs^{137}). The basis for selecting one source over another depends on the type of radiation event to be studied.[24]

Ground Simulation Methods

Flash X-Ray generators produce radiation as X-rays in a very short, intense pulse (~ 80 ns). An illustration of a typical flash X-ray generator is displayed in Figure 2.20. The signal is generated by the interaction of electrons with elements of high atomic number (e.g. tungsten). The resultant interaction yields secondary radiation as high-energy photons (Bremsstrahlung) with energies between 1 MeV to 10 MeV. The ionizing dose can be controlled to deposit 10^1 - 10^5 rads (Si) per pulse (Dose rate of 10^9 - 10^{12} rads (Si) per second). The rapid dose rate and pulsed nature of the applied radiation makes the flash X-ray chamber a better candidate for the study of transient effects rather than using total dose accumulation studies.[24]

For electron particle radiation studies, the use of a linear electron accelerator (LINAC) can simulate transient high-energy, particle radiation effects and total dose affects. The illustration in Figure 2.21 describes how the pulsed electron beam is produced. Polymer degradation by total dose accumulation can be studied reliably using the LINAC for electron energies up to 2 to 3 MeV. The method suffers from

field uniformity that is critical to applying a uniform dose. Dosimetry is critical in characterizing the uniformity of the dose rate at any position in the test chamber, which can and does vary from test run to test run.

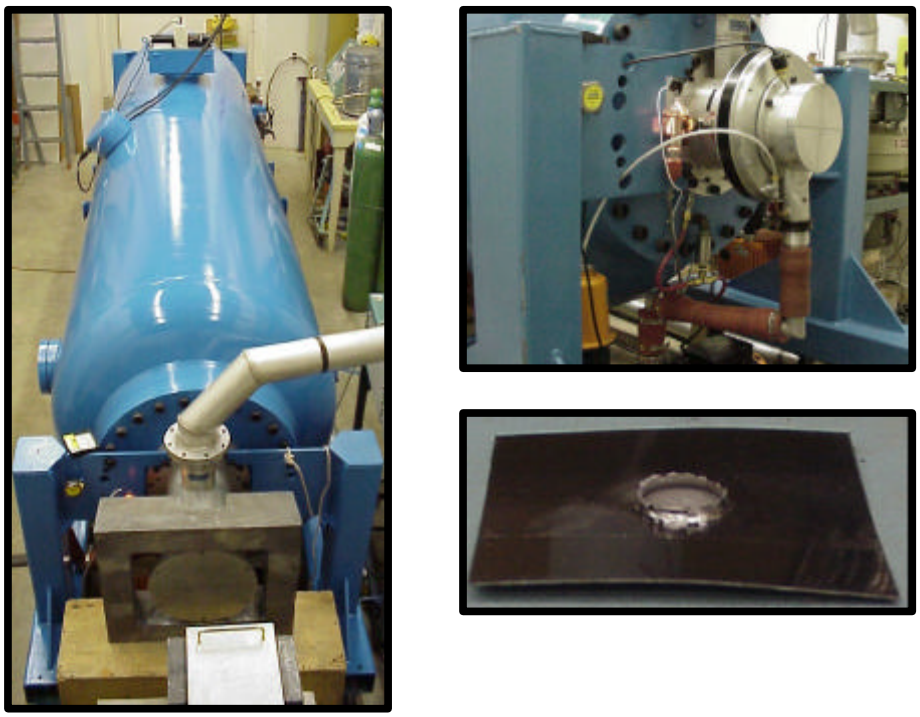

Figure 2.20. Illustrations of a Flash X-Ray Ionization Chamber, Source and W Target.

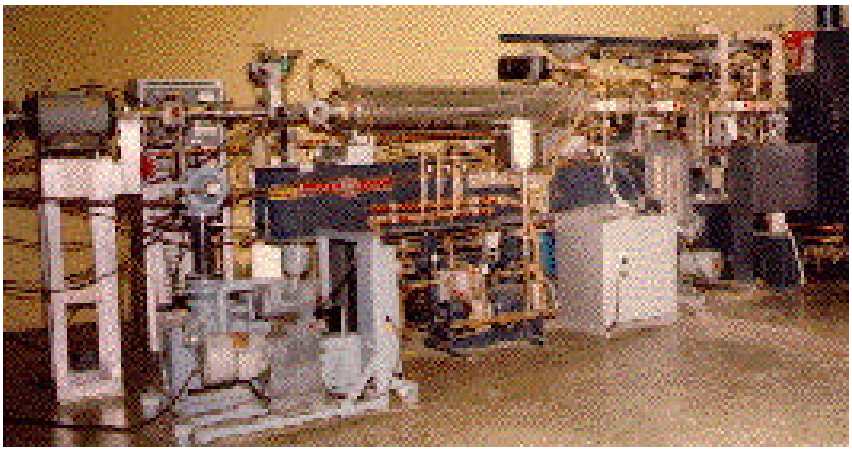

Figure 2.21 Illustration of LINAC Electron Beam Ionization Chamber

^{60}Co Cell Energy and Fluence

In polymer studies, most investigators prefer the use of a nuclide source (^{60}Co). The ^{60}Co nuclide decays slowly to the ground state of ^{60}Ni through *b* decay. The ^{60}Co is a long life isotope (~5.26 years) that provides γ photons with energies of 1.17 MeV to 1.33 MeV. High-energy ^{60}Co photons easily penetrate thick samples ensuring that the bulk mass of the target sample will receive a uniform dose. Having a uniform dose for a radiation hardness testing chamber simplifies the dosimetry for the analyst, while the long half-life of the ^{60}Co nuclide provides for a constant, uniform dose over time. The ^{60}Co source at Honeywell Space Systems in Clearwater, FL is illustrated in Figure 2.22, and is used to discuss the approach to dosimetry.

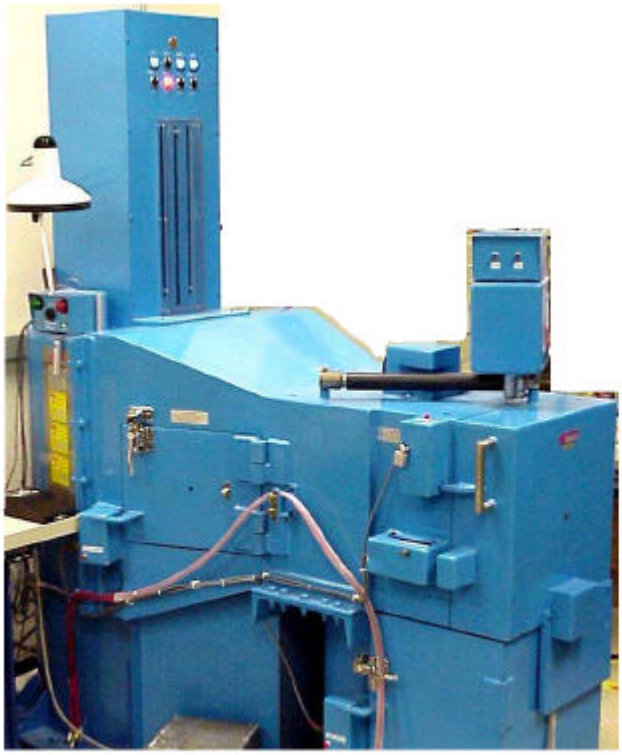

Figure 2.22. Illustration of ^{60}Co Ionization Chamber.

It is necessary to account for the influence of oxygen if ground simulation experiments are to be conducted in air. At ambient air pressure, the polymer sample is permeated with oxygen which, as discussed in Chapter 1, will act as a scavenger for free radical intermediates formed during the irradiation exposure period. The competitive formation of oxidation products can diminish the critical radiation-induced events of interest to the space investigation, and thereby limit the study of the effects of molecular weight and free volume.

The initial concentration of oxygen in the sample is at a saturation level based on the material under study. As the oxygen is consumed through reaction with the newly formed radical intermediates, the diffusion of air into the polymer can lead to additional consumption of oxygen, and can interfere with the study. Gillen, et. al.[25] demonstrated that this effect could be overcome through the use of a sufficiently high dose rate (i.e. greater than one Mrad per hour). The gamma source selected for this study uses a dose rate greater than three Mrads per hour. The dosimetry used to establish the dose rate follows in the next section.

Dosimetry and Mapping

Dosimetry is the tool for measuring the total dose of energy absorbed by a sensitive material in an ionizing radiation environment. Total dose is expressed in units of rads (100 ergs / gram of material). Materials of differing atomic number will display a different absorbed dose for a specific radiation spectrum, particularly for lower energy spectra. The ^{60}Co source emits a γ spectrum with an average kinetic energy value of 1.25 MeV. Variations in the absorption coefficients and stopping powers for materials are minimal at this energy level. Total dose absorbance in silicon (rads (Si)) is used to simplify comparisons of absorbed dose between materials with differing elemental composition.[26]

Dosimeter options vary in specific dose and dose rate sensitivity along with displaying differences in accuracy, precision, and stability. There is also a consideration for dosimeter response dependence on the kinetic energy or LET (Linear Energy Transfer) of the transient particle or photon regime. Polymer degradation is not the result of single event ionization, but rather the accumulation of dose absorbtion and

ionization. Thermoluminescence detectors (TLDs) are integrating dosimeters that are preferred for the evaluation of the relationship between dose accumulation and time.[27]

In radiation hardness testing dosimeters are mounted at the same coordinates intended for the material under study. The dose rate at the selected coordinates is assayed as the amount of absorbed dose in the dosimeters at predetermined time intervals. If the source is subject to variability, it is advisable to include the dosimeters alongside the sample during radiation hardness testing. The basis of selection of right dosimeter depends on a number of factors.

As an example of the use of dosimetry and a γ source for the simulation of a space particle environment, several polymeric powder samples are to receive sufficient γ radiation to deposit a total dose of up to 250 Mrads. Calcium fluoride (CaF_2: Mn) thermoluminescence dosimeters (TLDs) were used to perform time-integrated dose measurements and establish the dose rate distribution grid at multiple source-to-centerline distances from the γ source. All of the dosimeters used to establish the grid underwent a pretest to assess the uniformity of response to the radiation field. The pretest is performed with a batch of 30 dosimeters. The dosimeters are annealed prior to radiation, tested using a TLD phosphor reader (primarily of a heating stage and a photomultiplier) and then exposed at low total dose level and read again. The dosimeters must display post-irradiation TLD readings within a 95% confidence limit ($\sigma? < 8\%$) with a mean reading within 25% of the true value of the TLD. These dosimeter samples are reusable for calibration testing of the chamber.

Total Dose Determination and Equivalence to Space

An assessment of TLD response to total dose rate was measured by testing a batch of dosimeters at multiple points along the centerline from the source. The dose rate sensitivity is evident if the TLD readings drift from the confidence level of 95%. Figure 2.23 illustrates the change in dose rate as a function of distance from the γ? source of the ^{60}Co chamber.

The 12,000 Ci γ source at Honeywell uses twin ^{60}Co cells (6,000 Ci each) with a sampling area of 7.5” x 7.5”. The isodose curves for the sampling areas at multiple points along the centerline from the source are displayed in Figures 2.23.

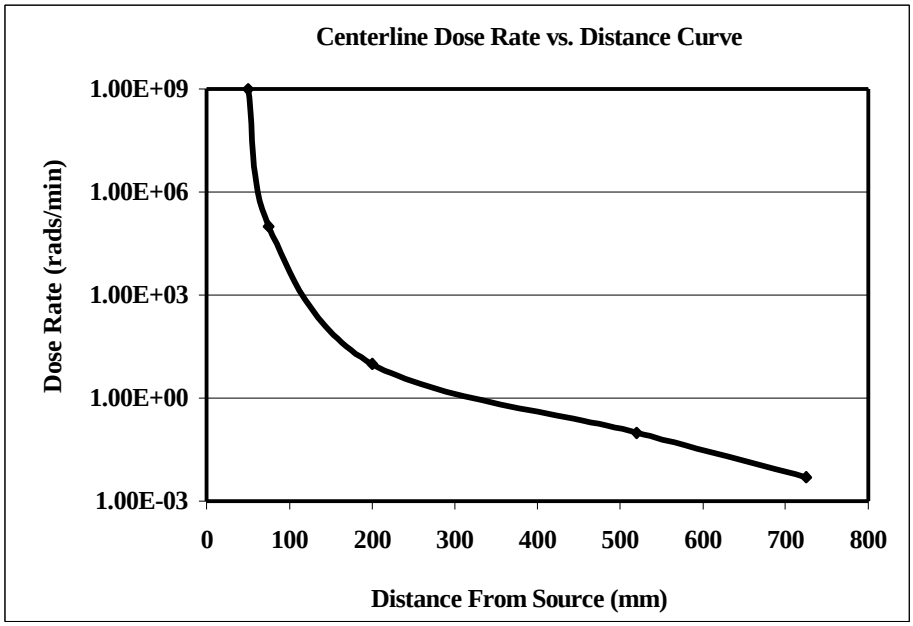

Figure 2.23. Dose Rate (rads (Si)/min) vs. Distance From Radiator ^{60}Co Source.

The approach to irradiation of the polymer samples required the samples to be placed at 85 mm from the source. At 70 mm the isodose curve displayed a constant field for 100% of the calibrated dose rate (26,759 rads (Si)/min) within an area 3.5" in diameter around the centerline (Table 2.2). Dosimetry testing provided the absorbed dose rate values (rads (Si)/min) used to prepare an isodose curve for a region 2.4" x 1.6" at 85 mm from the source (Figure 2.24). These chamber coordinates were used for all polymer radiation experiments in this study. A MATHCAD program was used to develop the isodose curve contour map for the entire sampling area (Figure 2.25). The TLDs display a maximum absorbance range of 1 x 10^6 MeV. The dose rate established during dosimetry testing was used to determine the exposure times necessary to prepare samples with a total absorbed dose of 40 Mrads, 80 Mrads, 120 Mrads and 250 Mrads. An evaluation of changes to the chemical and physical properties of the polymer in a proposed, distant radiation environment is now possible based on modeling, source selection and dosimetry.

Dosimeter	Dose	Position		APR DOS	25000	rad(Si)
6	23071	POS 1				
7	22094	POS 2		TRANS	350	rad(Si)EST
8	24473	POS 3				
9	25512	POS 4		EXP TIME	1.74	MIN
10	24727	POS 5				
11	27836	POS 6		MAX	28476	rad(Si)
12	27591	POS 7		AVG	25822	rad(Si)
13	26431	POS 8		MIN	22094	rad(Si)
15	28016	POS 9				
16	28476	POS 10		%MAX/MIN	28.88%	
				%AVG/APR	3.29%	
	DOSE RT	14841	rad(Si)/MIN : W/TRANS : W/MIN			
	DOSE RT	244	rad(Si)/SEC : W/O TRANS : W/AVG			

Table 2.3 Dosimetry Table Yielding Dose Rate for ^{60}Co Shepherd 484 Chamber.

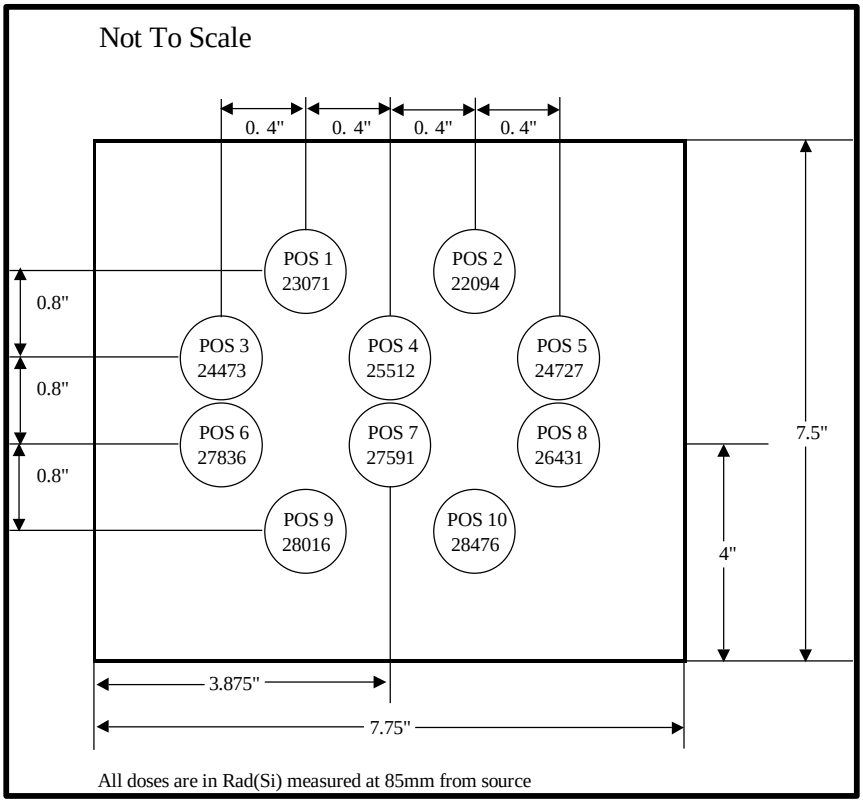

Figure 2.24. Isodose Curve for the ^{60}Co Source at 85 mm.

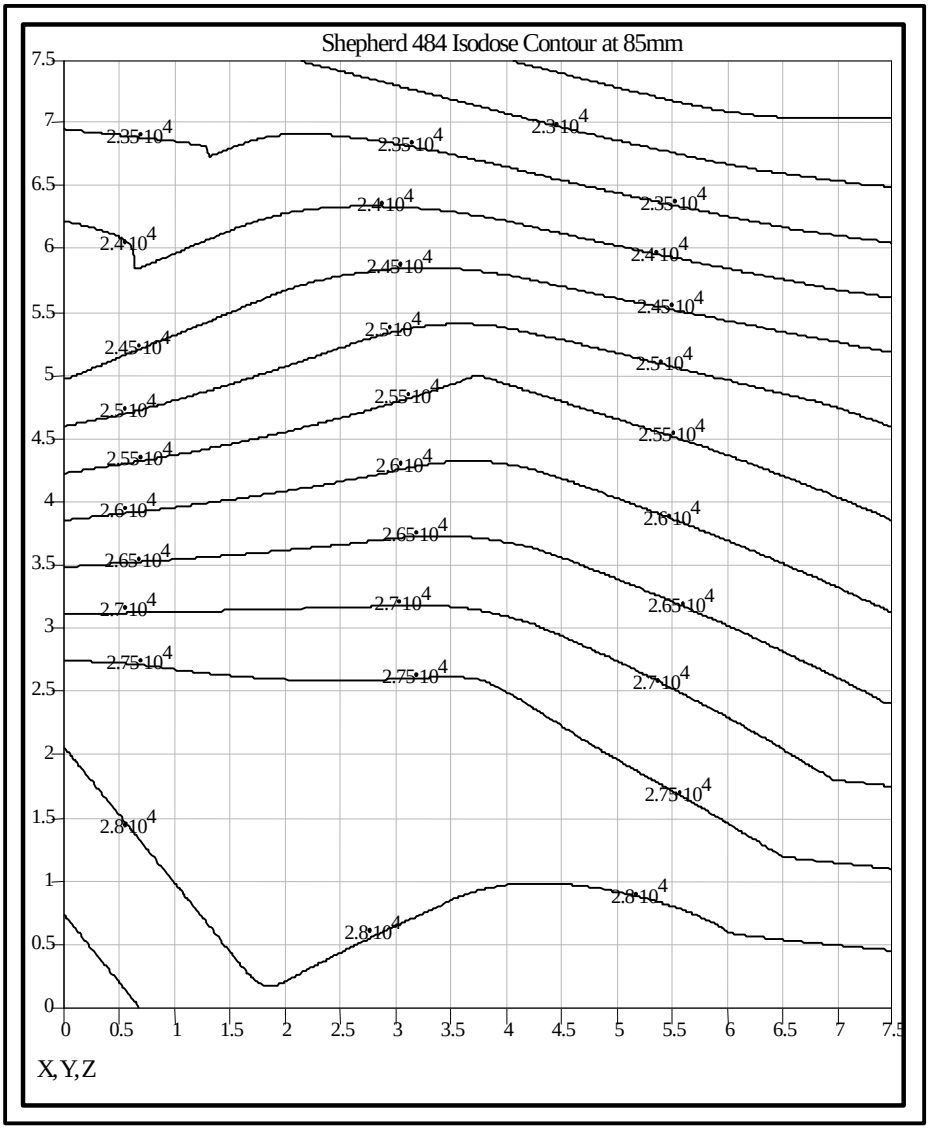

Figure 2.25. Shepherd 484 Isodose Contour Map for the ^{60}Co Source at 85 mm.

References

1. Makhlis, F. A.; *Radiation Physics and Chemistry of Polymers*, Wiley, New York, **1975**.

2. Biggin, H. C.; *Irradiation Effects on Polymers*, Clegg, D. W. and Collyer, A. A., Eds., Elsevier Applied Science, Oxford, **1991**, p. 1.

3. *Space Vehicle Mechanisms*; Conley, P. L., Ed..; John Wiley & Sons: New York, **1998**, p. 621.

4. *The Effects of Radiation on Electrically Insulating Materials*; Hanks, C. L. and Hammon, D. J.; REIC Rep. 64, Battelle Memorial Institute, Columbus, OH, **1969**.

5. *An Overview of the First Results on the Solar Array Materials Passive LDEF Experiment (SAMPLE), A0171*; Whitaker, A. F.; LDEF – 69 Month in Space-First Post Retrieval Symposium, NASA CP-3134, June **1991**.

6. *Space Environmental Effects on Materials*; Swinghamer, R. J., NASA-TM-78306, Marshall Space Flight Center, Huntsville, AL, Aug. **1980**.

7. Schnitzer, F., et. al., *Proc. Of the 8th International Plastic Optical Conference '99*, Chiba, Japan; **1999**, pp. 209-212.

8. Harmon, J. P., et. al.; *American Chemical Society Symposium Series 620*; Clough, R. L. and Shalaby, S. W., Eds.; American Chemical Society, Washington, D.C., **1996**, p. 302.

9. Taylor, E. W.; "Space and Enhanced Radiation Induced Effects in Key Photonics Technologies"; *IEEE Aerospace Conf. Proc.;* ISBN 0-7803-5427-3, Snowmass, CO, March 1999.

10. Sawyer, D. M. and Vette, J. I.; *AP8 Trapped Proton Environment for Solar Maximum and Solar Minimum*, NSSDC-76-06, National Space Science Data Center, Greenbelt, MD, 1976.

11. *AE8 Trapped Electron Model*, National Space Science Data Center, NASA-Goddard Space Flight Center, Greenbelt, MD, 1989.

12. Seltzer, S.; NBS Technical Note 1116, *SHIELDOSE: A Computer Code for Space-Shielding Radiation Dose Calculations*, National Bureau of Standards, Washington, D.C., 1980.

13. Seltzer, S. M., *SHIELDOSE, A Computer Code for Space-Shielding Radiation Dose Calculations, National Bureau of Standards, NBS Technical Note: 1116*, U.S. Government Printing Office, Washington, D.C., 1980.

14. Seltzer, S. M., Electron, *Electron-Bremsstrahlung, and Proton Depth-Dose Data for Space-Shielding Applications, IEEE Trans. Nuclear Science, 26*, 1979, p. 4896.

15. Davis, G.; *GPS-Based Navigation and Orbit Determination for the AMSAT AO-40 Satellite: AIAA 2002-5004*, AIAA Guidance, Navigation and Control Conference, Monterey, CA, Aug 2002.

16. Seltzer, S. M., Updated calculations for routine space-shielding radiation dose estimates: SHIELDOSE-2, *NIST Publication NISTIR 5477*, Gaithersburg, MD., December 1994.

17. Ott, M. N.; *Electron Induced Scintillation Testing of Commercially Available Optical Fibers for Space Flight*, Proceedings of the Nuclear and Space Radiation Effects Conference Data Workshop, Norfolk, VA, 1999.

18. Specifications provided by Boeing Radiation Effects Laboratory (BREL), Seattle, WA.

19. Specifications provided by University of California-Davis, Crocker Nuclear Laboratory, Davis, CA.

20. Kudoh, H., et. al.; *Radiation Physics and Chemistry*, *48*, 5, 1996, p. 555.

21. Serway, R. A. and Faughn, J. S.; *College Physics*, Harcourt Brace Javonovich Publisher, 1985.

22. Seguchi, T., et. al.; *Radiation Physics and Chemistry*, *50*, 3, 1997, p. 299.

23. Schnabel, W.; et. al.; *American Chemical Society Symposium Series 620*, Clough, R. L. and Shalaby, S. W., Eds.; American Chemical Society, Washington, D.C., 1996, p. 44.

24. Messenger, G. C. and Ash, M. S.; *The Effects of Radiation on Electronic Systems*, Van Nostrand Reinhold Company, New York, 1986.

25. Gillen, K. T. and Clough, R. L.; *Irradiation Effects on Polymers*, Elsevier Applied Science, Clegg, D. W. and Collyer, A. A., Eds., Oxford, 1991, p.215.

26. Profio, A. E.; *Radiation Shielding and Dosimetry*, John Wiley and Sons, New York, 1979, p. 255.

27. ASTM E-668-97, *Annual Book of ASTM Standards*, West Conshohocken, PA, 1998.

Chapter 3

Experimental

Materials

The experimental work for this study required analytical methods that would yield information about chemical changes in polymer structure and free volume information through instrumental analysis of polymer thermal properties. The selected methods included differential scanning calorimetry (DSC) to determine the glass transition temperature (T_g) for free volume information, and Fourier transform infrared (FTIR) spectrometry and gel permeation chromatography (GPC) for data on changes to the chemical structure.

Discussion of PMMA and Polystyrene Polymerization Process

The polystyrene (PS) and polymethyl methacrylate (PMMA) polymers used for this study were reference standards prepared by Polymer Source (Province of Quebec, Canada) and Scientific Polymer Products, Inc. (Ontario, NY). Table 3.1 describes the properties of the polymers as reported by the manufacturers.

Polymer Source reported the synthetic procedures for the stereospecific polymerization of *atactic*-polymethyl methacrylate and *iso*-polymethyl methacrylate. *atactic*-PMMA was prepared from methyl methacrylate monomer added drop-wise under positive nitrogen pressure to a dried THF solution containing the initiator adduct (R^-M^+) cooled at $^-78^oC$. The final solution was stirred for 30 minutes. Polymerization was terminated with methanol. The product was recovered by precipitation in methanol / water (8/2:v/v) and dried under vacuum at 60^OC for 48 hrs. SEC and GPC chromatography was used to establish molecular weight and polydispersity.

Reference Standard and Tacticity	Manufacturer	Mw	Mn	Mw/Mn
Polystyrene	Scientific Polymer Products	590	550	1.07
(GPC - Manufacturer Data)	Scientific Polymer Products	2,430	2,300	1.06
Atactic	Scientific Polymer Products	6,400	6,100	1.05
(By FTIR)	Scientific Polymer Products	13,200	12,400	1.06
	Scientific Polymer Products	19,300	18,100	1.07
	Scientific Polymer Products	44,100	41,200	1.07
	Scientific Polymer Products	75,700	64,900	1.17
	Scientific Polymer Products	151,500	139,500	1.09
	Scientific Polymer Products	223,200	200,600	1.11
Polymethyl Methacrylate				
(GPC - Manufacturer Data)	Polymer Source	6,800	6,400	1.06
Syndiotactic	Polymer Source	14,200	13,800	1.03
(By NMR - Manufacturer Data)	Polymer Source	17,900	16,200	1.06
(By FTIR)	Scientific Polymer Products	68,200	60,600	1.13
	Scientific Polymer Products	147,100	139,900	1.02
Isotactic	Polymer Source	4,200	3400	1.24
(By NMR - Manufacturer Data)	Polymer Source	11,500	10,500	1.09
(By FTIR)				

Table 3.1. Properties for PMMA and PS Reference Standards

Iso-PMMA was prepared from methyl methacrylate monomer added drop-wise by syringe to a dried, degassed toluene solution containing the initiator adduct (*t*-butylmagnesium bromide) cooled at $^{-}78^{o}$C under positive nitrogen pressure. The reaction vessel was sealed and the polymerization was allowed to proceed at $^{-}78^{o}$C for four days. The reaction was terminated with methanol. The product was recovered by precipitation in methanol and dried under vacuum at 90^{O}C for 48 hrs. SEC and GPC chromatography was used to establish molecular weight and polydispersity.

Tacticity was determined by Fourier transform infrared spectroscopy (FTIR) and proton nuclear magnetic resonance spectroscopy (NMR). The manufacturer determined the isotactic content of the iso-PMMA standards using a 500 MHz spectrometer and calculating the ratio of the peak area of the isotactic α-CH_3 protons at 1.20 ppm to that of syndiotactic and heterotactic fractions observed at 0.82 and 1.03 ppm respectively.[1] The manufacturer's NMR results show peak area ratios of 0.91_{iso} / 0.09_{hetero} for PMMA Mw = 4,200 g/mole and 0.90_{iso} / 0.03_{syndio} / 0.07_{hetero} PMMA Mw = 11,500 g/mole [Polymer Source Data].

Determination of Mw, Mn, PD and G Values

Molecular weight determination is a primary method in assessing the chemical damage to a polymeric material.[2] The method can be used to assay the amount of polymer chain scission and crosslinking by radiation-induced polymer degradation.[3] Early molecular weight studies used viscometric methods for the determination of the viscosity average molecular weight M_v, and relating the M_v to the intrinsic viscosity.[4] The method was useful for the study of polymers in the liquid state as neat fluids or as solutions in selected solvents for the evaluation of scission and crosslinking. Early radiation studies made use of the gel point as a physical property for assessing the crosslinking mechanism of polymer degradation.[2] The data was used to develop the early models of Saito and others[5] in demonstrating the significance of scission, end-group depolymerization and cross-linking as the primary degradation pathways for radiation-induced ionization of the polymer chain..

Gel Permeation Chromatography

The introduction of gel permeation chromatography (GPC), also known as size exclusion chromatography (SEC), made it possible to characterize the distribution of chain lengths in the polymer. This allowed characterization of simultaneous events of solids undergoing scission and crosslinking.[6]

The assessment of polymer molecular weight can be evaluated as number average molecular weight (M_n) which is the total molecular weight of all molecules divided by the number of molecules (Figure 3.1).

$$M_n = \frac{\sum_i N_i M_i}{\sum_i N_i}$$

Figure 3.1. Formula for the Determination of Number Average Molecular Weight.

The term *N* denotes the molar concentration, *M* is the Molecular Weight and *i* represents a running index that denotes the degree of polymerization of the *ith* species in the polymer mixture. Alternatively, molecular weight can be evaluated as the weight average molecular weight (M_w) that represents the mass average molecular weight that can be determined using the formula in Figure 3.2. The methods used to determine Mn and Mw are categorized as absolute methods and relative methods. The absolute methods for Mn include: osmometry, ebulliometry, cryoscopy and end group analysis, whereas, the absolute method for Mw is light scattering. Viscometry and gel permeation chromatography (GPC) are established, relative methods for the determination of molecular weight distribution and Mw.[6] The GPC method requires calibration using a series of standards of known molecular weight distribution.

$$M_w = \frac{\sum_i N_i M_i^2}{\sum_i N_i M_i}$$

Figure 3.2. Formula for the Determination of Weight Average Molecular Weight.

The two molecular weight terms combine (M_w/M_n) to provide the polydispersity index. These expressions can provide insight into the preferred mechanism of radiation-induced degradation. In the LDEF experiments, the preference for cross-linking was predicted and confirmed when exposed polystyrene panels displayed a drop in the M_n value indicating the presence of fewer molecules, along with a significant increase in M_w and polydispersity.

The GPC technique is a separation method based on the size of molecules comprising the polymeric material. In the case of linear polymers (oligomers of polystyrene, PMMA, etc.), the chain length defines the size of the molecule and the molecular weight. As polymeric materials are synthesized,

the polymerization is carried out in a manner that produces chains of different length (or molecular weight). The recurrence of polymer chains of specific lengths leads to a distribution of molecular weights in the polymer mixture. In condensation polymer synthesis, the reaction stoichiometry and kinetics can be controlled to yield a product with a narrow polydispersity.[7] Free radical chain building reactions are more difficult to control with respect to the degradation reactions that compete with the synthetic process, and thereby yield product with high polydispersity. Figure 3.3 illustrates the GPC features of polydispersed polystyrene as an example of the values of interest with respect to the molecular weight.

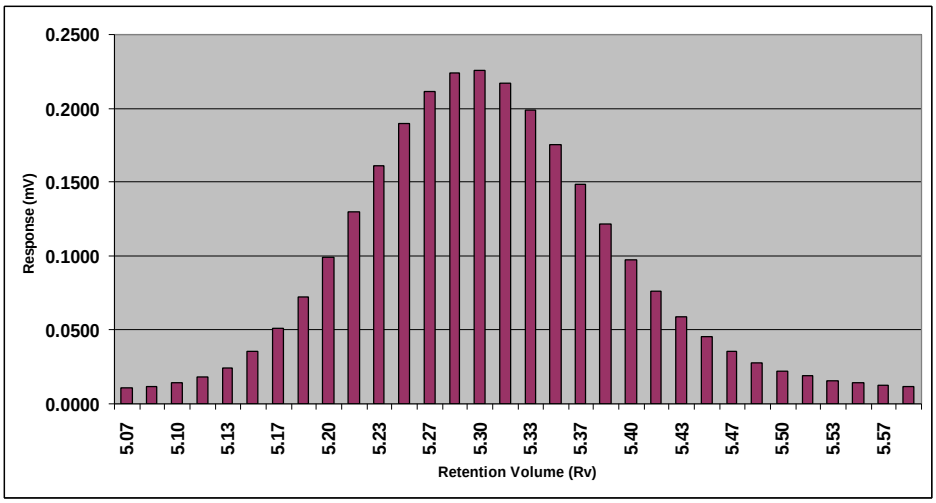

Figure 3.3. Chromatogram for a Polydispersed, Polystyrene Standard with Mw = 6,400 g/mole (The higher molecular weight fractions are eluted at lower retention volume).

Standard Curve and Molecular Weight Distribution

The GPC data for the polystyrene standards used for this study is presented in Table 3.2. The linearity of the calibration curve was verified using WINCHEM software program for polymer analysis.

The data in Figure 3.4 demonstrates that the GPC procedure can resolve the molecular weight of this class of polymeric compounds.

Mw	Mn	Mw/Mn
2,430	2,300	1.06
6,400	6,100	1.05
13,200	12,400	1.06
19,300	18,100	1.07
44,100	41,200	1.07
75,700	64,900	1.17

Table 3.2. Polystyrene GPC Standards.

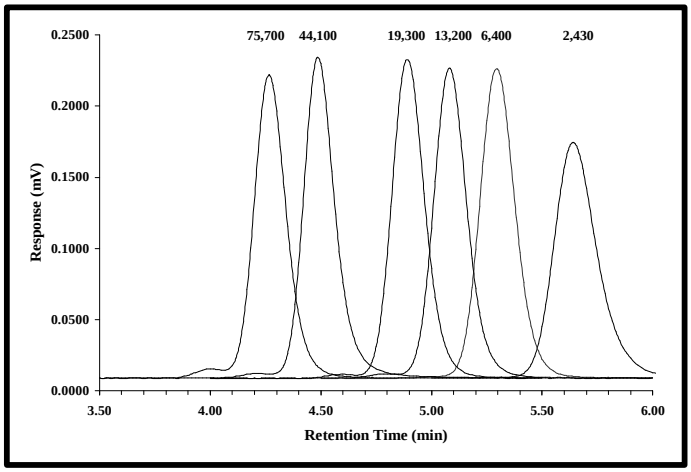

Figure 3.4 GPC PS Standard Chromatograms.

A power curve was defined for the estimation of molecular weight in the determination of weight-average (M_w) and number average (M_n) molecular weight and the polydispersity index (Figure 3.5) for the gamma-irradiated PMMA linear series.

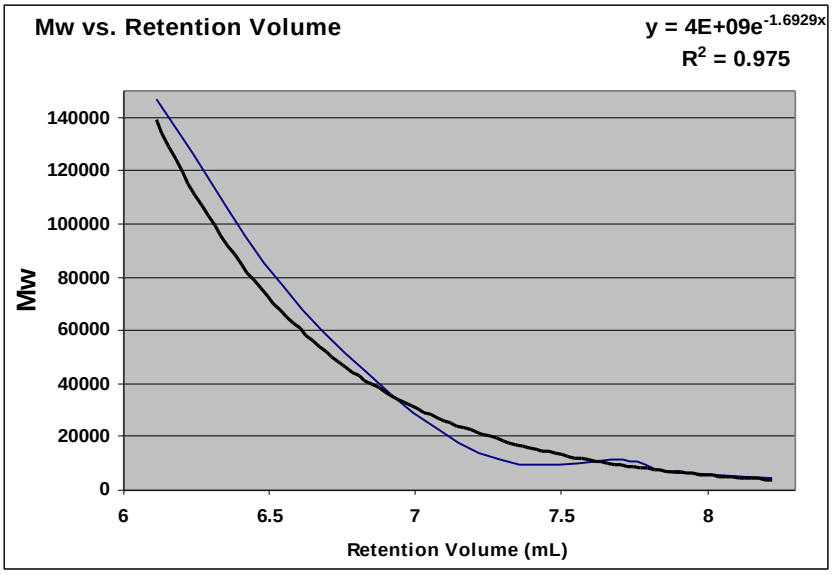

Figure 3.5 Calibration Curve for PMMA Standards with Best-Fit Function.

A calibration curve can be established from the retention volumes for polymer standards of known molecular weight and narrow molecular weight distributions.[8] The resolution of the GPC column determines the quality of separation between oligomers of specific chain length. The calibration curve can be used to assign a molecular weight range to each of the vertical segments of the chromatogram. The height (H_i) of the vertical segment describes the concentration for the specific molecular weight represented by the *ith* segment. The equation for M_n can be redefined in terms of the H_i values for the chromatogram presented by the polymer mixture (Figure 3.6).

Previous work has demonstrated that GPC can be applied to describe the radiation damage observed for a linear polymer sample.[9,10,11] The studies showed that by monitoring changes in the values for Mn, Mw and PD, the mechanism of degradation via crosslinking or chain scission could be distinguished. The G(s) values were calculated using the radiochemical yield equations of Saito, et.al. (Equation 3.1).[5]

$$M_n = \frac{\sum H_i}{\sum \frac{H_i}{M_i}} \qquad M_w = \frac{\sum H_i M_i}{\sum H_i}$$

Figure 3.6 Determination of the Number and Weight Average MW Using GPC Absorbance Values.

$$1/Mw = 1/Mw0 + [(G(s)/2) - (2G(x)] \times (D \times 1.038 \times 10^{-5}) \qquad (Eq.\ 3.1)$$

Characterization of the Polymer Chemical Structure

Post-irradiated polymers undergo changes in chemical structure as chain scission or cross-linking reactions occur. Unreacted free-radical intermediates that remain in the irradiated polymer sample in air can react with oxygen molecules to form peroxides and other oxidization products.[12] Several tools have been applied to analyze the chemical structure of the irradiated polymer to gain information useful to assuring the affected chemical bonds.[13] Polymer formulation experts use such information in the design of polymers with structural features that harden the polymer structure against radiation-induced structural degradation.

Scission

Instrumental analysis using nuclear magnetic resonance spectroscopy, mass spectrometry, and vibrational spectroscopy(e.g. Fourier Transform Infrared Spectroscopy (FTIR)) has been applied to the chemical analysis of irradiated polymeric materials.[14,15] The use of infrared spectroscopy is an effective tool for chemical analysis of the bulk polymer that maintains the chemical integrity of the sample without

dissolution or other experimental preparation techniques that may quench reactive intermediates or halt other physical changes in polymer properties.[16,17]

In previous work, infrared analysis has been applied to UV-irradiated thin films of polymethyl methacrylate (PMMA).[18] The chemical structure of PMMA allows several different degradation pathways that include main chain scission, ester removal, change in the three-dimensional structure (tacticity) and oxidation. Moore and Choi demonstrated that while main chain scission can be assessed by FTIR, the loss of ester can be tracked using the carbonyl band at ~ 1730 cm^{-1} (Figure 3.7). [15] Other key peaks can be monitored as well (e.g. alkene formation – 1367 cm^{-1}). The spectrum can also be used to evaluate the tacticity of the PMMA polymer chain structure (isotactic vs. atactic vs. syndiotactic) using the vinylic and carbon oxygen bond cluster bands at 1085 to 1312 cm^{-1} (Figure 3.8)[16,18,19]

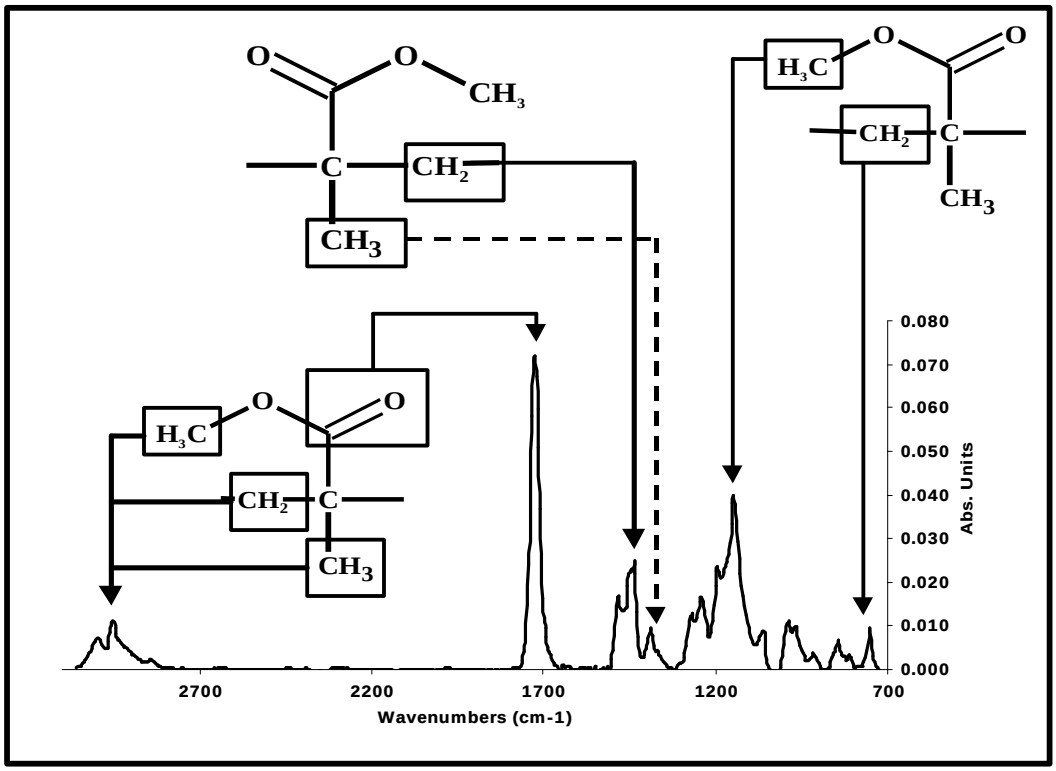

Figure 3.7. Specific FTIR Bands of Interest for PMMA Degradation

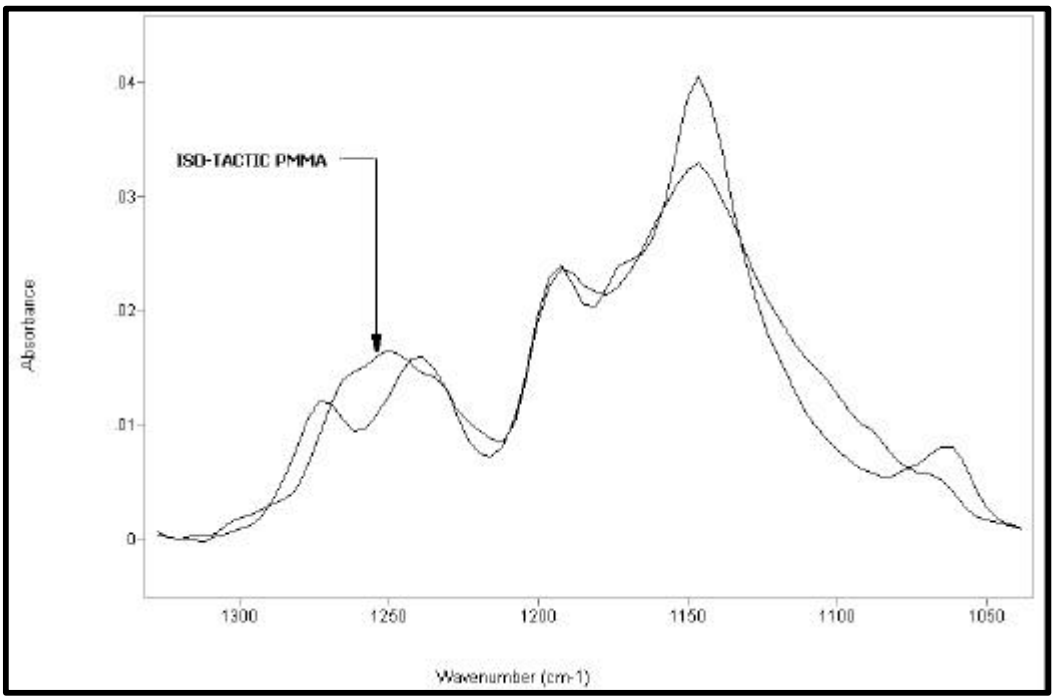

Figure 3.8. Comparison of FTIR Bands for Isotactic and Atactic PMMA .

ATR Fourier Transform Infrared Spectroscopy

In performing the FTIR analysis, the samples used to conduct the microtransmittance analysis of the polymer samples were too thick for establishing a quantitative comparison of the relative peak heights. For film samples analyzed by transmittance FTIR, it is important to maintain a maximum peak height of no more than 0.3 absorbance units to maintain linearity of the absorbance band as a function of concentration. The FTIR method is reported to lose linearity at an absorbance maximum of 0.3 absorbance units.[22] The true linear range for comparing FTIR peak heights is 0.3 absorbance units or less. In preparing thinner films that achieved 0.3 absorbance units, two problems affected the acquisition of acceptable spectra. One, the signal-to-noise ratio was too great for resolution of more subtle spectral features, and two, the pressure required to prepare a neat, thin film sample for analysis had reflowed the polymer. The internal mechanical stress in the sample presented a concern for further distortion of the peak heights, and a continuation of the

similar problem in assessing the relative peak heights. These issues lead to an attenuation approach to assessing structural degradation.

The above problems were solved through the use of a single-bounce attenuated total reflectance (SB-ATR FTIR) accessory made by Thermo-SpectraTech. A comparison of the microtransmission method and the SB-ATR method are shown in Figure 3.9. In the microtransmission method, the IR beam must pass through the sample to the detector. This leads to the problems of sample thickness and stress-induced distortion of the sample spectrum. The SB-ATR method holds the polymer sample in contact with a hemi-spherical, diamond window with minimal force. The infrared beam is directed into the diamond window from below toward a single reflectance at the sample-diamond interface that is incident with the sample surface. The beam does not pass through the sample (Figure 3.10). The beam then is directed to the MCT detector, and a spectrum of reasonable absorbance is obtained. The spectra for this study are included in Appendix 2.

All PMMA and PS spectra were obtained using a BIORAD FTS 40 FTIR spectrometer equipped with a mercury cadmium telluride detector and a SB-ATR reflectance microscope assembly. The co-added spectra were collected and averaged over 100 scans at a range of 4,000 – 750 cm^{-1} at 8 cm^{-1} resolution.

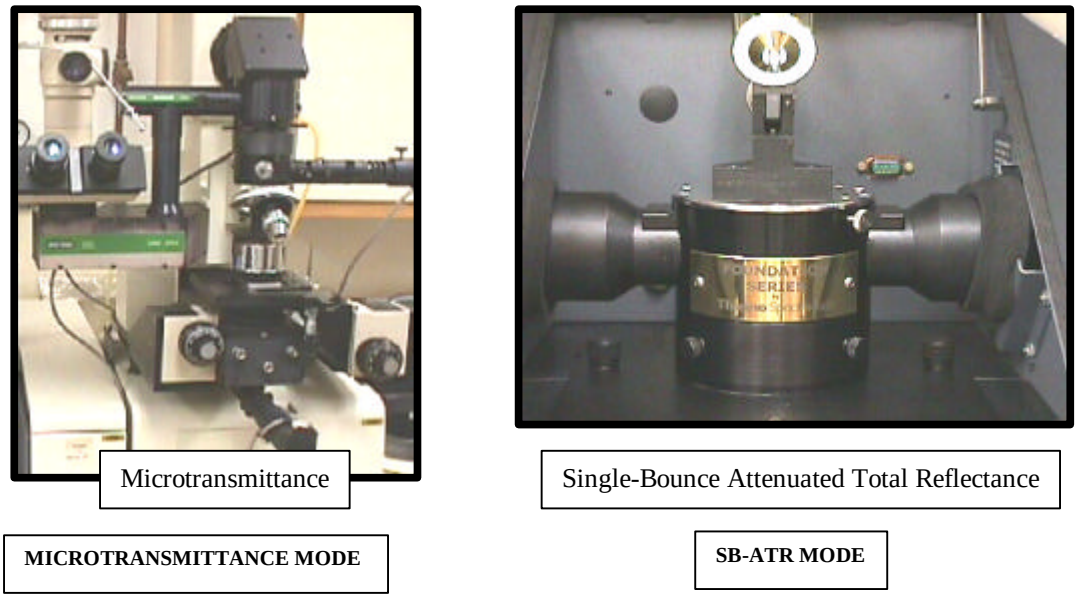

Figure 3.9. Comparison of Microtransmittance and SB-ATR FTIR Methods.

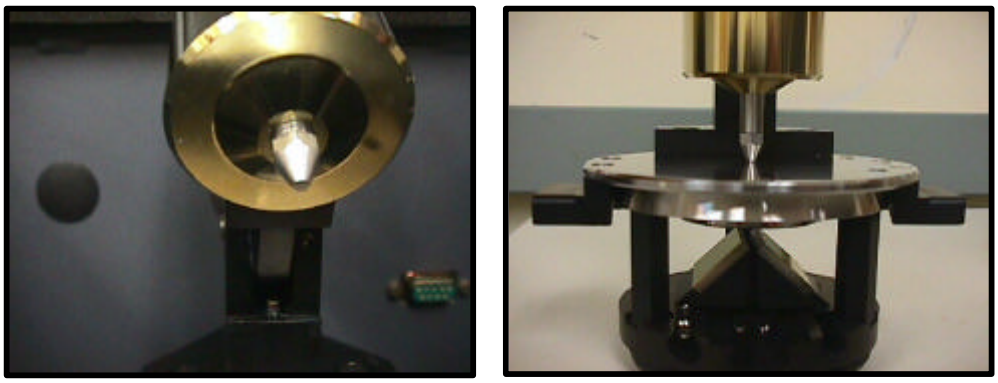

Figure 3.10. Illustration of the SB-ATR FTIR Accessory.

Crosslinking

There are specific FTIR bands of interest in the crosslinking reactions expected for the polystyrene molecule as well. Using FTIR, Parkinson and Keyser followed the changes in the polystyrene chemical structure observed following exposure to gamma irradiation.[23] Even with significant total dose, the changes in the polystyrene spectrum are nearly imperceptible and are not practical for comparison purposes. Parkinson's work showed that irradiation of polystyrene led to degradation of the phenyl side chain with losses in peak intensity for the ring C-H bands at 3061 cm-1 to 3083 cm-1 and an increase in the peak at 825 cm-1 that is attributed to crosslinking through the phenyl side chain (implying that the primary cross-linking mechanism occurred between the ring carbons of neighboring polystyrene chains).

Moore and Choi reported that specific infrared absorbtion bands can be observed to diminish, appear, increase or decrease in line with the mechanism of degradation of irradiated PMMA.[19] Loss of the methyl ester group results in a decrease in the intensity of the bands assigned to the PMMA side chain: 2997 and 2936 (methyl C-H), 1730 (carbonyl), 1484 (methyl C-H), 1446 (methyl C-H), and 1265–1145 cm^{-1} (carboxyl C-O).[15] If the PMMA is irradiated in the presence of oxygen, an increase in the absorbance

band from 3100-3500 cm^{-1} may signify the formation of PMMA hydroxyl (O-H) moieties. The formation of double bonds in the main chain formed through the elimination of the ester group led to the appearance of a new band at 1650 cm^{-1} demonstrating the usefulness of infrared spectroscopy in defining changes in the chemical structure of polymeric compounds.

Characterization of the Polymer Physical Properties

Ultimately, the concern for the effect of radiation on the polymer chemical structure of the polymer is the potential for a change in the performance of the polymer in application such as optoelectronics, satellite instrumentation and electronics packaging. There are many tools to evaluate key physical properties of interest for polymeric materials. Changes in refractive index, coefficient of thermal expansion (CTE), α–β ? transitions, elastic modulus or storage modulus can introduce risk to the flight mission in most spacecraft. Many optoelectronics systems are based on interferometric principles where a change in refractive index or an extended light path can result in signal attenuation or an increase in baseline noise. Electronic assemblies rely on adhesive polymeric materials to bond electronic components to the printed wiring board. In space environments that exert repetitive thermal cycling at extreme temperatures in rapid succession at high acceleration, the components may lose adhesion. Adhesive polymers are formulated to match the CTE of the board substrate and the mounted components of the electronic assembly. A change in the α–β transition temperatures due to radiation-induced chemical degradation may change the CTE of the adhesive in the critical temperature range of the spacecraft mission. The critical properties of the polymer material must be maintained to enhance spacecraft mission performance.

The tools used to measure the properties of the typically include:

Thermal Mechanical Analysis	–-	Coefficient of Thermal Expansion (CTE)
Differential Scanning Calorimetry	–-	*a* - ? Transitions
Dynamic Mechanical Analysis	–-	*a*- *b* ? Transitions and Moduli
Dielectric Analysis	–-	*a*- *b* –γ ? Transitions and Dielectric Constant

Differential Scanning Calorimetry

Differential scanning calorimetry (DSC) is a commonly used method for characterizing phase changes or a change in the physical state of polymers. Heat energy is consumed or evolved as a material undergoes melting, a change in crystalline form, or participation in a chemical reaction. The enthalpies of these processes are measured as a function of differential heat flow required to maintain two materials [The sample and an inert reference material] at the same temperature. Figures 3.12 and 3.13 are schematics describing the principle of operation of a differential scanning calorimeter.

The changes in state presented by a polymer, other than first order transitions, over a specified temperature range can be pertinent to changes in the physical properties of the polymer (e.g. specific heat, coefficient of thermal expansion, free volume and the dielectric constant), and thereby may significantly affect the performance of the polymer. The conventional designations for these second order phase changes begin with the phase change that occurs at the highest temperature called the α-transition, or glass transition temperature (T_g) or α-relaxation.

The DSC measures heat flow (Δdq/dt) in the polymer material. The endotherm or exotherm presented in the DSC thermogram can represent chemical reactions that are readily observed as a first order change of state. At the glass transition temperature, a second order phase transition phenomenon occurs where there is a step change in heat capacity. Experimental observations demonstrate that factors such as molar mass (M), degree of cross-linking and size of pendant groups (including branching) on the main polymer chain can influence the Tg value of a polymeric material. These factors are based on a change in the chemical structure of the polymer that are similar to the chemical changes that are the basis for degradative effects of radiation, thus helping to validate the selection of DSC as an appropriate tool in the study of radiation effects on polymers.

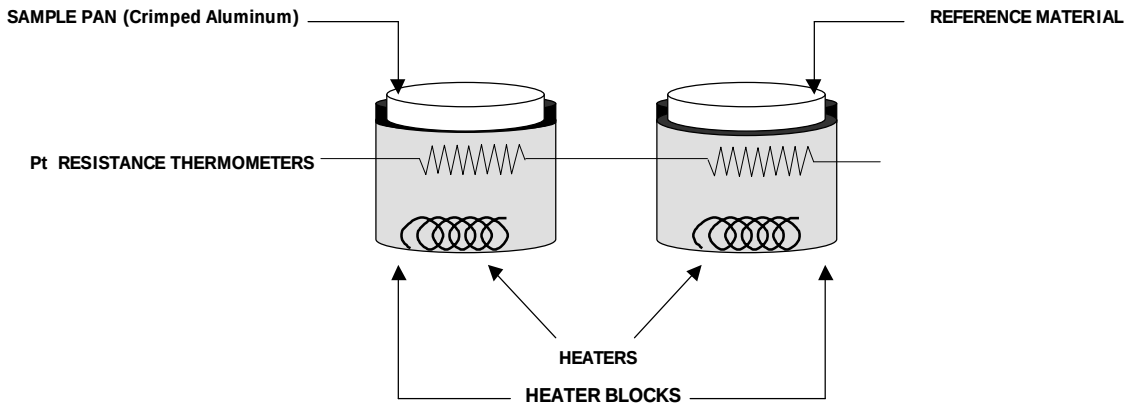

Figure 3.12. Illustration of DSC Holding Pan, Sensors and Heater Blocks.

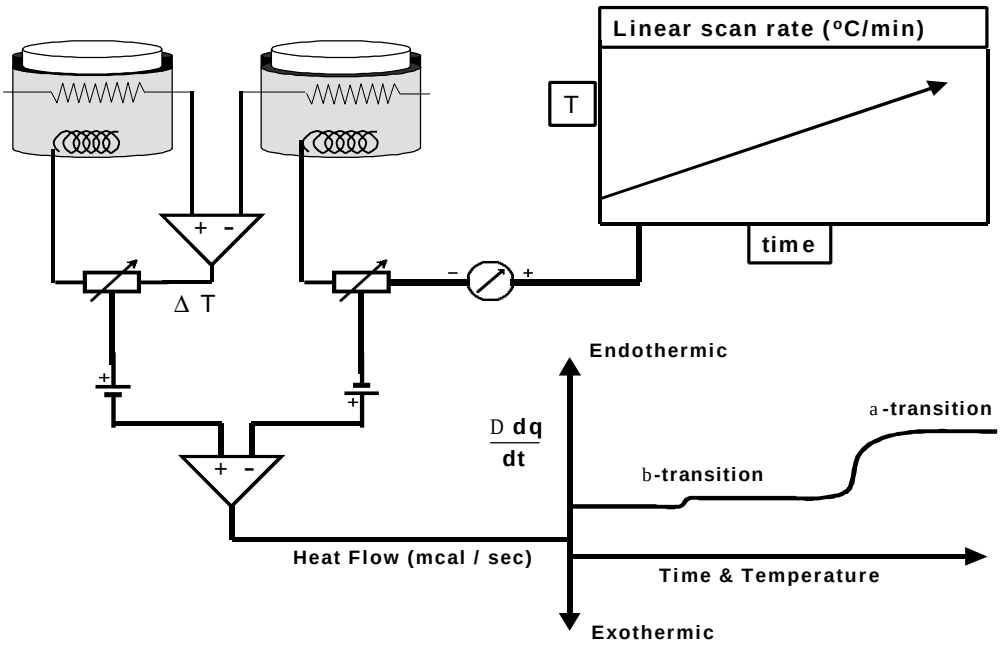

Figure 3.13. Illustration of Differential Scanning Calorimetry – Controllers and Data Output.

Thermal Analysis and Free Volume

During the glass transition phenomenon, a polymer undergoes a change in brittle, glass-like form to a rubbery state as the thermal energy is now sufficient to increase the vibration between atoms comprising the polymer. The segmental motion (e.g. vibrational, rotational and diffusional) increases and is expressed as a change in heat capacity. The molecular structure of the monomeric unit, and the length of the oligomeric chain, influence the segmental motion of the component atoms. Oligomeric chains of increasing length (higher molecular weight) or an increase in the size of side group moieties influence the free volume of the material and will shift the Tg to higher values. Analysis of narrowly dispersed PMMA standards shows that the Tg occurs at lower temperature as a function of molecular weight. Previous work attributes the drop in Tg to the additional free volume that occurs at the end group of the oligomers

comprising the polymeric molecular structure. Lower molecular weight materials have considerably more end groups that implies more free volume and can be addressed in the Fox-Flory equation (Figure 3.10).[24,25,26] The $T_{g\infty}$ refers to the glass transition temperature obtained by extrapolation of M_n to infinity and K is a dimensionless constant independent of molecular weight (25×10^3).[25]

$$Tg \sim Tg_{\infty} - (K/M_n)$$

Figure 3.14. Flory-Fox Equation Illustrating the Effect of Mw and Free Volume on Tg of PS.

References

1. Bovey, F. A., and Tiers, G. V. D.; Journal of Polymer Science, 1960, *44*, p. 173.
2. Charlesby, A., et. al.; *Proceedings of the Royal Chemical Society of London, Series A, Mathematical and Physical Sciences*, 1954, *224*, 1156, p. 120.
3. O' Donnell, J. H., et. al.; *Macromolecules*, 1979, *12*, p. 113.
4. Baxendale, et. al.; *Journal of Polymer Science*, 1947, *1*, p. 237.
5. Saito, O.; *Journal of the Physical Society of Japan*, 1958, *13*, 198, p. 1451.
6. Gedde, U. W.; *Polymer Physics*, Chapman and Hall, London, 1995, p. 9.
7. Odian, G.; *Principles of Polymerization*, McGraw-Hill Book Company, New York, 1970, p. 75.
8. Mahabadi, H. K.; *Journal of Applied Polymer Science*, 1985, 30, p. 1535.
9. Ichikawa, T., et. al.; *Journal of Polymer Science: Part A: Polymer Chemistry*, 1994, 32, p. 2487.
10. Limin, D., et. al.; *Journal of Applied Polymer Science*, 1996, *59*, p. 589.
11. Kudoh, H., et. al.; *Radiation Physics and Chemistry*, 1996, *48*, 1.
12. Reich, L., and S. Stivala; *Elements of Polymer Degradation*, MacGraw-Hill Book Company, New York, 1971, p. 31.
13. Harmon, J. P., et. al.; *Polymer*, 2003, *44*, p. 167

14. Dong, L.; et. al.; *Macromolecules*, 1995, *28*, 3681

15. O'Donnell, J. H.; Radiation Effects on Polymers, *American Chemical Society Symposium Series 620*, Clough, R. L. and Shalaby, S. W., Eds.; American Chemical Society, Washington, D.C., 1991, p. 402.

16. Bohn, P. W.; et. al.; *Analytical Chemistry*, *53*, 1981, p. 1082.

17. Nagai, H.; *Journal of Applied Polymer Science*, 1963, *7*, p. 1697.

18. Suarez, J. C. M., et. al.; *Journal of Applied Polymer Science*, *85*, 2002, p. 886.

19. Moore, J. A., and Choi, J. O.; Radiation Effects on Polymers, *American Chemical Society Symposium Series 620*, Clough, R. L. and Shalaby, S. W., Eds.; American Chemical Society, Washington, D.C., 1991, p. 156.

20. Havriliak, S., Jr., and Roman, N.; *Polymer*, 1966, *7*, 387.

21. Sundararajan, P. R.; *Journal of Polymer Science*, 1977, *15*, 699.

22. Griffiths, P. R., and DeHaseth, J. A.; *Fourier Transform Infrared Spectrometry*, John Wiley & Sons, Inc., New York, 1986.

23. Parkinson, W. W., Keyser, R. M.; *Radiation Chemistry of Macromolecules Volume II*, Dole, M., Ed.; Academic Press, New York, 1972, p 57.

24. Fox, T. G., and Flory, P. J.; *Journal of the American Chemical Society*, 1948, *70*, p. 2384.

25. Fox, T. G., and Flory, P. J.; Journal of Applied Physics, 1950, *21*, p. 581.

26. Fox, T. G., and Flory, P. J.; Journal of Physical Chemistry, 1951, *55*, p. 221.

Chapter Four

Variations in Response to Gamma Radiation for PMMA

Abstract

Modeling methods are required for predicting the chemical stability of macromolecular materials used in critical spacecraft components of satellites orbiting in the high-energy radiation environment of near earth and deep space planetary magnetic belts. Methods for predicting and simulating the total absorbed dose and ionization for long term space missions are presented herein. This paper evaluates main-chain scission and elimination products in a chain length series of narrowly dispersed polymethyl methacrylate (PMMA) polymers (6,800 - 147,100 M_w). A kinetic model comparison is made of the scission radiation yield (G_s) predicted for the simulated ionization data to the results of PMMA degradation in a ground-based simulation of the space radiation environment using a ^{60}Co source. The influence of molecular weight on the stability of post-irradiated PMMA is evident in the degree of change observed for each molecular weight series with respect to the degradation products produced by exposure to gamma radiation. The analysis of the specific polymer degradation products and changes in the average molecular weight (M_w) were performed using chemical analysis (FTIR and GPC) and thermal analysis (DSC). The analytical results for PMMA radiation-induced degradation products demonstrate that, depending on Mw, the amount and types of degradation products will vary with respect to decarboxylation, chain scission and other oxidative pathways. The results support a deviation from the modeled degradation pattern based on Mw and end group loss with free volume properties driving the observed differences in the G(s) values.

Introduction

The influence of chemical structure on the interaction of particle radiation with polymeric materials is a subject of interest to the space industry.[1-4] The broad range of polymer technology advancements for high-speed data processing, remote sensing and imaging, and system control and communications include electro-optical networks, flat panel displays, thin-film sensors and embedded miniature electromechanical sensors that are transitioning into aerospace and spacecraft designs. These

advancements use new polymeric formulations that have demonstrated successful performance in product applications for ground-based environments. Polymeric chemical structures display unique levels of change in physical and chemical properties following exposure to the space radiation environment that is a risk to spacecraft performance. This concern is driven by the potential for degradation of polymer performance and the production of outgassed degradation products that must be quantified in advance of spaceflight to determine the suitability of polymer innovations for spacecraft systems.[4-7]

The high cost and limited opportunity for on-orbit experimentation necessitates radiation modeling, ground simulation and analytical methods that accurately assess the amount of total ionizing dose deposited in a polymeric material over the duration of the space flight mission and to assess the resultant radiation-induced changes in the chemical structure. As an example in assessing the impact of polymer instability in space missions, a space flight environment is considered for a ten-year, low earth orbit (LEO) mission. The projected LEO particle spectrum and fluence can be modeled to yield data for ground simulation experiments that subject the polymer with an energy deposition equivalent to the projected ten-year mission dose.

Using the polymeric structural formula and total dose, a modeling analysis can be done to assess the potential for polymer degradation leading to changes in the critical chemical and physical attributes and performance factors required for stable polymer performance throughout the mission life (Figure 1). The risk of radiation-induced changes in polymer attributes and factors are the basis for the need to develop accurate modeling methods.

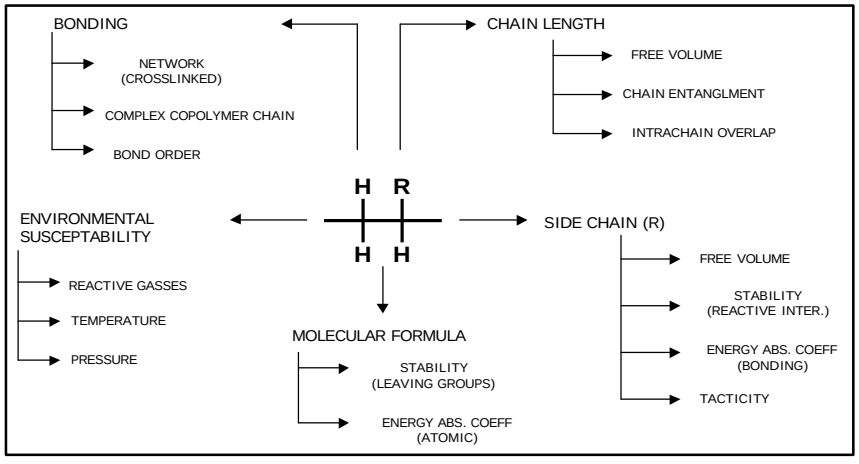

Figure 4.1. Summary of Chemical and Physical Factors Affecting Polymer Radiation Hardness.

Molecular weight and side groups are typical structural attributes that determine the properties of a polymer, such as coefficient of thermal expansion and modulus over the spacecraft system's thermal operating range. The effect of chain length and side groups on solid state polymer stability in a simulated mission flux spectrum can be studied using polymethyl methacrylate (PMMA) linear polymer series.[8,9]

Previous studies report irradiated PMMA undergoes two primary degradative pathways: loss of the carboxymethyl side-chain moiety and scission of the main chain (Figure 1). [10,11,12] Both radiation-induced degradation pathways illustrate an unfavorable condition for spacecraft systems with respect to outgassing effects and changes in physical properties of PMMA caused by main-chain scission-based change in average molecular weight (Mw). The PMMA, therefore, provides preferred attributes as a model compound for modeling and assessing the effects of radiation on polymer chemistry and properties.

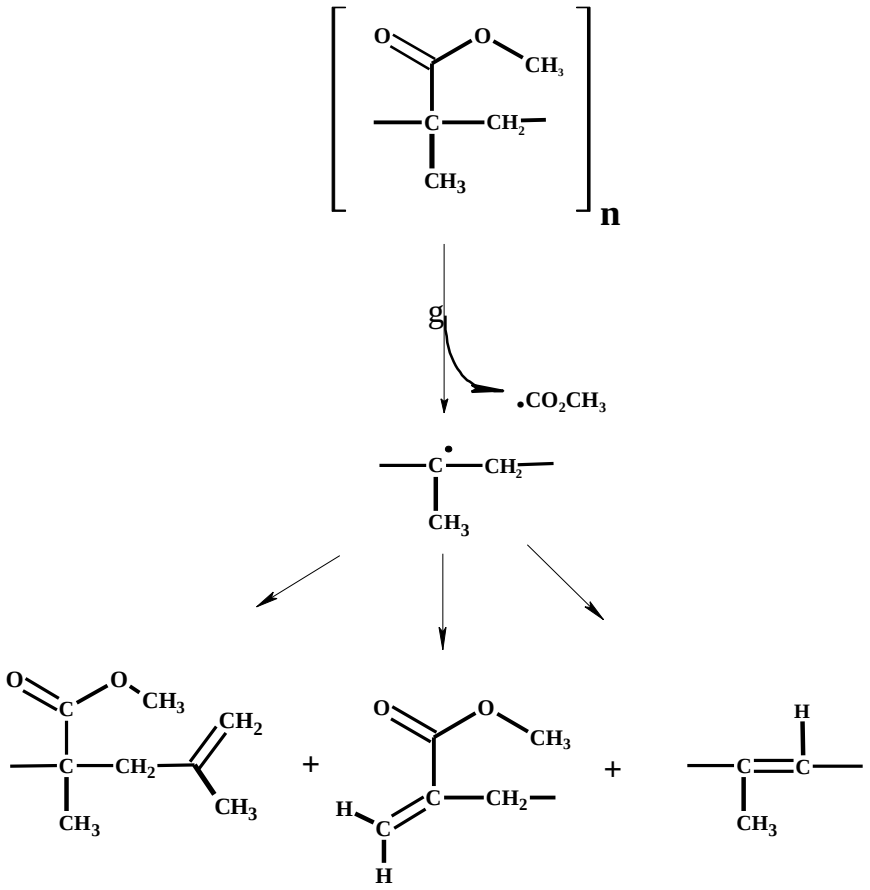

Figure 4.2. Radiation-Induced Degradative Pathways for a-PMMA.

Modeling the Space Mission Environment

Using a suite of established modeling tools, the total dose of deposited energy for a polymer material in a specific flight path application can be estimated. The most intense interplanetary space radiation environments are observed in the trapped magnetic particle belts surrounding planets in the solar system. Using NASA's modeling software: AP-8 proton, JPL-91 solar proton and AE-8 electron modeling and the spacecraft orbit flight path and the near Earth orbit integrating flux can be determined.[13,14] Using the particle flux and spectrum determined by the NASA models, the estimated total ionizing dose absorbed by PMMA can be determined using NIST SHIELDOSE-2.[15] The total dose describes the energy imparted to the PMMA polymer sample that is used to predict the extent of chemical degradation based on conventional radiation yield coefficients (G value) for specific PMMA degradation products shown in Figure 4.2.

Using the total dose projections provided by the SHIELDOSE-2 modeling, ground-based simulation of the total ionizing dose can be performed with a ^{60}Co gamma source irradiator. Using dosimetry, the simulated total dose and uniformity of the dose rate in the exposed field is verified with dosimetry. Analysis is performed to determine changes in the chemical structure and physical properties of the polymer following irradiation. Definition of the space radiation environment and total dose simulation conditions provides the target environment for ground simulation and thereby enables a representative mission assessment of the effects of the polymeric chemical structure on radiation-induced degradation.

Modeling the Degradation Chemistry

Previous statistical modeling studies have yielded numerical and algebraic kinetic equations for predicting the change in Mw distribution for solid state, linear series of oligomeric units as a result of scission events.[16-20] The modeling methods use assumptions in the Mw distribution and polydispersity of the polymer, and do not address contributions from crosslinking, recombination, end-group loss or tertiary

structure effects. The models also assume an equivalency in the probability of scission of each oligomer in the linear polymer series.

By comparison, predictions can also be made using radiation yield values (G values) for specific changes in structural features that, in turn, are based on experimental observations from numerous studies in the literature. The G values are based on total dose deposited in a specific mass of the polymer and the change in Mw distribution for pre- and post-irradiated polymer. The G values for a polymer can represent specific events in the free radical initiation or ionization process, and the subsequent formation of degradation products following ionization or free radical formation.

Using G values, a demonstration of the effects of chemical structure on susceptibility to radiation-induced degradation can be made. Using G value data for linear polyethylene (PE), polypropylene (PP) and PMMA, the change in polymer radiation susceptibility with a change in polymeric structure can be demonstrated (Table 1.2).

The G values described in Table 1 compare the degradation products formed by polymers with a common, linear, saturated, carbon-carbon chain that differ by the side group moieties.[21]

The polyethylene structure is provided as the baseline polymer where no side groups are present, and the degradation product yields are represented by G(x) for crosslinking bond formation, G(s) for cleavage of the main chain (or scission), and $G(H_2)$ for hydrogen gas formation as a result of an elimination reaction along the main chain (or abstraction).

As side groups are added to the main chain, the formation of additional degradation products alters the yield values for $G(X,S,H_2)$ while adding the formation of other products from decomposition of the side chain itself. For polypropylene, the formation of methane, $G(CH_4)$, is accompanied by an increase in the G(s) value, a stable G(X) value and, as expected, a decrease in the $G(H_2)$ value. The degradation chemistry becomes more complex for PMMA, where the loss of the carboxy-methyl side chain, $G(-COOCH_3)$, and the sterically hindered pathway of the resultant, tertiary free radical intermediate to a crosslinked product, are thought to influence the preference for a scission-based degradation over crosslinking, and $G(H_2)$ is insignificant by comparison to polyethylene. The ratios of gamma-induced, main chain scission to crosslinking (G(S)/G(X)) for polyethylene, polypropylene and PMMA are 0.2, 1.1, and 10.0 demonstrating the influence of the side groups in linear polymers. Previous studies have

reported that the total dose (gamma radiation) required to achieve a significant change (25%) in the mechanical properties of is 3 x 10^8 rads for polyethylene, and 3 x 10^7 for polypropylene and PMMA.

Recent studies using E-beam and proton sources yielded G(-COOCH3) PROTON = 3.22 and G(-COOCH3) ELECTRON = 2.59 along with G(S) PROTON = 0.75 and G(S) ELECTRON = 0.46.[22] The variation in reported results illustrates the difficulty in defining a universal value for the radiation yield polymer degradation products. Several factors influence this variation. There is the inability to reproduce the precise fluence and flux spectrum of the designated space environment. There is also the influence of the stopping powers (H^+, e^-, vs. γ of the composite atoms and covalent bonds comprising the polymeric target sample that influence the evaluation of the polymer with respect to the depth of penetration of the particle or photon into the experimental target.[23, 24,25] In addition, there is the cumulative effect of the structural and tertiary structure of the polymer that effects the propagation reactions that follow the incipient formation of the radiation-induced reactive intermediate as the irradiation exposure continues to be applied to the target.

The affect of oxygen for polymers exposed to radiation in the presence of air is another consideration in radiation studies. The formation of alkyl radicals in the polymer chain can be scavenged by oxygen that has diffused into the polymer to a saturation level that is controlled by the crystallinity of the polymer and the ambient temperature and pressure of the surrounding air environment. The resultant peroxide radical intermediate products, formed by reaction of the alkyl radical with oxygen, decompose to form oxidized products from the carbon-carbon backbone of the main chain (alcohols, ethers, organic peroxides, aldehydes, carboxylic acids, along with carbon monoxide and carbon dioxide gas). A comparison of the affect of oxygen on radiation yield values for polyethylene, polypropylene and PMMA are presented in Table 4.1.

Polymer	G (H_2) in air	G (H_2) in vacuum
Polyethylene	4.0	3.7
Polypropylene	2.5	3.2
PMMA	0.4	0.3

Table 4.1. Radiation Yield Values (G) for Linear Polymers in Vacuum vs. Oxygen Atmosphere.

The degree of immobilization of the polymer chain decreases the yield of oxygen-based oxidation products in the decomposition of irradiated polymers. To minimize interference from oxygen in this study, a constant, high dose rate (>3 million rads/hr), and ambient constant temperature (below Tg) were used throughout the exposure period for the irradiated PMMA samples, and all samples were analyzed in a single batch analysis. [26,27]

The effect of average molecular weight on the physical properties of polymers has been reported.[28] The molecular structure of the monomeric unit and the length of the oligomeric chain influence segmental motion of the component atoms, and thereby alter the physical properties displayed by the polymer. Oligomeric chains of increasing length (higher molecular weight) influence the free volume of the polymer and will shift the glass transition temperature (Tg) to higher values.[29] An increase in the length of the side groups on the polymer chain can decrease the Tg value while the addition of a stiff, smaller group (phenyl or *tert*-butyl) will increase the polymer Tg.[30]

Previous work with respect to chain length attributes the decrease in Tg to the additional free volume that occurs at the end groups of the oligomers comprising the polymeric molecular structure. Analysis of narrowly dispersed, polymethyl methacrylate standards shows that the Tg varies as a function of molecular weight. Lower molecular weight materials have considerably more end groups that implies more free volume as addressed in the Fox-Flory equation (Eq. 4.1).[31]

$$T_g \sim T_{g\infty} - (K/M_n) \qquad (Eq.\ 4.1)$$

The chain scission mechanism of degradation reported for PMMA can lead to main-chain scission or loss of end groups. The free volume between the end-groups of oligomeric segments influences the free volume of the polymer. Longer polymeric chains undergo alignment and entanglement that reduces free volume and restricts mobility between chains. As ionization of the main chain segments of the oligomer occurs during irradiation, higher molecular weight oligomers with lower, main-chain segmental mobility have the potential for recombination.

PMMA can be synthetically prepared as narrowly dispersed, linear polymers with known average molecular weight (M_w) thereby enabling the evaluation of the effects of molecular weight on

main chain stability. The PMMA polymer chain is a preferred model compound for studying the effects of chain length on polymer stability in ionizing radiation. Simpler, straight chain aliphatic hydrocarbon chains display a higher radiation yield for elimination and crosslinking reaction products. The carboxymethyl side chain on the hydrocarbon backbone of the PMMA polymer predisposes the polymer chain to decomposition upon ionization by yielding methane and carbon dioxide gasses that diffuse into the polymer matrix and provide no opportunity for recombination of the side chain. The resultant main-chain tertiary radical decomposes into the scission products shown in Figure 4.2. The influence of the PMMA side chain in driving scission-based degradation permits a focused evaluation of the chain length as a structural feature in the stability of polymers. In this study, the effects of PMMA chain length in the scission yield and side chain loss were modeled and determined experimentally. The methods for the analysis of PMMA include gel permeation chromatography (GPC) for the determination of molecular weight and polydispersity values, Fourier transform infrared (FTIR) spectroscopy for the characterization of the chemical structure, and differential scanning calorimetry (DSC) for the assessment of glass transition temperatures. The final model defining the influence of PMMA molecular weight is developed on the basis of the radiation yield and the distribution of degradation products. The developed model is compared to the predicted degradation based on the empirical data reported to date and is discussed with respect to the chemical influence of chain interaction, chain length and free volume.

Experimental

The PMMA polymers used for this study were certified reference standards prepared by Polymer Source (Province of Quebec, Canada) and Scientific Polymer Products, Inc. (Ontario, NY). The data for each sample has been presented n Chapter 3.0.

FTIR spectra for all PMMA samples were obtained using a BIORAD FTS 40 FTIR spectrometer equipped with a mercury cadmium telluride detector and a Thermo-SpectraTech single-reflection attenuated total reflectance (ATR) assembly. The co-added spectra were collected and averaged over 100 scans at a range of 4,000 – 750 cm^{-1} at 1 cm^{-1} resolution. Samples were analyzed as

neat powders supported on a spherical diamond single crystal and held in point-to-point contact by a standard-tipped pressure tower. The spectral range affected by the diamond itself (2700 – 1800 cm-1) did not overlap the spectral bands of interest for the PMMA samples).

The glass transition (Tg) measurements for all PMMA samples in this study were obtained by differential scanning calorimetry (DSC) using a Perkin-Elmer Series 7 Thermal Analysis System. The Tg values were assessed by semi-automated determination of the half-step height temperature between the onset and peak of the heat flow curve (half vitrification). Powder samples (5 – 16 mg) from the standard and irradiated powders were weighed into open aluminum pans and analyzed by the following thermal profile. All samples were analyzed under nitrogen purge gas. The thermal profile began at 25°C, heated from 25°C to 150°C at 10°C/min., held at 150°C for 5 min., then cooled from 150°C to 25°C at 10°C/min. The samples were reheated from 25°C to 150°C at 10°C/min. and any transitions were measured and recorded.

The gel permeation chromatography (GPC) was performed using a Dynamax UV-1 liquid chromatograph equipped with an ultraviolet detector (λ = 254 nm). Separations were performed with a Waters Styragel HR 4E; 7.8 x 300 mm GPC Column with 5μ rigid particle packing having 16,000 plates per column using THF solvent [Burdick and Jackson High Purity UV – Grade]. The LC Flow Rate was 1.5 ml / min. using a back-pressure of 400 psi. PMMA samples were dissolved in THF. Sample concentrations for Mw less than 25,000 g/mole were 0.25 % by weight. Sample concentration for PMMA with Mw greater than 25,000 g/mole were 0.10 % by weight. The sample injection size was 20 μL. Calibration was conducted with polystyrene standards.

PMMA samples where irradiated in air with a gamma irradiator using a Shepherd 484 Cobalt-60 nuclide source (Co^{60}). The Co^{60} nuclide source was calibrated with a Victoreen 570 with 621 ion chamber secondary standards. The Co^{60} provides γ photons in the range of 1.17 MeV to 1.33 MeV. The 12,000 Curie (Co^{60}) *g*source uses twin Co^{60} cells (6,000 Ci each) with a sampling area of 7.5" x 7.5". The samples were irradiated to three levels: 40, 80 and 120 Mrads at a dose rate of (26,759 rads (Si)/min).

Results and Discussion

GPC Analysis and Radiochemical Yield Data

In any ground-based study for the simulation of total dose deposition in materials, there are assumptions that must be made regarding the annealing effects for the resultant reactive intermediates that can persist over the mission life that have not been characterized in ground simulation. The assumption is made, in this study, that the PMMA scission and side-group degradation mechanisms and the G values observed for the ground-based simulation are similar to the long-term, in-flight degradation chemistry of PMMA.

Using this assumption, the predicted radiation-induced degradation for a linear PMMA polymer series can be modeled using the G values and total dose absorbed by one gram samples of the polymer. The current study evaluates four PMMA samples of differing Mw (Table 4.2).

Mw	Mn	Mw/Mn
6458	6025	1.07
18463	17894	1.03
60170	57899	1.04
145062	130396	1.11

Table 4.2. M_w Properties for PMMA Standards.

Using the G values for PMMA (Table 1.2), an expected new Mw distribution based on the composite radiation yield values can be prepared for each PMMA standard. This is discussed in the pages that follow. In assessing the contributions for each degradative pathway, with respect to

molecular weight, the radiation yield at a specific total dose of 120 Mrads can be determined (Eq. 4.2) as a function of molecules per gram of PMMA (Table 4.3) .

Charlesby, Saito, and others[16-20] have used the randomness of ion formation in a single volume of bulk polymer under exposure to radiation. The assumption is important when studying the expected degradation for different molecular weights of a polymer. To illustrate, a planar layout of a fully extended PMMA molecule (Mw 145,062) is partitioned into three additional sectors representing the relative chain lengths of the other lower Mw standards used for this study (Figure 4.3). Ziegler, et. al.[32], has demonstrated the uniformity of flux for high energy particles incident to a solid surface, and through the use of TRIM and CASINO analysis, it was determined that the field would be uniform (random) throughout the small (100 – 200 micron) spherical solids comprising the PMMA standards used for this study.

Dose (eV/gram) x G/100 eV = Molecules or chain events produced/gram of material (Equation 4.2)

	G VALUES	Gs	Gx	GH_2	G-$COOCH_3$
		1.2	0.2	0.4	1.0
Mw	# molecules/ gram	# of scission/ molecule	# of crosslinks/ molecule	# of hydrogen molecules/molecule	# of carboxymethyl side groups lost/molecule
6458	9.3×10^{19}	0.15	0.03	0.06	0.13
18463	3.3×10^{19}	0.44	0.07	0.14	0.36
60170	1.0×10^{19}	1.44	0.24	0.48	1.2
145062	4.1×10^{18}	3.51	0.59	1.18	2.93
Note: Values are based on 120 Mrads total dose absorbed by one gram PMMA					

Table 4.3 Predicted Degradative Events/molecule of PMMA for 120 Mrads Total Dose.

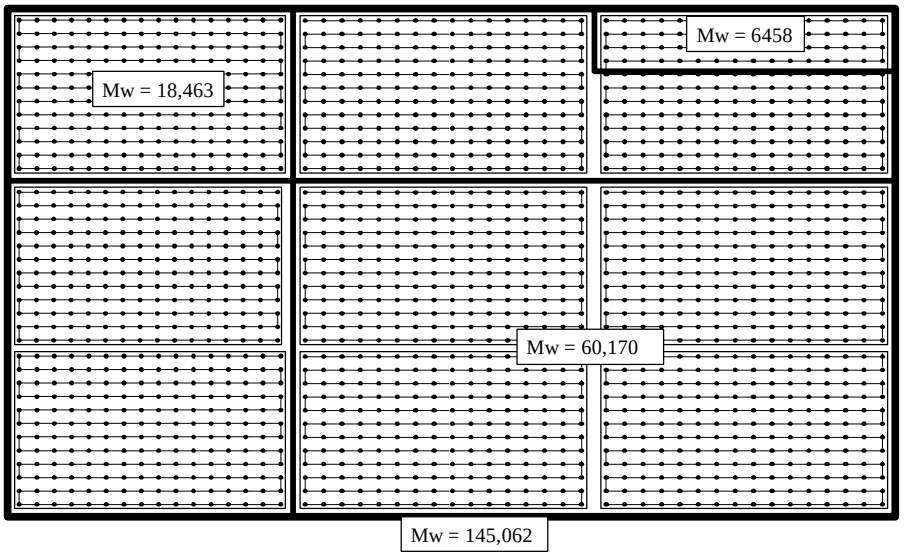

Figure 4.3. Partitioned 142K Mw PMMA Chain Illustrating the Probability of Scission for Three G-Based Scission Events per 147K Mw Single Chain at 120 Mrads Total Dose.

G values report chemical degradation events per gram of material. This suggests for a specific total dose (e.g. 120 Mrads), most smaller chains remain relatively unaffected compared with longer chains that are vulnerable to multiple scissions on each chain comprising the bulk polymer (As shown in Figures 4.4 to 4.7).

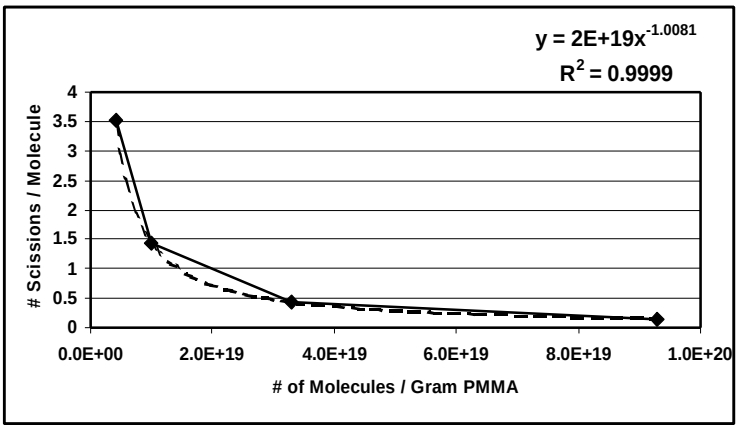

Figure 4.4. Predicted Scission Events/Molecule of PMMA for 120 Mrads Total Dose.

[Solid line and diamond are experimental – Figures 4.4 to 4.7]

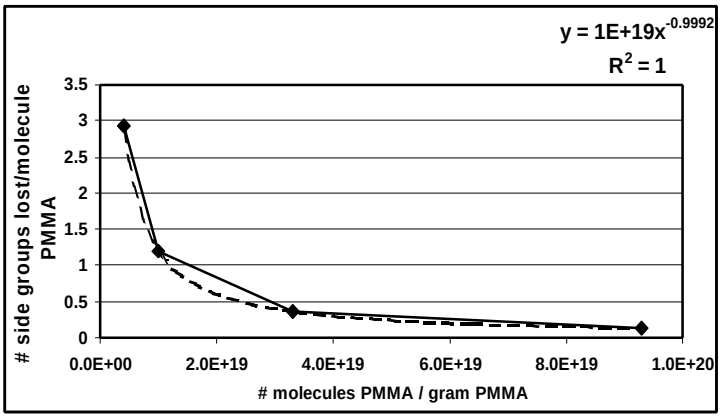

Figure 4.5. Predicted Decarboxylation Events /Molecule of PMMA for 120 Mrads Total Dose.

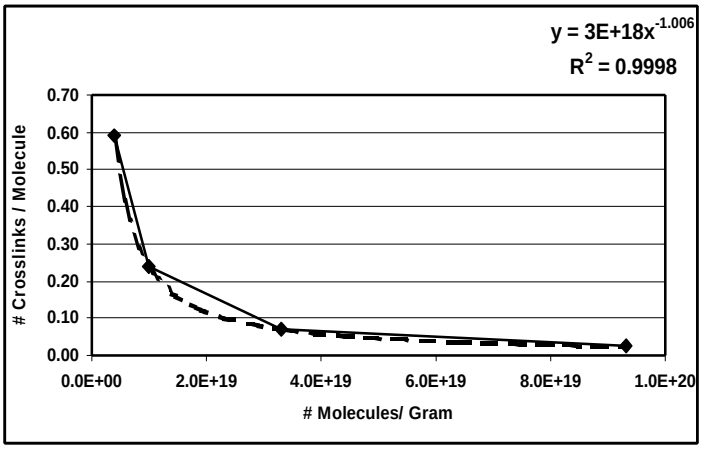

Figure 4.6. Predicted Crosslinking Events/Molecule of PMMA for 120 Mrads Total Dose.

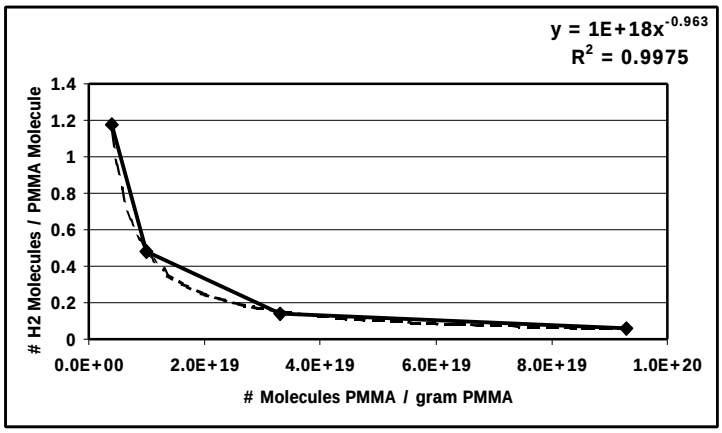

Figure 4.7. Predicted H_2 Events/Molecule of PMMA for 120 Mrads Total Dose.

Using what is known about the scission process for PMMA, the G-Value and GPC data can be used to complete the modeling process for narrow partitions of a Gaussian distribution of narrowly dispersed 6450 Mn PMMA standard. For scission reactions, as one assumes that the scission is random along the PMMA chain segments, then the counts (CTs -peak height) for the GPC partitions are useful in validating random scission along the chain. Using peak height as a measure of chain length, the equation for scissions/molecule as a function of CTs (assuming that the fragmentation is equally probable at all segments (Figure 4.8)) the new distribution of peak heights can be determined (Equation 4.3 – where X is the number of molecules of PMMA per gram of polymer). Molecular weights below the lower limit of the initial Mw distribution increase in the same number of fragments, but not in total number of absorbing segments. The results of the GPC:G-value-based modeling are presented step-wise as follows.

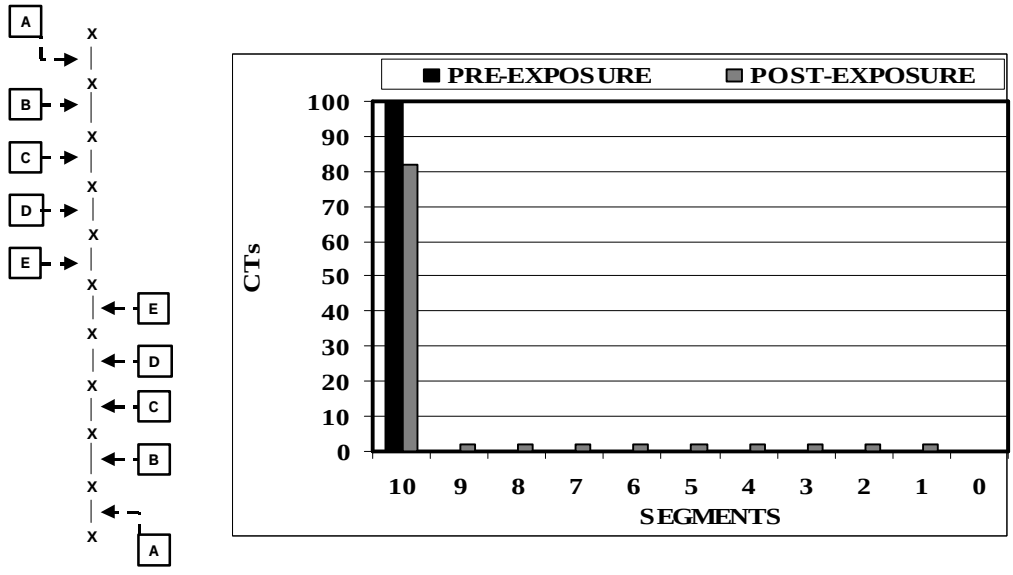

Figure 4.8 Illustration of Random Chain Scission of a Single Mw Oligomer W/ Fragment Distribution.

*# Scissions per Molecule = S = (2 x 10^{19}) * X$^{1.081}$ (Equation 4.3)*

In Figure 4.8 the PMMA oligomer is assumed to fragment with equal probability at any segment on the mainchain. The fraction of CTs lost from the affected PMMA chains for each Mw partition is determined using Equation 4.3. The resultant fragments are evenly distributed to the successive series of shorter chains continuing to the monomer CTs [Primarily from end group loss]. Therefore, in conjunction with the G-value based loss in counts for each Mw partition, there is a cumulative effect of fragments from successively higher Mw partitions that are evenly apportioned to each successively lower Mw partition (Figure 4.9). The distribution of fragments and the associated increase in CTs per partition remains constant over each partition as the molar weight of the partition increases in proportion to the value of S. As the S approaches one, all molecules in the molar weight partition undergo scission. As the value of S exceeds one, a reiterative, integral process is applied to successive fragment distributions.

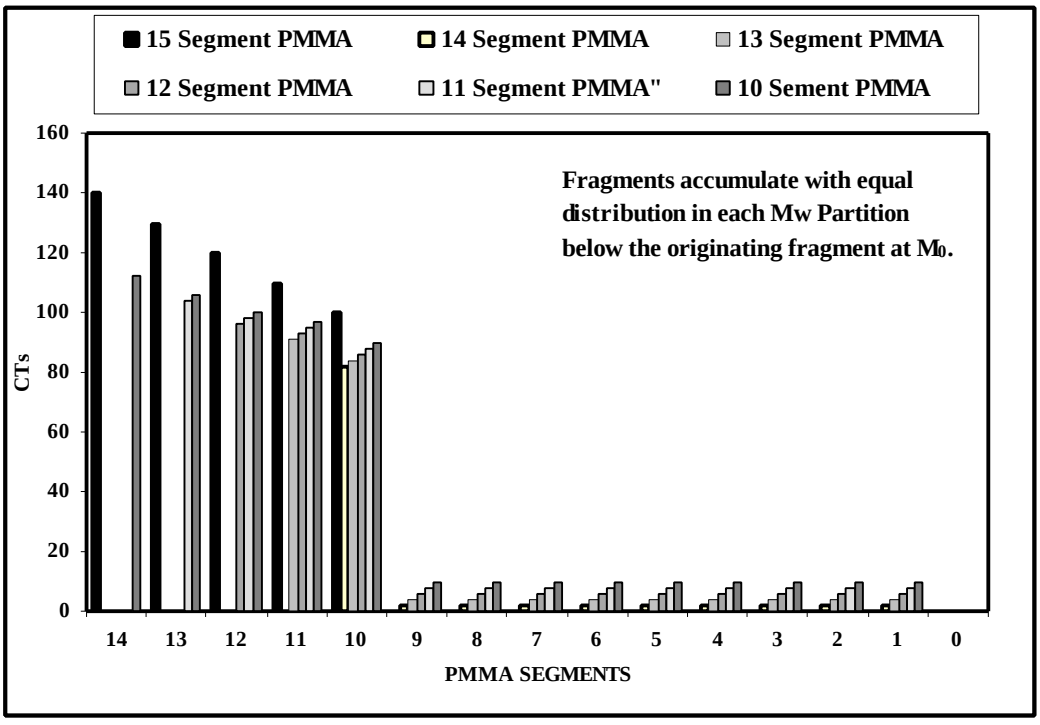

Figure 4.9 Demonstration of the Accumulation of Fragments at Lower Molecular Weights.

Based on the predicted scissions per molecule, the loss of the carboxymethyl side group (G-$COOCH_3$ = 1.00) leads to a proportionate reduction in the GPC response for the affected fraction of oligomers at each molecular weight. The loss of a side group on a single segment of the oligomeric chain does not affect the GPC elution time significantly, and therefore the Mw distribution following absorbed dose of 120 Mrads is only diminished in the peak intensities for the original molecular weight distribution due to loss of the absorbing carbonyl of the ester moiety (Figure 4.10). The predicted affect of hydrogen abstraction is shown in Figure 4.11 where, again, there is little change to the molecular weight distribution based on the loss of hydrogen. The affect of crosslinking shown in Figure 4.12 displays a modest increase in higher molecular weight fractions, but still retains much of the original distribution. The scission component and the composite distribution predicted by the collective radiation yield are shown in Figures 4.13 and 4.14 respectively. Gel permeation chromatography (GPC) results provided the weight average molecular weight values (M_w) and dosimetry yielded the total dose values (D in eV units) to calculate the G(s) values (scissions per 100 rads) summarized in Table 4.4. The experimental Mw distribution is included as a comparison to the predicted distribution.

Compliance with Predicted G-Based Modeling

Using the scission equation only (Eq. 4.4), similar comparisons were made between projected composite degradation and the experimental Mw change for the higher molecular weight materials (Figure 4.14-4.16).

$$m_{Ir} = m_I - [m_{I-} (m_I [k_s(N_A/M_I)^{-1.0081}])] \qquad (Eq.\ 4.4)$$

The G(s) values were calculated using the established radiochemical yield equation.. No detectable evidence of crosslinking was observed in the GPC data, and the G(x) term is thereby set to zero yielding Equation 4.5.[16]

$$G(s) = \frac{\left[\frac{1}{M_w} - \frac{1}{M_{w\,0}}\right]}{(D/100\ N_A)} \qquad \textit{(Eq. 4.5)}$$

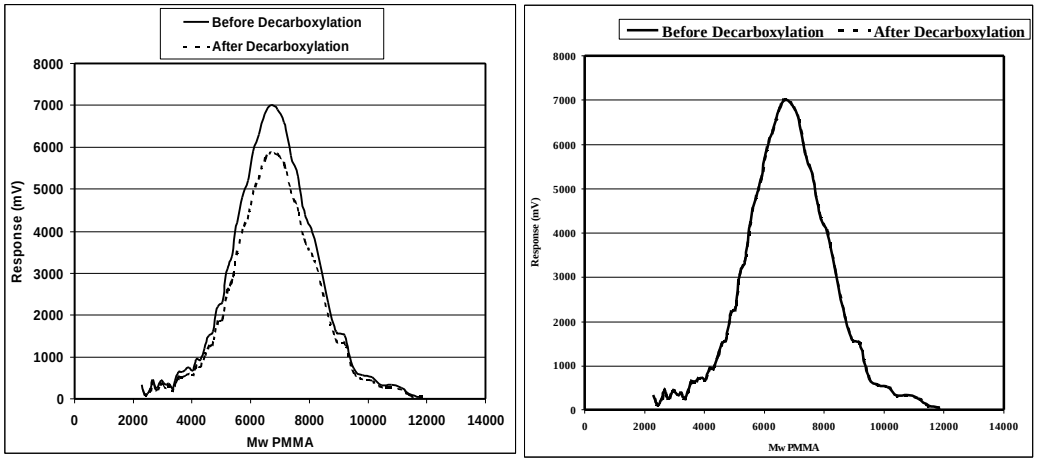

Figure 4.10. Predicted Affect of Radiation-Induced Decarboxylation on PMMA 6450 Mw [120 Mrads]. Left: Predicted number of chains affected. Right: Actual impact to GPC peak height.

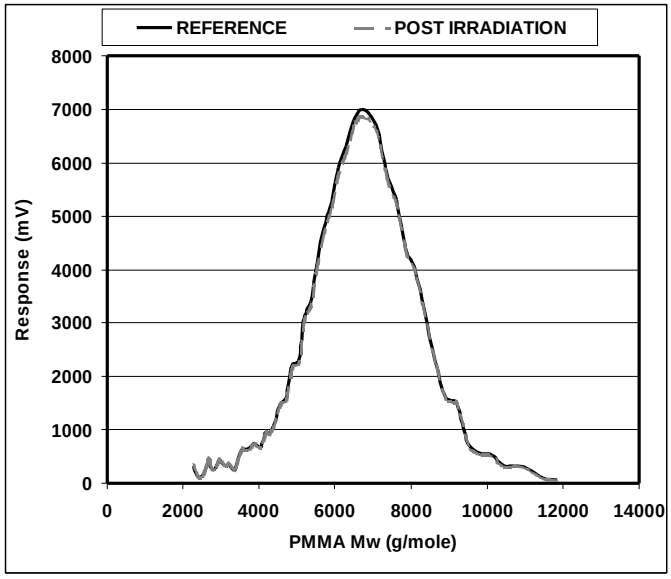

Figure 4.11. Predicted Number of Affected Chains for Radiation-Induced H_2 Abstraction on PMMA Mw 6450 [120 Mrads].

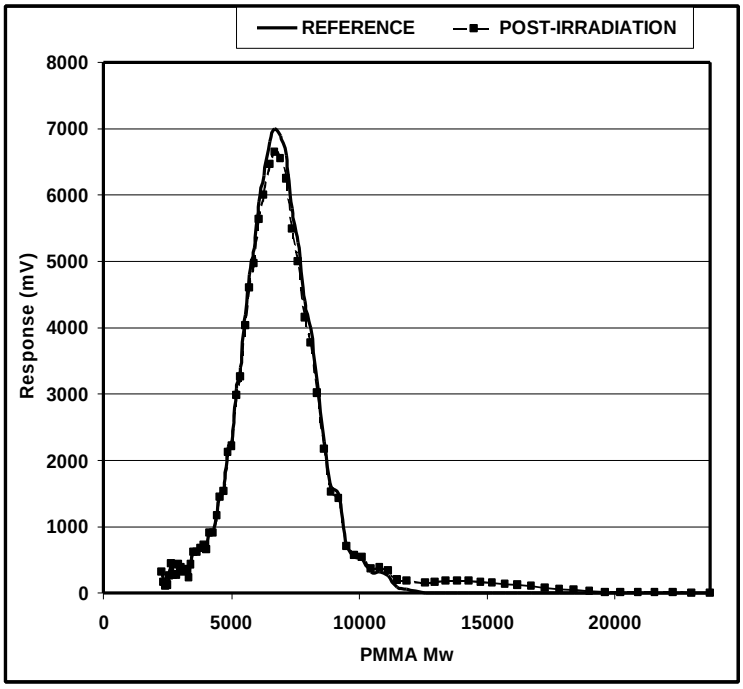

Crosslinking

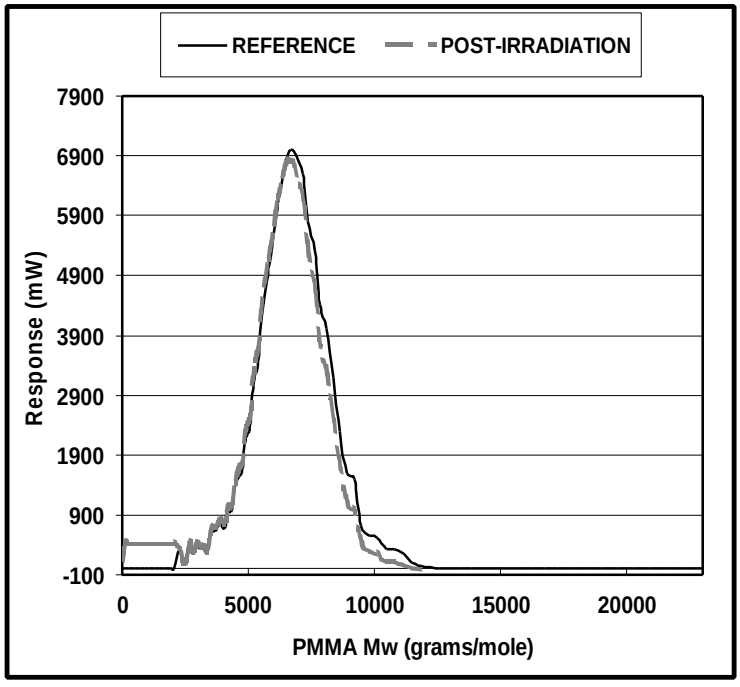

Scission

Figure 4.12. Predicted Affect of Radiation-Induced Scission and Crosslinking on PMMA Mw 6450 [120 Mrads].

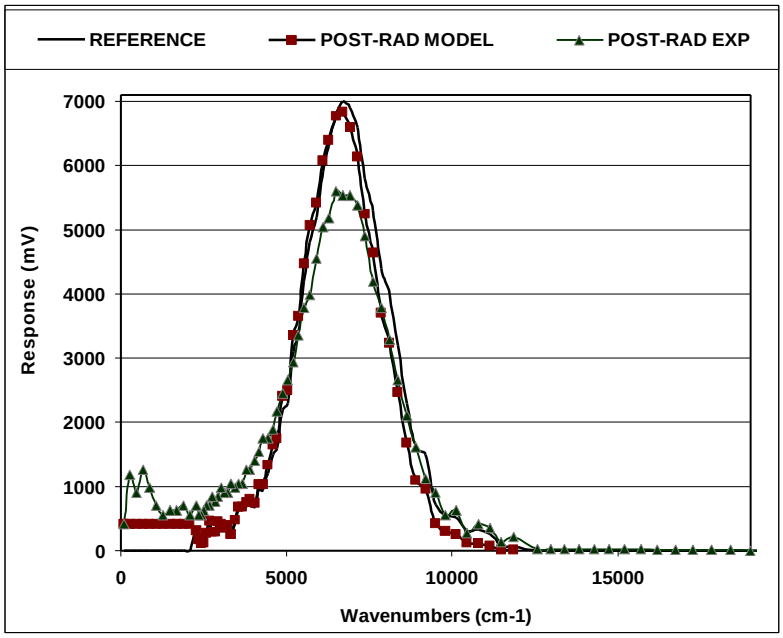

Figure 4.13. Predicted Composite Affect vs. Experimental Data PMMA Mw 6450 [120 Mrads].

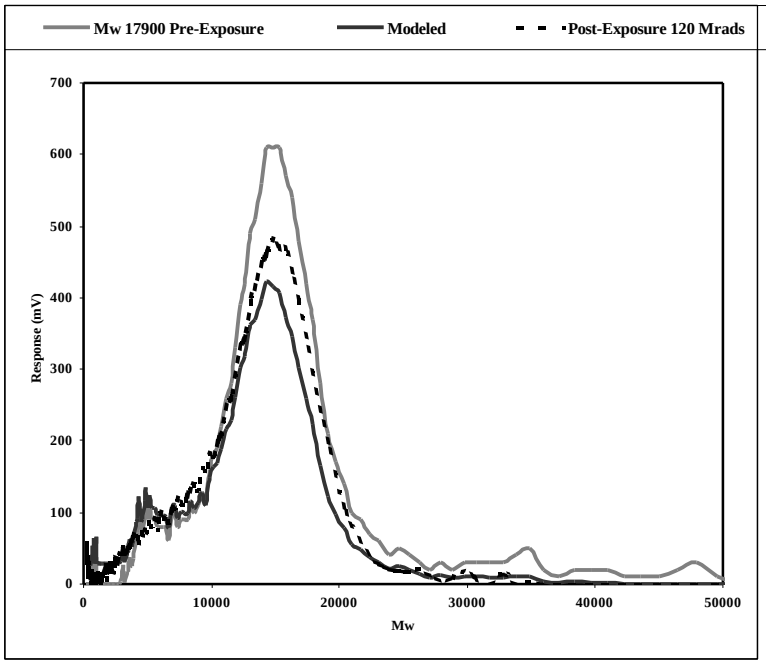

Figure 4.14. Predicted Scission vs. Experimental Data PMMA Mw 17,900 [120 Mrads].

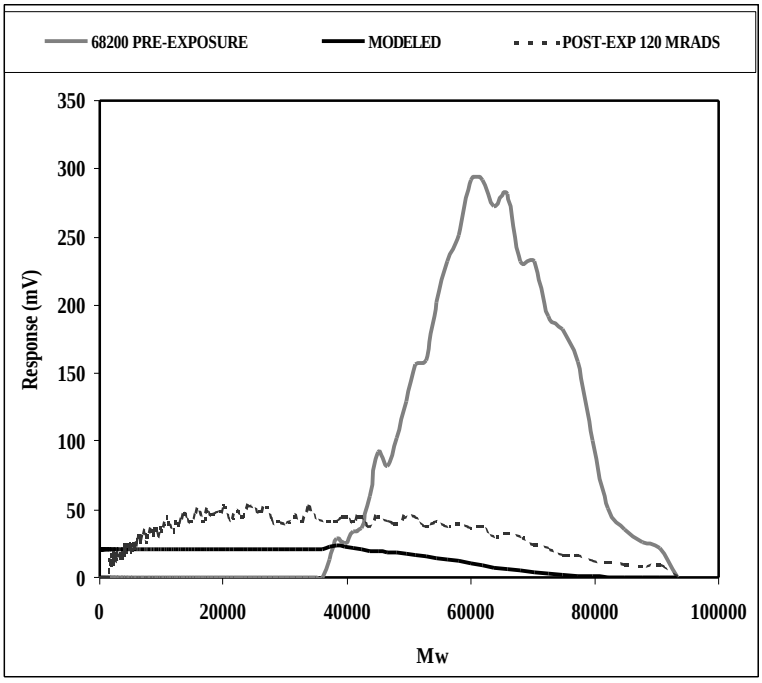

Figure 4.15. Predicted Scission vs. Experimental Data PMMA Mw 68,200 [120 Mrads].

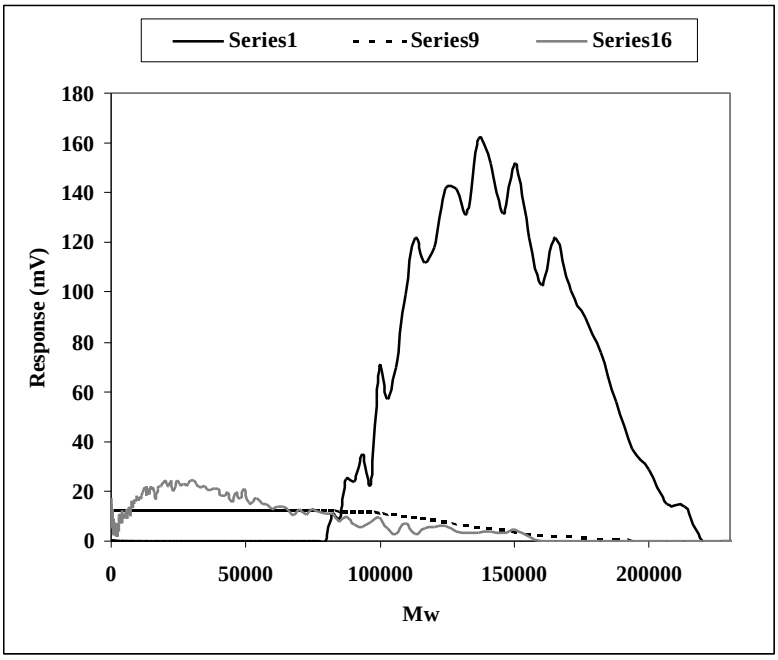

Figure 4.16. Predicted Scission vs. Experimental Data PMMA Mw 147,100 [120 Mrads].

Dose (rads - Si)	G(s)	Mw_x	Mw_0	N_a	D (eV)
0	N/A				
4.00E+07	1.86	5338	6726	6.02E+23	2.50E+21
8.00E+07	0.58	5789	6726	6.02E+23	4.99E+21
1.20E+08	1.57	4062	6726	6.02E+23	7.49E+21
0	N/A				
4.00E+07	0.91	11792	15165	6.02E+23	2.50E+21
8.00E+07	0.45	11841	15165	6.02E+23	4.99E+21
1.20E+08	0.36	11333	15165	6.02E+23	7.49E+21
0	N/A				
4.00E+07	0.41	41079	62837	6.02E+23	2.50E+21
8.00E+07	0.42	29824	62837	6.02E+23	4.99E+21
1.20E+08	0.37	25748	62837	6.02E+23	7.49E+21
0	N/A				
4.00E+07	0.46	60353	143620	6.02E+23	2.50E+21
8.00E+07	0.40	42485	143620	6.02E+23	4.99E+21
1.20E+08	0.41	30892	143620	6.02E+23	7.49E+21

Table 4.4. Mw, D and G(s) Values for Gamma-Irradiated PMMA.

The terms Mw_0 and Mw are the pre- and post- Mw distribution respectively. N is Avagadro's number. The higher Mw PMMA G(s) values compare well to values reported by previous investigators for samples in air (G(s) = 0.6 – 0.85).[33] For lower Mw PMMA (6726 to 15,165), the scission rate is higher. Graphical analysis of the GPC data yields the integrated second order rate equation (Equation 5), where k is in units of moles per $gram^{-1}$ per hr^{-1}

$$\frac{1}{Mw} = kt + \frac{1}{Mw_0} \qquad \textit{(Eq. 5)}$$

The equations describing the rate of degradation in Figures 4.17 display good correlation coefficients. From the equations, a comparison of the scission rate for the linear series of PMMA samples demonstrates that the rate increases as the chain length decreases. The second order character of the reaction would suggest that more reagent is available for scission as the chain length decreases.

Role of End-Groups and Free Volume

The GPC data also suggests that end-group loss is the preferred path of degradation where low molecular weight, monomeric fractions appear at high elution times that has also been observed using

MALDI–MS by our laboratory.[34] The monomeric fragments indicate a depolymerization at the terminal ends of the polymer chains that correlates well with the negatively skewed distribution and widened PD values of the symmetrically distributed, pre-radiated standards (Figure 4.16). Further, random main-chain scission would lead to a flat distribution of polymer segments with high kurtosis as observed with the higher molecular weight PMMA samples.

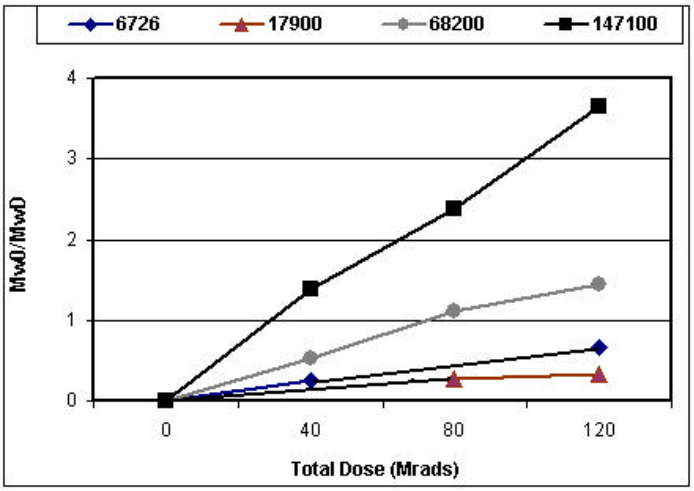

Figure 4.17. PMMA Mw vs. Total Dose (Rad Si).

The rate constant increases significantly as the PMMA molecular weight approaches Mw = $1x10^4$ chain length as the number of end-groups per unit mass of linear PMMA polymer decreases (Table 4.5). The change in rate constant coincides with a rapid change in the pre-radiated and post-irradiated values of the Tg of the PMMA samples (Figure 4.18). The effect of the free volume present at the end-groups of the PMMA polymer reaches a critical value for the total free volume in the PMMA polymer.

Mn	End Groups / gram PMMA	Rate constant (25°C)
6,726	1.79×10^{20}	1×10^{-6}
15,165	7.94×10^{19}	3×10^{-7}
62,837	1.92×10^{19}	3×10^{-7}
143,620	8.38×10^{18}	3×10^{-7}

Table 4.5. Comparison of Rate Constants vs. End Group Units/gram of PMMA.

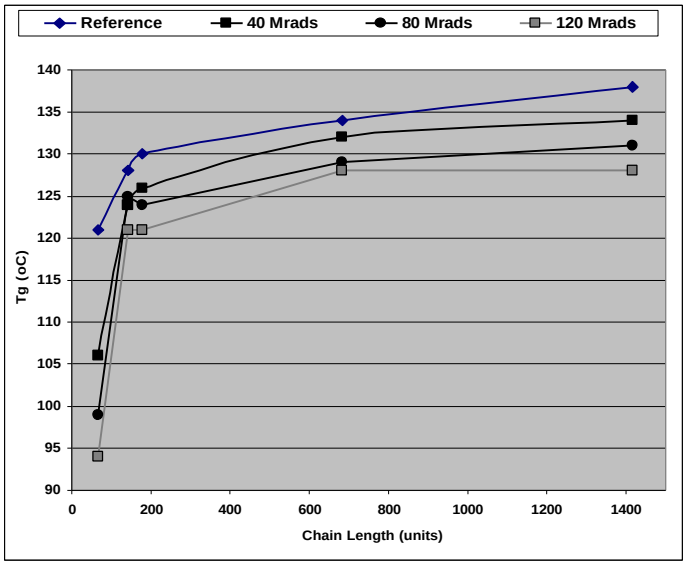

Figure 4.18. Changes in Tg vs. PMMA Chain Length and Total Dose.

At temperatures below the Tg, limitations in molecular motion (relaxations) are driven by higher activation energy (ΔH_a) for the segments of a polymer chain as a function of chain length. The limitation in motion is attributed to diminishing free volume that is associated with an increase in molecular weight. The change in ΔH_a expressed in kcal/mole for the irradiated PMMA polymers under this study can be determined using the Williams-Landis-Ferry (Eq. 4.6) and the Tg values as summarized in Table 4.6. Here, temperature is in Kelvin, R is the gas constant (1.99×10^{-3} Kcal/^{o}K.mole), C_1 and C_2 are universal constants (-17,44 and 51.6 ^{o}K respectively) for a wide range of polymers. The C_1 constant has importance in assessing the fractional free volume (f_g) in the glass transition region where $f_g = B/(2.303 \times C_1)$, and B is unity.[35] The C_2 constant is used to determine the CTE of a polymer using the fractional free volume [$a_f = f_g/C_2$].

$$DH_a = 2.303\left(\frac{C_1}{C_2}\right) RT_g^2 \qquad \textit{(Eq. 4.6)}$$

The expected, proportionate decrease in the ΔHa value as the linear PMMA series approaches lower Mw is observed. In addition, the PD values increase most significantly for the lower Mw PMMA series. The data shows that a preference for end-group scission is in effect. Random main chain scission would lead to broader PD values and would progressively expand the PD values for the high Mw PMMA series. The preferential loss of end-group segments of the PMMA chain is driven by the free volume and unoccupied volume associated with end-groups.

Mw	Pre-Exposure	Mw40	40 Mrads	Mw80	80 Mrads	Mw120	120 Mrads
	ΔHa(Kcal/mole)		ΔHa(Kcal/mole)		ΔHa(Kcal/mole)		ΔHa(Kcal/mole)
6458	240	4675	222	4583	214	3807	209
18463	252	16480	247	14170	244	13007	240
60170	257	56241	254	34916	250	23738	249
145062	262	68535	257	39363	253	29600	249

Table 4.6. ΔH_a Values (Kcal/mole) at T_g vs. Mw vs. Total Dose for PMMA.

Previous reports describing the role of decarboxylation of the carboxyalkyl side groups in the main chain scission of poly (alkyl methacrylate) is thought to drive random main chain scission in PMMA that has been exposed to high energy photons (γ radiation).[36] The ratio of main chain scission to pendant ester scission is typically very high (50:1). However, the Mw distribution data for this investigation suggests that the effect of a higher scission rate is observed at the end-group moieties and not in the random segments of the main chain polymer. The observation helps to explain the higher G(s) values and observed for the lower Mw PMMA samples and the lower apparent rate of reaction (k) for the higher Mw samples.[37]

The data further shows that the overlapping, entangled segments of longer chains in the higher Mw PMMA polymer are limited in motion as intermediate ionic species are formed following irradiation. The ionic intermediates formed in the motion-restricted segments prefer the lower entropy and lower enthalpy path of chain abstraction to the formation of two products in the limited free volume of the main-chain. The lack of a random pattern of chain scission segments in the GPC results supports this conclusion.

The FTIR results would confirm decarboxylation and the formation of unsaturated carbon-carbon bonds to support the preferred abstraction path. To confirm the extent of decarboxylation and abstraction in the bulk polymer sample, FTIR spectra were compared for the PMMA reference and post-irradiated materials. The assignments for key pre-exposure absorption bands are presented in Chapter 3.0. The projected post-irradiated PMMA absorbtion bands following 120 Mrads total dose accumulation are presented in Figure 4.19.

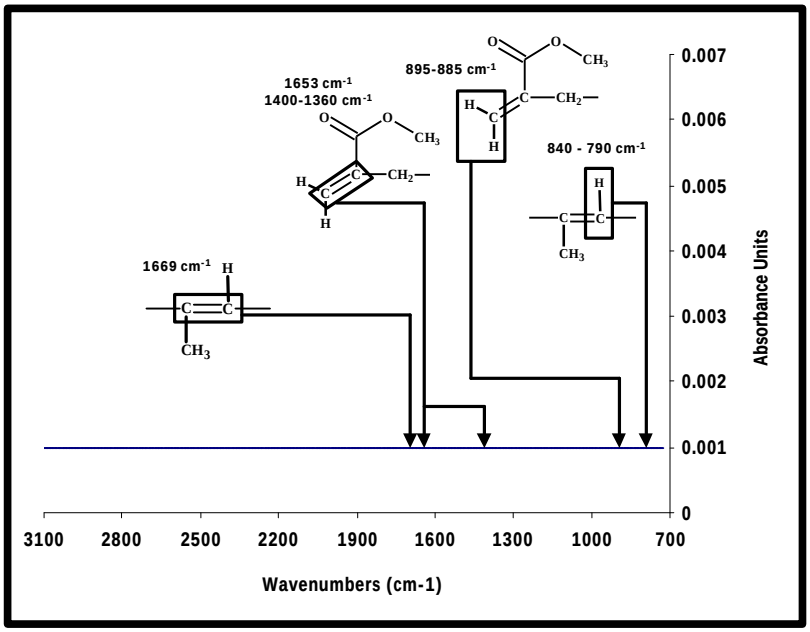

Figure 4.19. Projected FTIR Bands for Observation of Alkenyl PMMA Degradation Products.

The use of the single-bounce ATR method permitted analysis of the relative peak intensities of the PMMA structure by FTIR without concern for linearity affects due to sample thickness or stress-induced distortion of IR bands due to plastic deformation of high-stress pellets or wafer samples. The ATR method used for this study evaluated the surface of the powder samples held in contact against a conical diamond window. The method was repeatable in the duplication of the relative intensity of IR

bands for the PMMA samples. The method also provided sufficient energy to yield distinctive peaks for the identification of the decomposition bands described in Figure 4.19.

The pre- and post-exposure spectra for the Mw = 6450 PMMA sample provided no apparent evidence of peak distortion. There was strong evidence for the decarboxylation in comparing the bands for the carbonyl double bond 1732 cm^{-1} and cluster bands (1360 – 1108 cm^{-1}) for the main-chain vinyl carbon-carbon bonds, acyl-oxy and methoxy carbon-oxygen bonds (Figure 4.20). The loss is progressive throughout the radiation regime at 40 Mrads and 80 Mrads total dose.

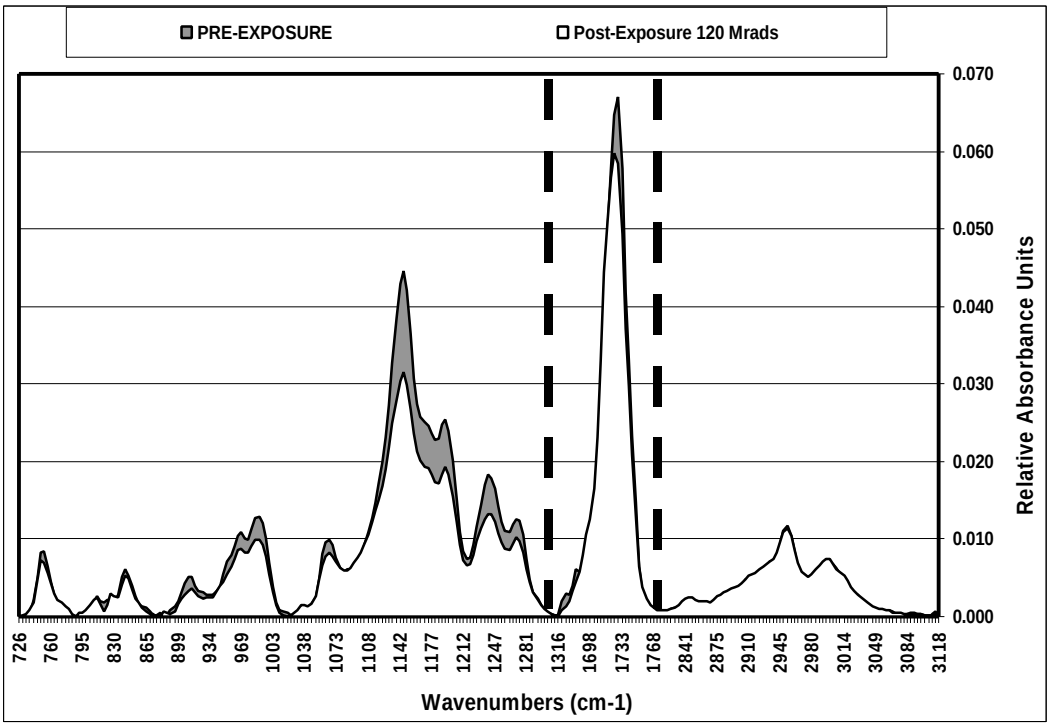

Figure 4.20. Comparison of the Pre- and Post-Exposure (120 Mrads) FTIR Spectra Highlighting PMMA Decarboxylation .

The FTIR data for higher molecular weight PMMA samples displays a more random distribution of relative peak height ratios (Table 4.7). This is to be expected when scission and decarboxylation ratios approach unity as previously reported for higher Mw PMMA. [32]

PMMA Mw	Pre-Exposure	40 Mrads	80 Mrads	120 Mrads
6726	5.8	5.5	5.3	5.2
15165	6.5	6.7	6.3	7.1
62837	6.1	7.1	6.3	7.2
143620	6.6	-	6.3	7.3

Table 4.7. Varying Ranges of SB-ATR-FTIR Absorbance Ratios (C-H 2952 cm^{-1}/C=O 1728 cm^{-1}).

Conclusions

Previous modeling studies to date[34] use two working ranges with respect to projecting and validating the predicted G-based molecular weight distributions. One group of modeling studies evaluates the liquid polymer using the viscoelastic region of the viscosity to assess crosslinking behavior using gel point. G-values for polymers in the liquid state are significantly higher than those for the solid state (e.g. 10:1). For space applications, the need of liquid state polymer modeling is not as prevalent as polymers in the solid state. The modeling studies carried out for higher molecular weight polymers are subject to multiple events per molecule, and have less free volume leading to a higher probability of recombination by chains that are highly restricted in segmental and rotational motion. The modeling studies do not address the intermediate molecular weight linear range of the Fox-Flory function (Eq. 2). This study has evaluated a solid polymer that displays high preference for scission-based main-chain degradation in this region.

The results show that the region displays a significant effect from Mw through free volume effects for radiation-induced, scission in a linear series of polymer Mw. The effect of depropagation and end-group population in the represents a region of interest for modeling polymer degradation behavior with respect to stability of physical properties in space missions. The results have shown that the partitioning approach to modeling random, scission-based degradation enables a closer evaluation of the events in progress throughout the Mw distribution range of the polymer. The experimental chromatographic data complements the partitioning approach to modeling degradation by reporting the composite yield following all degradation events. The comparison of the modeled and experimental partitioning results illustrate degradation information beyond current modeling methods by introducing

the introduction of factors for conformational energy, end-group population, density, depropagation, thermal effects, oxygenation and free volume, and permits the introduction of these factors into the modeling formula for each Mw partition.

References

1. *Space Vehicle Mechanisms*; Conley, P. L., Ed..; John Wiley & Sons: New York, 1998, p. 621.

2. *The Effects of Radiation on Electrically Insulating Materials*; Hanks, C. L. and Hammon, D. J.; REIC Rep. 64, Battelle Memorial Institute, Columbus, OH, 1969.

3. *An Overview of the First Results on the Solar Array Materials Passive LDEF Experiment (SAMPLE), A0171*; Whitaker, A. F.; LDEF – 69 Month in Space-First Post Retrieval Symposium, NASA CP-3134, June 1991.

4. *Space Environmental Effects on Materials*; Swinghamer, R. J., NASA-TM-78306, Marshall Space Flight Center, Huntsville, AL, Aug. 1980.

5. Schnitzer, F., et. al., *Proc. Of the 8th International Plastic Optical Conference '99*; Chiba, Japan; 1999, pp. 209-212.

6. Harmon, J. P., et. al.; *American Chemical Society Symposium Series 620*; Clough, R. L. and Shalaby, S. W., Eds.; American Chemical Society, Washington, D.C., 1996, p. 302.

7. Taylor, E. W.; "Space and Enhanced Radiation Induced Effects in Key Photonics Technologies"; *IEEE Aerospace Conf. Proc.;* ISBN 0-7803-5427-3, Snowmass, CO, March 1999.

8. Reich, Leo, and Stivala; et. al.; *Elements of Polymer Degradation*; MacGraw Hill Book Company, 1971, p. 31.

9. Siedle, A. H. and Adams, L.; *Handbook of Radiation Effects*; Oxford University Press, New York, 1993.

10. Williams, F.; *Radiation Chemistry of Macromolecules Volume I*; Dole, M., Ed.; Academic Press, New York, 1972.

11. Charlesby, A.; *Atomic Radiation and Polymers*; Permagon, Oxford, 1960.

12. Charlesby, A. and Thomas, D. K.; *Proceedings of the Royal Chemical Society of London, Series A, Mathematical and Physical Sciences*; 1954, *223*, 1154, p. 392.

13. Sawyer, D. M. and Vette, J. I.; *AP8 Trapped Proton Environment for Solar Maximum and Solar Minimum*; NSSDC-76-06, National Space Science Data Center, Greenbelt, MD, 1976.

14. *AE8 Trapped Electron Model*; National Space Science Data Center, NASA-Goddard Space Flight Center, Greenbelt, MD, 1989.

15. Seltzer, S.; NBS Technical Note 1116, *SHIELDOSE: A Computer Code for Space-Shielding Radiation Dose Calculations*, National Bureau of Standards, Washington, D.C., 1980.

16. Charlesby, A., et. al.; *Proceedings of the Royal Chemical Society of London, Series A, Mathematical and Physical Sciences*, 1954, *224*, 1156, p. 120.

17. Saito, O.; *Radiation Chemistry of Macromolecules Volume; I*Dole, M., Ed.; Academic Press, New York, 1972.

18. O' Donnell, J. H., et. al.; *Macromolecules*, 1979, *12*, 113.

19. Wolf, B. A.; *Macromolecules*, 1981, *14*, 654.

20. Kashiwagi, T., Et. al.; *Macromolecules*, 1986, *19*, 2412.

21. Dole, M.; *Radiation Chemistry of Macromolecules Volume; I*Dole, M., Ed.; Academic Press, New York, 1972, p 3.

22. Moore, J. A. and Choi, J. O.; *American Chemical Society Symposium Series 620*Clough, R. L. and Shalaby, S. W., Eds.; American Chemical Society, Washington, D.C., 1996, p. 156.

23. Anderson, H. H. and Zeigler, J. F.; *The Stopping and Ranges of Ions in Matter*, Permagon Press, NY, 1977.

24. Garth, J. C. and J. R. Turinetti, *IEEE Transactions on Nuclear Science*, *44*, 6, 1977, p. 2058.

25. Wall, L. A. and Brown, D. W.; *Journal of Research for the National Bureau of Standards*, 57, 30, 1956, p. 131.

26. Wall, L. A. and Brown, D. W.; *Journal of Physical Chemistry 61*, 2, 1957, p. 129.

27. Gillen, K. T. and Clough, R. L.; *Irradiation Effects on Polymers*, Clegg, D. W. and Collyer, A. A., Eds.; Elsevier Applied Science, Oxford, 1991, p.157.

28. Hill, D. J. T., et. al.; *American Chemical Society Symposium Series 620*Clough, R. L. and Shalaby, S. W., Eds.; American Chemical Society, Washington, D.C., 1996, p. 130.

29. Gedde, U. W.; *Polymer Physics*, Chapman & Hall, London, 1995.

30. Hill, D. J., et. al.; *Journal of Applied Polymer Science*, 1996, *59*, 589.

31. Fox, T.G.; *Bulletin of the American Physical Society*, *1*, 1956, 123.

32. Ziegler, J. F. et. al.; *The Stopping Range of Ions in Solids*, 1985, Pergamon Press, New York.

33. Wall, L. A. and Brown, D. W.; *Journal of Physical Chemistry* 1957, *61*, 2, p. 129.

34. Tatro, S. R., Baker, G. R., Bisht, K., Harmon, J. P.; *Polymer*, 2003, *44*, p. 167.

35. Emran, S. K., Newcome, G. R., Weis, C. D., Harmon, J. P.; *Journal of Polymer Science: Part B: Polymer Physics*, 1999, *37*, p. 2025.

36. Dole, M.; *Radiation Chemistry of Macromolecules Volume II*, Dole, M., Ed.; Academic Press, New York, 1973, p 97.

37. Suarez, J. C. M., et. al.; *Journal of Applied Polymer Science*, *85*, 2002, p. 886.

Chapter Five

Influence of Tacticity in Gamma Irradiation of PMMA Polymers of Varying Molecular Weight and Narrow Dispersity Indices.

Abstract

A previous study has evaluated a linear series of polymethyl methacrylate (PMMA) polymers to evaluate the influence of polymer Mw on the effectiveness of modeling methods to predict changes in molecular weight distribution following exposure to gamma radiation. The development of pertinent modeling methods is critical to the space industry were new polymer materials are used in high radiation environments. The results demonstrated that using conventional modeling methods, good agreement between the predicted redistribution of the average molecular weight was observed for higher molecular weight PMMA as the Tg approaches Tg_{∞} . The results also demonstrated that as values for PMMA glass transition temperatures begin to approach the region between Tg_{∞} and Mw = 0, the rate of degradation accelerates significantly. The higher rate of degradation is associated with the greater free volume associated with the lower Tg region enables depropagation reactions from the end groups that are more abundant in the lower molecular weight solids. As space missions require materials with semi-rigid properties with a moderate modulus range, the use of polymers just below the Tg_{∞} will be of strong interest for technology applications in space. This study evaluates tacticity as another structural feature of the PMMA polymer for modeling degradation chemistry. Iso-tactic polymer chain structure enables tighter tertiary structures with less free volume. Less scission is reported in favor of more crosslinking. As in the previous study, main-chain scission and elimination products will be evaluated in a chain length series of narrowly dispersed iso-tactic PMMA polymers (4,200 – 11,700 M_w). A comparison is made of the scission radiation yield (G_s) predicted for the simulated ionization data to the experimental results of PMMA degradation in a ground-based simulation of the space radiation environment using a ^{60}Co source. The influence of molecular weight and tacticity on the stability of post-irradiated PMMA is evident in the degree of change observed for each molecular weight series with respect to the degradation products produced by exposure to gamma radiation. The results further support the importance of free volume properties driving the observed differences in the G(s) values.

Introduction

Polymers used in advanced technology applications for the space environment must display stable properties throughout mission life. The presence of high energy particle radiation in the space mission environment presents a risk to polymer stability in space through radiation-induced ionization and the resultant degradation reactions of the polymer chain. As the chemical changes in the polymer component chains accumulate, a change in polymer properties (e.g. Tg , CTE, modulus, etc..) can occur. The latent nature of failure in polymer performance through radiation–induced changes in the chemical structure can be predicted through modeling and experimental ground simulation testing enabling the preferred selection of stable polymeric materials for space applications.[1]

Modeling methods examine two primary reaction pathways by which polymer degradation most pertinent to changes in polymer properties can proceed: main-chain scission and crosslinking.[2-6] The significance of these two pathways is the resultant change in molecular weight distribution of the polymer that accompanies these events. As previous studies have shown, a change in molecular weight distribution can alter the performance properties of a polymeric material.[7] While loss of side groups along the main-chain and abstraction of small molecules (e.g. hydrogen) also occurs, side-group loss is associated with main-chain scission, and is accounted for in the scission model. Hydrogen abstraction does not lead to a significant change in molecular weight distribution, and interest in these two degradation mechanisms is limited to outgassing which is a concern to spaceflight missions, but does not significantly contribute an added risk to the stability of polymer properties.

In a previous investigation, it was shown that established modeling methods were developed using one of two polymer states.[2-6] These included models to predict radiation damage in liquid polymers leading to crosslinking that could be measured by viscometric methods and the gel point. The other modeling approach used polymers of significantly higher molecular weight distribution where the Tg approached the Tg_{∞} values.[6] Using a linear series of narrowly dispersed PMMA standards with Gaussian distribution, the investigation showed that the radiation yield values for PMMA Mw standards in the linear region of the Fox-Flory function do not follow the modeling predictions, but show an enhanced M_n/M_w and a significant effect induced by end-group depropagation (Figure 5.1). Most polymers in space applications have

application-specific properties requiring minimal change in physical properties over the temperature range of use. However, this does not imply that polymers must be polymerized to the highest Tg to be used in the application of interest. Conversely, a semi-rigid, low modulus condition is preferred for most applications to endure the shock requirements and the thermal cycling regime that accompanies all space missions in ascent and deployment.[7] This pre-disposes the polymer material to a chemical structure with greater free volume than the rigid state, where free volume is limited by the immobility of free chains in a higher density network or a high Mw polymer with higher crystallite content. This suggests that the influence of Mw and the associated free volume effects of polymers is important to consider in spacecraft applications.

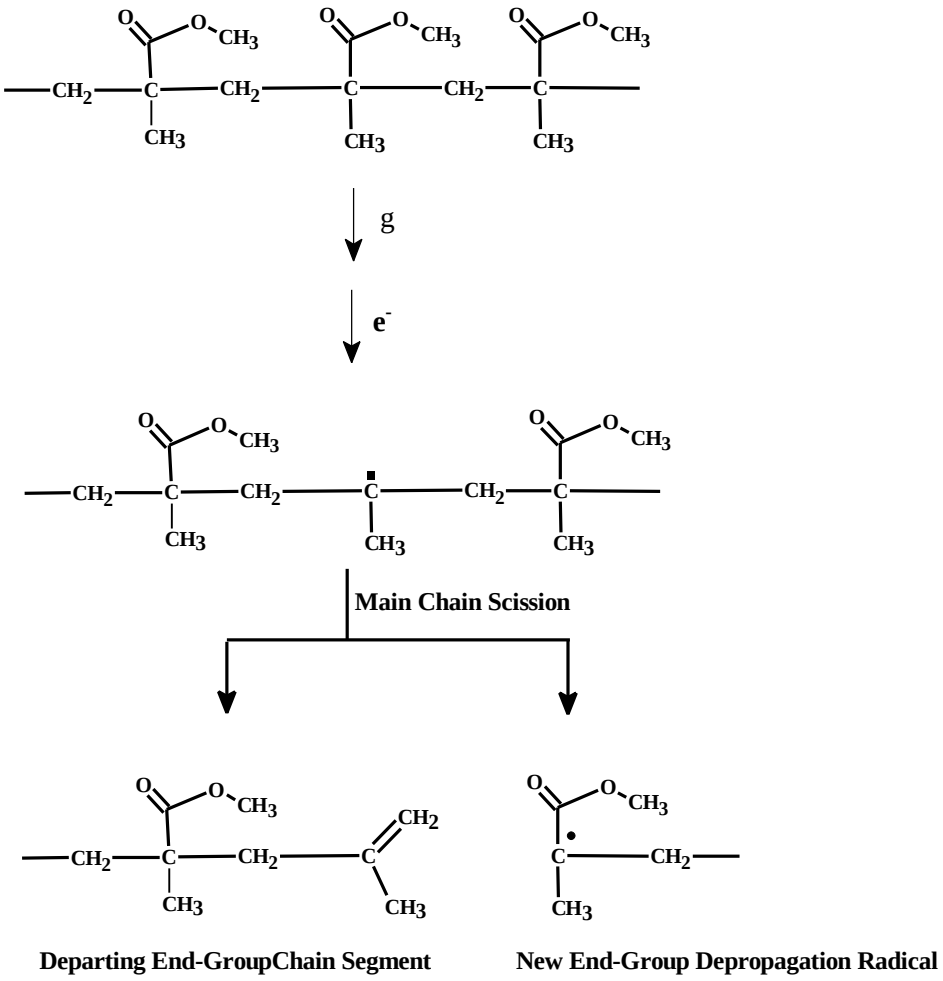

Figure 5.1 Gamma Radiation-Induced Degradation Leading to End-Group Depropagation.

Radiochemical Yield Comparisons

The previous study used established, mainstream G-values to demonstrate the effect of molecular weight on the fraction of molecules (chains) affected by a random scission following absorption of total dose typical of the space radiation environment.[6] The radiation yield value has units of events per gram of polymer, implying that smaller Mw components of a linear series of PMMA will have fewer events per molecule. However, the experimental G(s) values for atactic PMMA samples over the same molecular weight range yielded higher scission rates than expected for lower Mw standards and lower than expected G(s) values for higher Mw samples. This has been explained by the previous study and other investigators as differences in end-group composition of the PMMA sample and the rotational and translational mobility of the component PMMA molecules.[8,9]

The introduction of tacticity presents another structural feature to consider in modeling radiation-induced damage. Reports by Moore and Choi showed that the isotactic distribution of side groups in PMMA permitted main-chain conformations that allowed higher alignment between the carbonyl moiety and the α-methyl and methylene hydrogens on a neighboring chain (Figure 5.2).[10,11] The close orientation of the chains is reported to limit mobility and rotation between chain.. Moore and Choi went on to show an increase in the radiation yield of crosslinked PMMA chains (G(x), and that the yield of crosslinks increased with increasing molecular weight (6,000 Mw vs. 26,000 Mw). Using high molecular weight (> $1x10^5$), narrowly-dispersed iso-PMMA polymer standards, Pethrick also demonstrated the higher preference for crosslinking, and a higher rate of decomposition for *iso*-PMMA.[12]

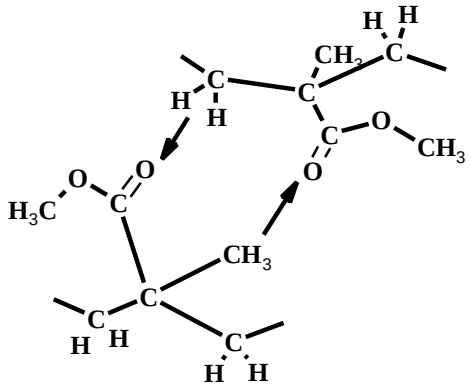

Figure 5.2 Illustration of the Interaction of the PMMA Side-Groups with Neighboring Main-Chains.

The lower G(s) values for stereoregular PMMA is attributed to the cage recombination effect wherein the inductive bonding between the neighboring chains maintains the reactive pair in close proximity to the original site of the scission break in the main-chain, thereby optimizing conditions for recombination.[13] The recombination reaction has been verified through the observation of racemization in the isotactic PMMA polymer following exposure.[14] The higher G(x) values reported by Moore are also a result of the close proximity of the neighboring chains during incipient radical formation along the main-chain.[10]

The cage recombination effect suggests that isotactic, stereoregular structure of PMMA would have an effect on the glass transition temperature by increasing it through the limited free volume. That is, while rotation is limited, translation is not. However, later reports show that lower molecular weight PMMA displays a lower Tg than atactic polymer and go on to attribute the behavior to the increased translational freedom between isotactic chains.[15,16]

It is of interest to assess the influence of the stereoregular structure on the degradation chemistry of PMMA by comparing the condition of atactic and isotactic polymers in the Mw range wherein the Tg is midway between the Mw = 0 and Tg_{∞}. The carboxymethyl side group is a key factor in the interaction between stereoregular chains of PMMA and can influence the degradation pathway for the polymer following irradiation. Highly-ordered, chain orientation of the iso-tactic PMMA structure restricts the decarboxylation reaction that yields the radical intermediates on the alpha methyl carbon and the main-chain beta carbon.. Instead degradation proceeds through an alternate Norrish I path as demonstrated in Figure 5.3 where the initial loss of the carboxymethyl side group is not required for scission.

Without rotational mobility in the isotactic main-chain segments neighboring the chain scission site, a stable bond orientation for depropagation is not readily achieved, and therefore end group loss rate is diminished. The stable radial intermediates can alternatively undergo recombination by scavenging radicals, crosslinking through translational motion in the chain, or undergo quenching by reaction of ambient oxygen with the resultant formation of peroxides and other carbonyl-based derivatives.

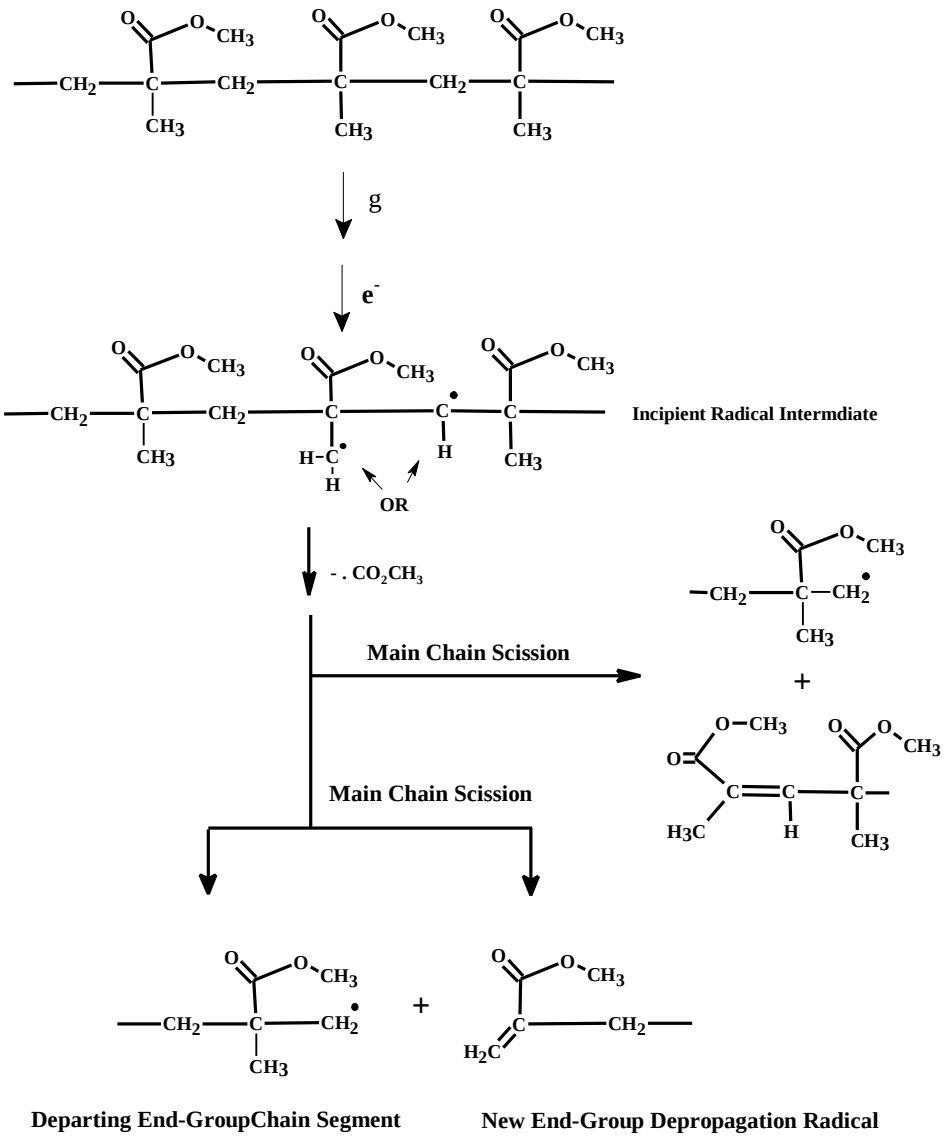

Figure 5.3 Gamma Radiation-Induced Degradation Leading to End-Group Depropagation.

The lower G(s) values reported for stereoregular PMMA are driven by the influence of the orientation and chain-to-chain interaction enabled by the functional groups present on the side chain. What is not yet understood is the extent to which the close-packed alignment of the isotactic chains align near the end groups where the continuity of the close-packed structure would be expected to diminish free volume.

Close-packed condition of neighboring chains is more ordered in syndiotactic PMMA (Tg = 126^{o}C) than in atactic (Tg = 120^{o}C), or isotactic PMMA (Tg = 48^{o}C) resulting in higher Tg values, smaller coil volume and more extensive chain entanglement.[16] The report also demonstrates the importance of these attributes in the progression of polymer depropagation.

Many of these studies performed experimentation in thermal ranges near Tg_{∞} or in the liquid state near the gel point. PMMA with a Tg in the thermal range between these two relatively stable regions offers an area of study that has significance to the preparation and application of polymeric materials. Previous work demonstrated deviations from established G-based and model-based predictions for PMMA standards with Tg distribution in this thermal region were concluded to be driven by the influence of higher free volume of polymers in this thermal region leading to a higher rate of depropagation. The evaluation of iso-PMMA standards with Tg values in the same thermal range would be one approach to understanding the effect of the carboxymethyl side chain on scission and depropagation mechanisms of PMMA degradation.

Experimental

Sample Preparation

The preparation of certified, stereoregular PMMA would be critical for this study. The synthesis of the iso-PMMA standards was performed by Polymer Source, (Province of Quebec, Canada). The isotactic content of the PMMA samples was calculated using the ratios of the α-methyl protons [1.20 ppm for isotactic, 0.82 ppm and 1.03 ppm for syndiotactic and heterotactic protons]. The isotactic content for both low molecular weight PMMA standards was greater than 90 %. The molecular weight distribution data and synthetic preparation methods for the atactic and isotactic PMMA standards used for this study have been presented in Chapter 3.

The PMMA standards are a white, granular powder (less than 1 mm diameter particle size) allowing full penetration of the gamma photon flux with insignificant shielding effects. The PMMA standards were used as received without further preparation or modification.

Methods of Analysis

GPC and Radiochemical Yield Data

The gel permeation chromatography (GPC) method and instrumentation developed and used for the evaluation of Mw, Mn and PD distribution of the experimental PMMA samples used in this study has been described in Chapter 3. The molecular weight distribution values were determined for pre-exposure and post-exposure conditions. The post-exposure levels included PMMA sample sets collected following total dose exposure levels of 40, 80 and 120 Mrads using the Shepherd 484 ^{60}Co Gamma Source. The samples were irradiated to three levels: 40, 80 and 120 Mrads at a dose rate of (26,759 rads (Si)/min). Samples were irradiated at room temperature with no detectable rise in temperature during the period of irradiation. Samples underwent analysis by GPC without post-exposure annealing within eight days after exposure.

The G(s) radiation yield data was determined using Equation 4.5. Based on the modeling approach described in Chapter 4.0, the determination of Mw and Mn used all partitions comprising the full distribution of chain lengths represented in the GPC chromatogram.

Differential Scanning Calorimetry

All PMMA samples [10-15 mg] were run in open aluminum pans to assay the Tg of the solid powders. The study used the instrumentation and thermal profile as described in Chapter 3. The instrument performance was confirmed through calibration. The Tg values for this study were confirmed independently using a TA Instruments modulated DSC 2910.

FTIR Analysis

All PMMA powder samples were run in transmission and ATR reflectance mode. The sample preparation methods and instrumentation are described in Chapter 3. The complete ATR spectra are provided in Appendix 3 as absorbance spectra.

Results and Discussion

In reporting the effects of tacticity on the sensitivity of PMMA to particle radiation, Pethrick attributed the higher sensitivity of isotactic PMMA to the competing degradation pathways by scission and crosslinking.[13] The thermodynamics associated with these findings are not fully understood. Entropic and kinetic considerations are used to explain the observation based on secondary thermodynamic transitions. Polymer chains that lack strong attractive forces (entropic) are more prone to chain disentanglement and end-group separation leading to Tg depression.

The enthalpic effect of the close packed interaction between the side chain oxygens and main-chain hydrogens is over come by the translation mobility along the chain. While the limited free volume in the highly-ordered array of side chains limits the scission initiating step of decarboxylation through decomposition of the carboxymethyl group, the alternative paths to decarboxylation (Figure 5.3) provide opportunity for translational separation of the chains. Thin film studies have examined the role of the orientation of i-, s-, and h-PMMA side groups with surfaces wherein s-PMMA polymer displayed the highest density of interaction and i-PMMA the least.[17]

Compliance with Predicted G-Based Model

Radiation yield values (G-values) for the primary degradation events in polymers are determined from the average molecular weight values of a polymer before and after irradiation (Equation 4.4). The calculated Mn, Mw and PD values for the polymer sample are presented in Table 5.1. G(s) values for the PMMA samples used for the current study are present in Table 5.2.

Correlation with Atactic PMMA Degradation Profiles

The GPC results verify the expectation for lower G(s) values using the stereoregular PMMA. As observed in the previous study on atactic PMMA, the G(s) values for the lower Mw iso-PMMA is greater than the G(s) for the higher Mw iso-PMMA standard, suggesting a similar affect of free volume. However, an evaluation of the DSC data (Table 5.3) does not show a significant change in the Tg for iso-

PMMA when compared with the atactic PMMA samples that could be attributed to insignificant change in free volume with total dose accumulation, and to the competing effects of chain scission and crosslinking.[13]

	4200 ISO REF	4200 ISO 40 MRADS	4200 ISO 80 MRADS	4200 ISO 120 MRADS
Mn	3459	3385	3356	2470
Mw	4088	3962	3898	3637
PD	1.18	1.17	1.16	1.47
	11500 ISO REF	11500 ISO 40 MRADS	11500 ISO 80 MRADS	11500 ISO 120 MRADS
Mn	9113	6723	7764	446
Mw	10099	9570	8879	2323
PD	1.11	1.10	1.14	5.21
	6800 REF	6800 40 MRADS	6800 80 MRADS	6800 120 MRADS
Mn	6025	1276	1221	871
Mw	6458	4675	4583	3807
PD	1.07	3.66	3.75	4.37
	14200 REF	14200 40 MRADS	14200 80 MRADS	14200 120 MRADS
Mn	17684	13896	9009	6706
Mw	18463	16480	14170	13007
PD	1.03	1.18	1.57	1.94

Table 5.1 Values of Mw, Mn and PD for PMMA Standards at Various Exposure Times.

Dose (rads - Si)	G(s)	Mn_s	Mn_0	N_s	D (eV)
6800 ATACTIC					
0	0.00	6726	6726	6.02E+23	1
4.00E+07	0.93	5338	6726	6.02E+23	2.50E+21
8.00E+07	0.29	5789	6726	6.02E+23	4.99E+21
1.20E+08	0.78	4062	6726	6.02E+23	7.49E+21
14200 ATACTIC					
0	0.00	15165	15165	6.02E+23	1
4.00E+07	0.45	11792	15165	6.02E+23	2.50E+21
8.00E+07	0.22	11841	15165	6.02E+23	4.99E+21
1.20E+08	0.18	11333	15165	6.02E+23	7.49E+21
4200 ISO	G(s)	Mn_s	Mn_0	N	D
0	0.00	4266	4266	6.02E+23	1
4.00E+07	0.39	3994	4266	6.02E+23	2.50E+21
8.00E+07	0.27	3696	4266	6.02E+23	4.99E+21
1.20E+08	0.37	3559	4266	6.02E+23	7.49E+21
11500 ISO	G(s)	Mn_s	Mn_0	N	D
0	0.00	10596	10596	6.02E+23	1
4.00E+07	0.09	10178	10596	6.02E+23	2.50E+21
8.00E+07	0.11	9663	10596	6.02E+23	4.99E+21
1.20E+08	0.60	5926	10596	6.02E+23	7.49E+21

Table 5.2 Comparison of the G(s) Values for PMMA Standards.

PMMA Mw	PRE-EXPOSURE	POST-EXPOSURE 40 MRADS	POST-EXPOSURE 80 MRADS	POSTEXPOSURE 120 MRADS
ISO				
4200	37	36	35	35
11700	49	47	45	45
ATACTIC				
6800	121	106	99	94
14200	128	124	125	121

Table 5.3 Comparison of the Tg Values for Atactic an Iso-Tactic PMMA Standards.

The translational movement of iso-PMMA chain segments and increased probability for crosslinking between chains are known to be driven by the orientation of chain alignment.[18] The difference was attributed to the Tg values conformational energy difference between diastereomers comprising the main-chain.[19] The resultant reduction in the glass transition temperature suggests that the there would be a greater opportunity for end-group loss as expected from the atactic results. A comparison of the proportion of end-group segments (e,.g.monomers, and dimers) observed at the high retention regions of the GPC chromatogram for atactic and isotactic PMMA samples demonstrates that end-group loss is suppressed in the iso-PMMA sample (Figures 5.4 and 5.5). The GPC data for the atactic PMMA sample also indicates composition of random scission products that is not observed in the iso-PMMA data.

The FTIR results support the suppression of scission in two areas of analysis. Iso-PMMA degradation through the reaction pathway in Figure 5.2 yields alkenyl products along the main chain or at the point of scission as a termination group. In several reaction products, the modified iso-PMMA chain retains the carboxymethyl side group, these reactions are not preferred in the atactic PMMA degradation where incipient decarboxylation is reported to initiate the scission process. Table 5.4 displays FTIR ratios for the carbonyl and saturated hydrocarbon bands for low molecular weight PMMA samples.

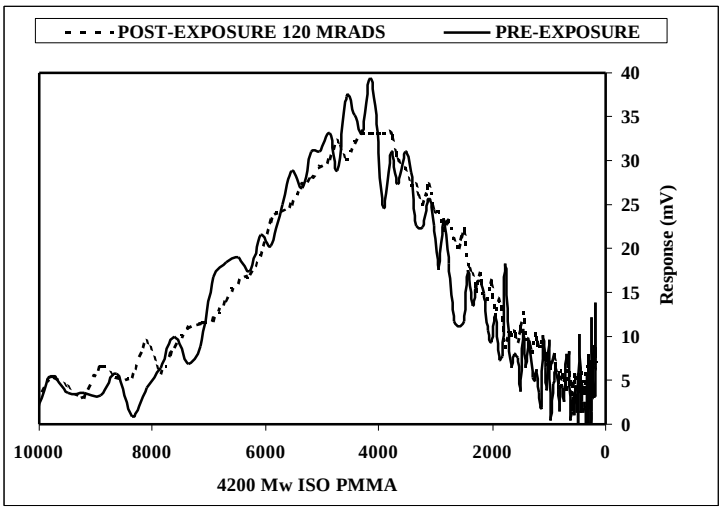

Figure 5.4 Pre- and Post –Exposure Iso-PMMA GPC Data Illustrating End-Group Depropagation.

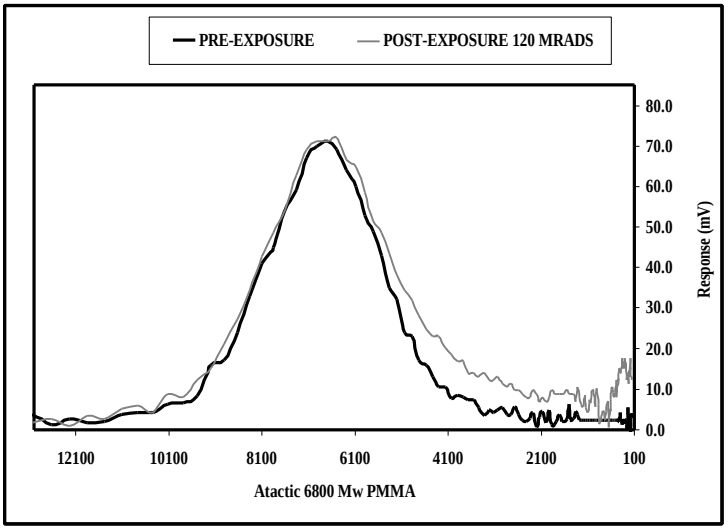

Figure 5.5 Pre- and Post –Exposure Atactic-PMMA GPC Data Illustrating End-Group Depropagation.

PMMA	6800 - REF	6800-40	6800-80	6800-120
2952	0.005	0.013	0.016	0.013
1728	0.029	0.069	0.084	0.068
RATIO	5.8	5.5	5.3	5.2
	4200 - REF	4200-40	4200-80	4200-120
2952	0.0167	0.0044	0.00847	0.00356
1728	0.078	0.018	0.031	0.0177
RATIO	4.7	4.1	3.7	5.0

Table 5.4 FTIR Ratios for Comparison of Side Chain Loss in PMMA.

The progressive side chain loss in the 6800 Mw atactic-PMMA supports the incipient decarboxylation pathway for the scission-based degradation. In the thermal mid-range between the Mw = 0 and T_{∞} for a linear series of polymers, atactic PMMA end-group loss and depropagation readily proceeds at the chain termini and at the point of chain scission. The iso-PMMA displays randomness in the peak ratios similar to the observation for high molecular weight PMMA samples in the previous study for atactic polymers. The highly ordered chain configuration of the iso-PMMA polymer limits scission through restricted rotation in the chain. These barriers to decarboxylation help to explain the effect of chemical structure on the differences observed in scission yield between atactic and isotactic PMMA in this study.

Another measurement of the scission activity in PMMA uses the FTIR spectrum to evaluate the region of 1100-1300 cm-1 (Previously discussed in Chapter 3). Assignments made to the cluster of IR peaks in this range are still the subject of debate, and are very sensitive to conformational changes.[19] The conformational energies for the main-chain backbone and the side chains depend on the tacticity, and could be obtained using the FTIR bands in this region. The FTIR spectra of this region of the IR spectrum for the stereoregular and atactic polymers are presented in Figures 5.6 – 5.7. The change in peak shape of the IR bands for the 4200 Mw iso-PMMA polymer suggests that some racemization has taken place. The same effect is not observed for the other polymer samples including the 11700 iso-PMMA sample. The analytical data continues to point out the importance free volume has in the behavior of linear polymers in the thermal range between T_∞ and the gel point. The unique observation of higher scission rate for the lower Mw iso-PMMA polymers in this thermal range continue in a manner consistent with the atactic PMMA reported in the previous chapter, albeit at a slower rate. In the absence of end-group depropagation the G(s) values for the iso-PMMA samples were significantly lower than the atactic polymers. The reduced G(s) values and recombination events support the effects of close packed structure in relation to the restrictive conformation of the PMMA side groups and the resultant limiting effect on end–group depropagation as reported in previous studies.

The decrease in Tg for the irradiated iso-PMMA samples was smaller compared to the exposed atactic polymer samples, confirming the previous reports on the resistance of iso-PMMA values to radiation-induced change in Tg. Moreover, these results support the proposition that tacticity, free volume and molecular weight produce a composite effect the kinetics of radiation-induced degradation in polymeric material.

As discussed in Chapter 4, modeling expressions assuming Schulz-Zimmer molecular weight distribution and random scission, the relation of scission yield to molar mass and dose is given in Equation 5.1.[4]

$$G(s) = 9.65 \times 10^{0}\ t_{avg.} / M_1 \qquad \text{(Eq. 5.1)}$$

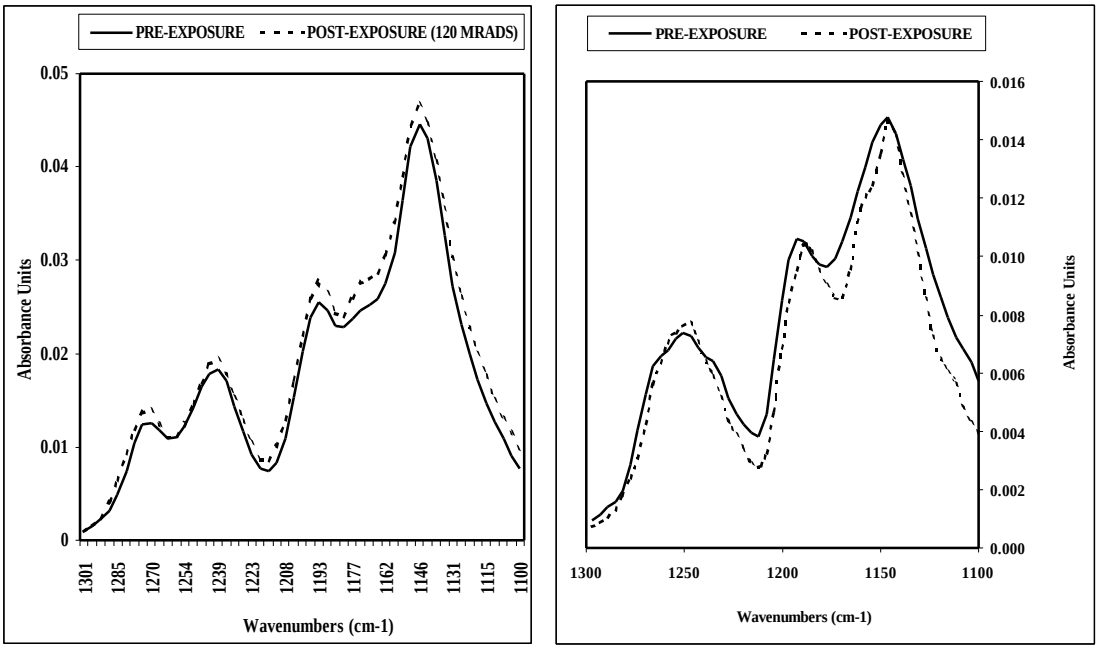

Figure 5.6 Comparison of FTIR Peaks 1100-1300 cm^{-1} for Atactic PMMA Mw 6800 (Left) and Isotactic PMMA Mw 4200 (Right) Illustrating the Affect of Stereochemical Scrambling.

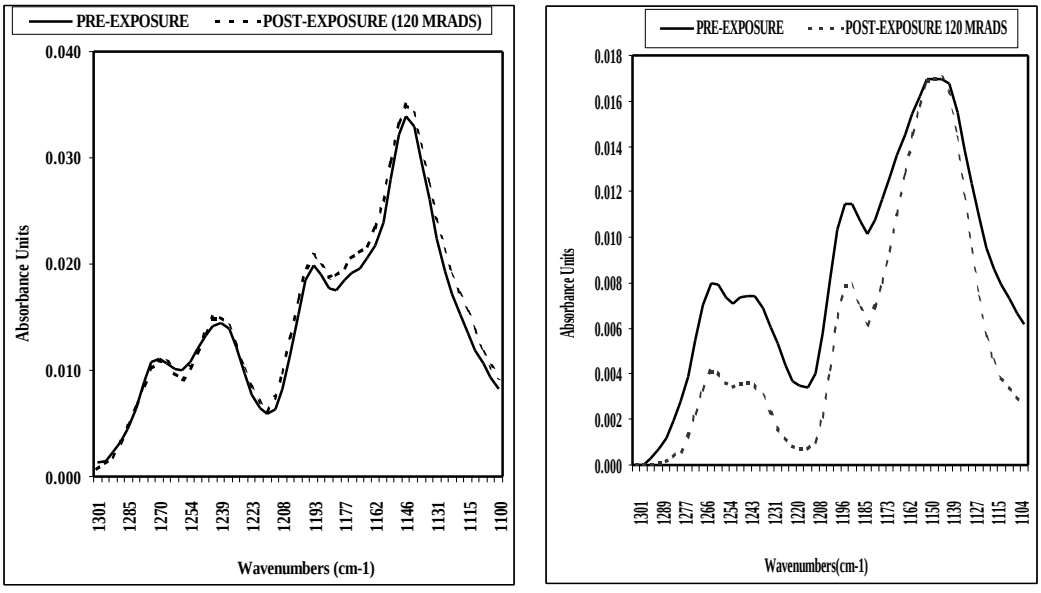

Figure 5.7 Comparison of FTIR Peaks 1100-1300 cm^{-1} for Atactic PMMA Mw 14200 (Left) and Isotactic PMMA Mw 11700 (Right) Illustrating the Affect of Stereochemical Scrambling.

Where G(s) is the scission yield value in scissions per eV per gram of polymer, t_{avg} is the average number of chain scissions per structural unit per unit dose, and M_1 is the molar mass of the structural monomeric unit. The equation has been applied to a specific predetermined distribution of partitions of molecular weight based on successive increments of one monomeric segment. The approach leads to complex integro-differential equations that limit the ability to introduce new structural or chemical parametrics in applying the model . The developers for current models warn that the expressions are only useful for liquid states of the polymer.[3-5] The current work in this study is focused on expressions that lead to greater flexibility to understand trends in polymer behavior as the foundation for approaching more exact solutions.

It was shown in the atactic PMMA study that, as a method for the determination of molecular weight distribution, GPC is useful for measuring Mn, Mw and PD. The instrument's detector uses UV spectroscopy to measure the partitioned molecular weight components of the dispersed linear PMMA polymer. The concentration of the absorbing component (carbonyl moiety) is the basis for describing the number of chains within the molecular weight partition on the basis of retention time and the resolving power of the GPC column selected for analysis. The approach to the development of an experimental model on the basis of GPC then, uses the partitions rather than individual chain lengths. This greatly simplifies the approach for higher molecular weight components of the molecular weight distribution, and allows close examination of the thermal range of interest to this study, where the greatest deviation from modeled polymer behavior is observed. The alternative expression for the composite change to the molecular weight partition in the GPC chromatogram can be used to evaluate the chain composition of the decomposed PMMA (Equation 5.2).

$$m_{Ir} = \#\ of\ molecules\ of\ M_I\ post\text{-}exposure = m_I - \#\ molecules_{\ scission} - \#\ molecules_{\ crosslinking} + m_{I\ fragments} \quad (Eq.\ 5.2)$$

Based on established G values for scission and crosslinking the expression prior to addition of the fragmented chains has been prepared for a specific molecular weight (m_I):

$$m_{Ir} = m_I - [m_{I-}(m_I[k_s(N_A/M_I)^{-1.0081}])] - [[m_{I-}(m_I[k_c(N_A/M_I)^{-1.0068}])] \qquad (Eq.\ 5.3)$$

Where m_I is the number of molecules at partition I, M_I is the molecular weight of the molecules at partition I, and k_s- k_c are the dose dependent rate constants for the scission and crosslinking events in PMMA. The derivation of the rate constants has been discussed in Chapter 4.

The approach to the inclusion of the accumulated fragments at m_{Ir} in the final Mw distribution can be determined by the initial molecular weight distribution and the polydispersity of the polymer. In random scission, the PMMA fragments m_{Ir} will originate from leveled distribution of fragments formed from higher molecular weight chains (See Figure 4.8). The PMMA fragments at m_{Ir} that are due to crosslinking will originate from lower molecular weight chains within the original Mw distribution.. The expression for m_{Ir} is modified for fragment accumulation using the pertinent six sigma range of the polymer (Eq. 5.4 and 5.5). The full expression is now ready for use in the prediction of Mw distribution following irradiation.

$$m_{Ir\ scission\ fragments} = [m_{max}[k_s(N_A/M_I)^{-1.0081}] / [(m_{max-}m_0)/M_0]] \ x\ (m_{max-}m_{Ir}) \qquad (Eq.\ 5.4)$$

$$m_{Ir\ crosslink\ fragments} = [m_{max}[k_c(N_A/M_I)^{-1.0068}] / [(m_{max-}m_0)/M_0]] \ x\ (m_{Ir-}m\ m_{max}) \ (Eq.\ 5.5)$$

Using the Mw distribution to illustrate the utility of the these equations when applied to each m_I partition of a Gaussian distribution, Figures 5.8 and 5.9 compare the experimental degradation results to expected G-based degradation. The model appears to predict the outcome of degradation for the lower molecular weight iso-PMMA sample. The higher Mw iso-PMMA sample displayed more degradation than expected when compared with the atactic PMMA samples in Figures 5.8 – 5.9.

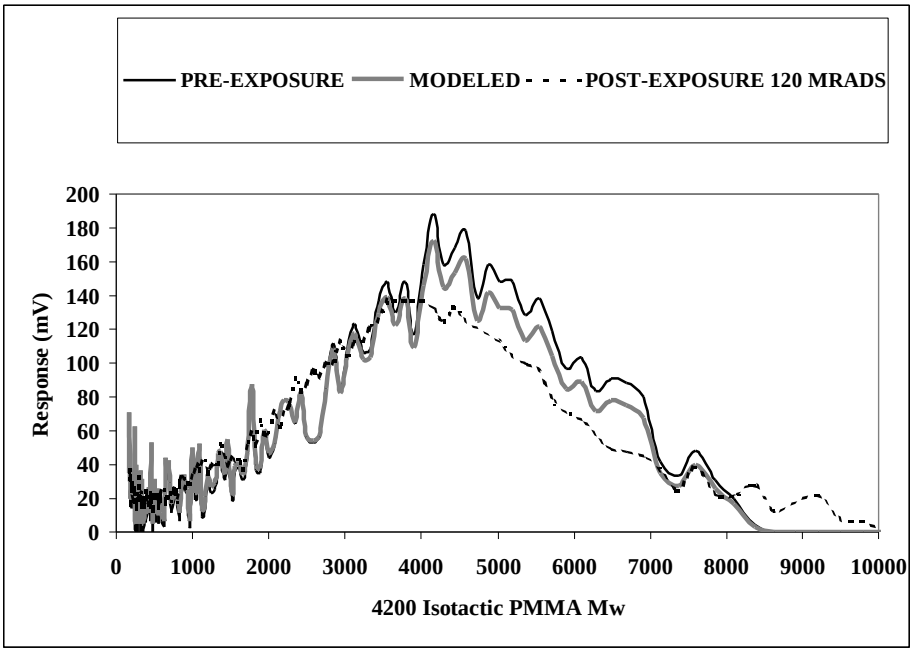

Figure 5.8. Predicted Scission vs. Experimental Data for *iso*-PMMA Mw 4,200 [120 Mrads].

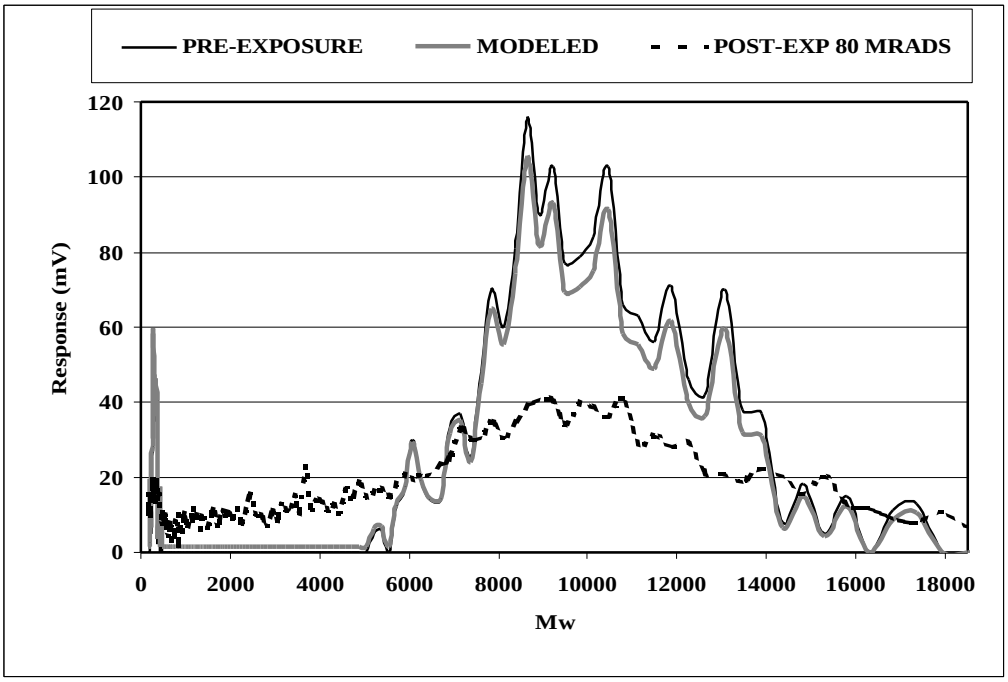

Figure 5.9. Predicted Scission vs. Experimental Data for *iso*-PMMA Mw 11,700 [120 Mrads].

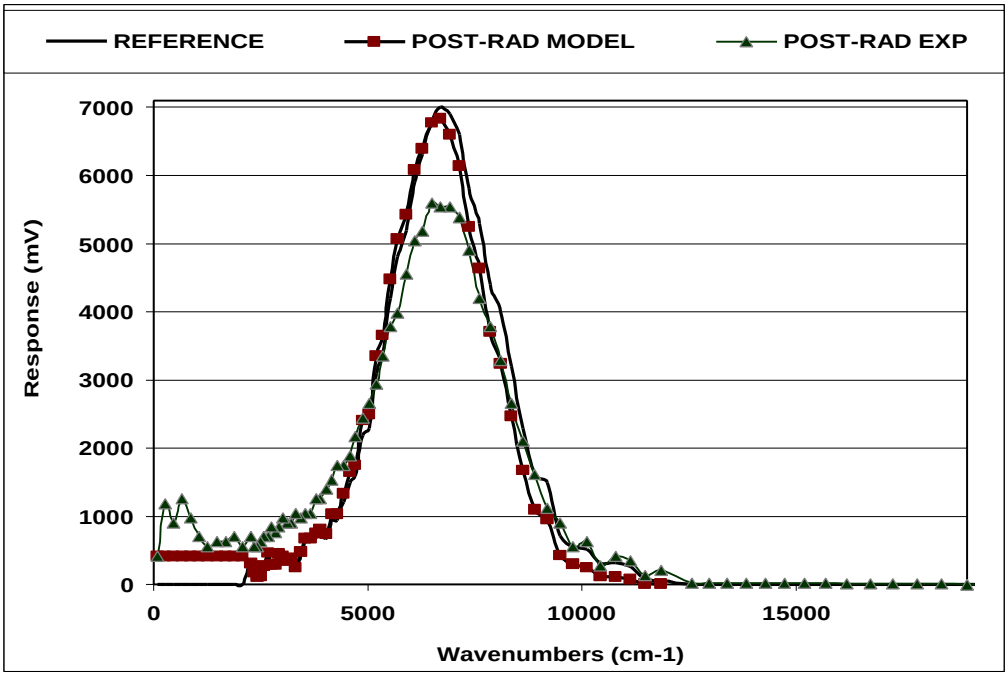

Figure 5.10. Predicted Scission vs. Experimental Data for *atac*-PMMA Mw 6,800 [120 Mrads].

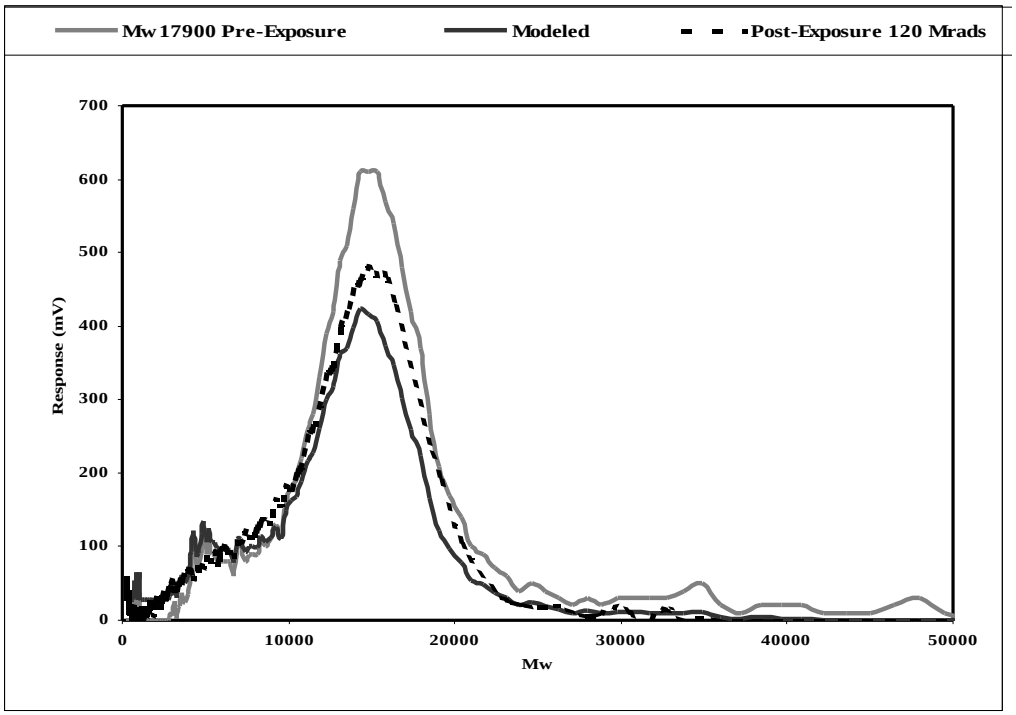

Figure 5.11. Predicted Scission vs. Experimental Data for *atac*-PMMA Mw 17,900 [120 Mrads].

Conclusions

Stereoregularity of the polymer chain structure influences the radiation-induced degradation chemistry of PMMA polymers. Iso-tactic PMMA displays post-exposure degradation pathways in accordance with the predictions of Moore, et. al. in the appearance of a higher proportion of crosslinks and a suppression of the scission rate.[11] Gel permeation chromatography results were used to compare the changes in molecular weight distribution for the iso-tactic and atactic low Tg PMMA standards. It was found that the iso-tactic PMMA polymer with high Mw displayed higher end-group loss, where the converse was observed for atactic PMMA in the same Mw range.

The close packing of the iso-PMMA chains enabled by the stereoregularity in main-chain, and the translational mobility of the aligned chains characteristic of iso-PMMA chain alignment, enables more crosslinking between chains. The end-group effects observed for atactic PMMA in the linear range of the Fox-Flory function between the PMMA Mw = 0 and Tg_{∞}? used for this study are not observed for the lower Mw stereoregular PMMA. The DSC data supports this finding in the lack of a change in the Tg as opposed to the significant decrease in Tg observed for the atactic polymer. The more ordered chain alignment for iso-PMMA limits the free volume at the end-groups, and thereby inhibits depropagation.

The presence of oxygen in the study of radiation affects on polymers can lead to oxidation products (e.g. peroxides, carboxylic acids, alcohols, etc..) that can interfere with the free radical propagation reactions associated with scission, crosslinking and end-group loss. This is important when also considering the reactive radical intermediates can persist with time below the Tg of the PMMA polymer and, without annealing, can contribute to the degradation of the PMMA samples long after exposure. The degradation is more pronounced with stereoregular polymers where caged intermediates reside without quenching if recombination does not occur, and accessibility by oxygen is restricted. The lack of oxidation products in the FTIR spectra for the isotactic and atactic PMMA polymers indicates that the presence of air did not significantly affect the degradation products of interest for this study.

The multiple, structural effects of the iso-tactic structure on the ability of PMMA to undergo established degradation pathways for scission and crosslinking demonstrates that established models may predict the number of scissions in the polymer chain, but does not accurately predict the new molecular

weight distribution. The successful assessment of free volume as it relates to the fraction of stereoregular chains in a highly-ordered configuration is needed before moving forward with validation of the modifications proposed in this study.

References

1. *Space Vehicle Mechanisms*, Conley, P. L., Ed..; John Wiley & Sons: New York, 1998, p. 215.
2. Charlesby, A., et. al.; *Proceedings of the Royal Chemical Society of London, Series A, Mathematical and Physical Sciences*, 1954, *224*, 1156, p. 120.
3. Saito, O.; *Radiation Chemistry of Macromolecules Volume I*; Dole, M., Ed.; Academic Press, New York, 1972.
4. O' Donnell, J. H., et. al.; *Macromolecules*, 1979, *12*, p. 113.
5. Wolf, B. A.; *Macromolecules*, 1981, *14*, p. 654.
6. Kashiwagi, T., Et. al.; *Macromolecules*, 1986, *19*, p. 2412.
7. Harmon, J. P. and Heffner, K. H.; *Forthcoming Publication*
8. Dallimore, G. R.; *Space Vehicle Mechanisms*, Conley, P. L., Ed., John Wiley & Sons: New York, 1998, p. 233.
9. Harmon, J. P. Tatro, S. R., Baker, G. R., Bisht, K.; Polymer, *44*, 2003, p. 167.
10. Goyanes, et. al.; *Journal de Physique IV*, Cooleque C8, supplement au Journal de Physique III, *6*, 1996, p. C8-587.
11. Moore, J. A. and Choi, J. O.; *American Chemical Society Symposium Series 620*; Clough, R. L. and Shalaby, S. W., Eds.; American Chemical Society, Washington, D.C., 1996, p. 156.
12. Sundararajan, P. R. and Flory, P. J.; *Journal of the American Chemical Society 96*, 16, 1974, p. 5025.
13. Pethrick, R. A.; *Irradiation Effects on Polymers*; Clegg, D. W. and Collyer, A. A., Eds.; Elsevier Applied Science, Oxford, 1991, p. 383.
14. Manring, L. E.; *Macromolecules*, 22, 1989, p. 4652.
15. Hill, D. J. T., et. al.; *Macromolecules*, *28*, 1995, 3681.
16. Zhang, G. and Thomas, J. K.; *American Chemical Society Symposium Series 620*; Clough, R. L. and Shalaby, S. W., Eds.; American Chemical Society, Washington, D.C., 1996, p. 55.
17. Kashiwagi, T., et. al.; *Polymer Bulletin*, *21*, 1989, p. 433.
18. Grohens, Y., et. al.; *Materials Research Society Symposium Vol. 629* Materials Research Society, 2000, p. FF1.7.1.

19. Pethrick, R. A. and Sharma, A. A,; *Polymer, 23*, 12, 1982, p. 1732.

20. MacKnight, W. and Karasz, F. E.; *Macromolecules*, 1, 1968, p. 537.

Chapter Six

Variations in Response to Gamma Irradiation of Polystyrene Polymers of Varying Molecular Weight and Narrow Dispersity Indices as Models for Assessment of Polymer Stability in Space Environments.

Abstract

The advanced polymeric materials used in spacecraft designs must display stable properties in the natural radiation environment of space. Forward knowledge through modeling and ground simulation of the cumulative effect of radiation-induced polymer degradation over the space mission life cycle can reduce risk to mission success. New considerations are studied in the application of current modeling methods for determining the radiation yields for crosslinking in polystyrene polymer. Previous work has assessed the effect of free volume and Mw on scission-based models using poly(methyl)methacrylate (PMMA). The previous studies have demonstrated an increase in the rate of degradation as molecular weight decreased in the linear range of the Fox-Flory function between the Mw = 0, and the asymptotic departure to Tg_{∞}. The studies showed the effect of higher free volume fraction imparted by an increase in the number of end groups, and the effect of conformational mobility for stereoregular polymer chains. The region displays a departure form the predicted redistribution of the polymer Mw using current scission yield values. The current study uses a similar approach in the evaluation of crosslinking behavior in a linear series of atactic polystyrene standards. The results of the polystyrene study demonstrate a similar observation to scission as lower Mw polystyrene polymers displayed less crosslinking than predicted by the modeling. Free volume is used to explain the departure from the predicted degradation rate.

Introduction

Modeling the Crosslink-Based Degradation Chemistry

The development of modeling methods and ground simulation techniques for predicting the radiation stability of solid polymeric materials is important to the space industry. As the two primary degradation reactions in polymeric materials, Main-chain scission and crosslinking reactions lead to alteration of the molecular structure of the polymer, and thereby change polymer material properties that are important to the performance of the polymeric material in the space environment. The chemistry of the two degradation reaction mechanisms can be studied through an evaluation of the polymer Mw distribution while the

resultant effect of degradation on the physical properties of the polymer can be monitored through thermal analysis methods.

Current kinetic expressions[1-2] for these mechanisms have progressively improved in accuracy with the use of new characterization methods for the assessment of the post-exposure changes to molecular structure. The more recent studies have examined simultaneous scission and crosslinking along with the evaluation of the pattern of distribution of polymer chains in the pre-irradiated molecular weight distribution (Schulz-Zimm or Gaussian) and the pattern of scission (Gaussian (mid-point) or random).[3-5] The methods also bound the fragmentation or crosslink products to a specific degree of randomness along the main-chain that is contradictory to the random nature of ionization of the bulk material as implied by the radiation yield values reported in the literature.

Our previous studies used the partitioning data from the chromatograms produced using gel permeation chromatography (GPC) to enable evaluation of the random fragmentation, the level-distribution of scission fragments, and the effects of free volume as a function of chain length.[6,7] The previous work addressed the issues with respect to scission-based degradation through results that reported that the predictive efficiency of current models is affected by assuming random main-chain scission, by chain length (i.e. Mw) and, more specifically, by the change in free volume. This was approached through recognition of the equivalency of chromatographic partitioning pattern to a quantitative expression of the molecular weight distribution of the polymer that has been documented in the literature (Equations 6.1 and 6.2).[8] The term *N* denotes the molar concentration, *M* is the Molecular Weight and *i* represents a running index that denotes the degree of polymerization of the *ith* species in the polymer mixture. By Beer's Law, the height (H_i) of the vertical segment relates to the concentration for the specific molecular weight (side group absorbance) chains represented by the *ith* segment of the polymer chain. Through the use of chromatographic *H* values, the work showed modeling of main-chain polymer degradation can be simplified to enable an improved understanding of the physico-chemical interactions that control the radiation yield kinetics.

$$M_w = \frac{\sum_i N_i M_i^2}{\sum_i N_i M_i} \qquad \textit{(Eq. 6.1)}$$

$$M_w = \frac{\sum H_i M_i}{\sum H_i} \qquad \textit{(Eq. 6.2)}$$

The previous work led to scission Equation 6.3 as a proposed modification describing the final count of polymer chains M_{Ipost} at a partition I (P_I) representing *ith* degree of polymerization for a specified level of absorbed dose. The components of m_{Ipost} include m_{Ir} (the fraction of unaffected chains at P_I determined by Equation 6.4) and the fragments contributing to the P_I population by degradation of the Mw partitions greater than P_I from Equation 6.5.

$$m_{Ipost} = m_{Ir} + m_{scission\ fragments} \qquad (Eq.\ 6.3)$$

$$m_{Ir} = m_{I-} (m_I [k_s(N_A/M_I)^{-1.0081}]) \qquad (Eq.\ 6.4)$$

$$m_{Ir\ scission\ fragments} = S \text{ for } j=m_{Ir} \text{ to } m_{max} \ [Ea_{max} / Ea_I] \times [(m_j [k_s(N_A/M_I)^{-1.0081}] /(P_j - P_0))]] \times (P_{max} - P_j/P_{max}) \qquad (Eq.\ 6.5)$$

The effect of free volume is most significant for the linear region of the thermal range where the Fox-Flory function (Eq. 1.1) predicts a linear polymer series will display a significant drop in the glass transition temperature (Tg).[9]

$$T_g \sim T_{g¥} - (K/M_n) \qquad (Eq.\ 1.1)$$

The scission model has yet to incorporate an accurate expression for the influence of chain depolymerization at the terminal ends of the polymer and at scission points along the main-chain. End–group loss is highly apparent by GPC analysis throughout the molecular weight range.[6] It is proposed that the expression would be a function of free volume and the post-exposure monomer concentration. The end group effect requires considerable forward knowledge of the rate of end-group loss at Tg_∞, and at several points in the linear range of the Fox-Flory function.

The increase in chain mobility that accompanies a decrease in Mw was important in considering the effect on the radiation-induced, scission-based degradation in previous investigations for PMMA. The change in conformational energy, higher end-group population, and the increase in free volume provided

the basis for the deviation from current scission models through higher end-group depropagation reactions. The thermodynamic relationship of the fractional free volume to polymer chain length and the flex energy of the chain segments has been described by Gibbs and DiMarzio.[10] The effect is significant in the study of the radiation stability of advanced polymers. The use of highly networked, high Mw polymers with limited free volume is not a general solution to hardening advanced polymers for use in space. Many applications require the introduction of copolymers, side chains and additives that impart preferred polymer performance through modification of the structural features that control critical properties such as modulus, refractive index and CTE. The resultant polymer structure displays features that affect free volume, and result in less rigid structures.

In developing models for crosslink-based degradation, free volume is expected to be an important factor. Polymers that display higher radiation yield values for crosslinking typically have a single, small, rigid side group.[11] Such structural features lead to restrictions to rotational and translational motion in the polymer chain that enhance the opportunity for crosslinking. In line with the results of previous studies, the increase in rotational and translational motion is expected to affect the efficiency of crosslinking in the polystyrene, and lead to a deviation from the expected modeling results. The current models employ various analytical solutions to the determination of the redistribution of degradation products, but each model relies heavily on experimental data and each numerically fits the model to experimental data. This approach seems to work for subsequent applications to other linear polymers in achieving predictability. However, the models do not account for the polymer features, or parametrics, that drive the need to fit the model to the experimental observations. The use of thermal analysis in conjunction with chemical analytical methods may provide insight into the basis for modeling expressions currently in use.

Experimental Section

The atactic polystyrene standards used for the study were prepared by Scientific Polymer Products, Inc. of Ontario, N.Y., and obtained as a linear series of narrowly dispersed standards. The certification data is presented in Table 6.1. The manufacturer's GPC certification data was used to confirm the Mw and polydispersity of each standard.

Mw	Mn	Mw/Mn
2,430	2,300	1.06
6,400	6,100	1.05
13,200	12,400	1.06
19,300	18,100	1.07
44,100	41,200	1.07
75,700	64,900	1.17

Table 6.1. Weight-Average and Number-Average Molecular Weights for Polystyrene Standards.

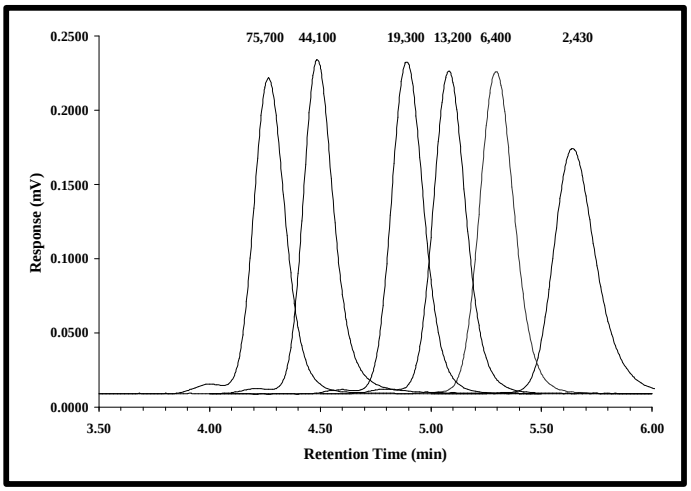

Figure 6.1. GPC Chromatograph Displaying the Distribution for Polystyrene Standards [Mw Values Denote Each Standard].

Gel permeation chromatography (GPC) was performed using a Dynamax UV-1 liquid chromatograph equipped with an ultraviolet detector (λ = 254 nm). Separations were performed with a Waters Styragel HR 4E; 7.8 x 300 mm GPC Column with 5μ rigid particle packing having 16,000 plates per column using THF solvent [Burdick and Jackson High Purity UV – Grade]. The LC Flow Rate was 1.5 ml / min. using a backpressure of 400 psi. Polystyrene samples were dissolved in THF. Sample concentrations for Mw less than 25,000 g/mole were 0.25 % by weight. Sample concentration for polystyrene with Mw greater than 25,000 g/mole were 0.10 % by weight. The sample injection size was 20 μL. Calibration was conducted with polystyrene standards.

The GPC data for the polystyrene standards is presented in Figure 6.1. The linearity of the calibration curve was verified using WINCHEM software program for polymer analysis. The data demonstrates that the GPC procedure can resolve the molecular weight of this class of polymeric

compounds. The GPC data was used for Mw, Mn and M_w/M_n calculations of the experimental polystyrene samples used in the study.

The post-exposure levels included polystyrene sample sets collected following total dose exposure levels of 80, 160, and 250 Mrads using the Shepherd 484 ^{60}Co Gamma Source. Samples were irradiated at room temperature with no detectable rise in temperature during the period of irradiation. Samples underwent analysis by GPC without post-exposure annealing within eight days after exposure. There were no detectable changes in the properties or chemistry of the polystyrene samples for exposures to 80 Mrads and 160 Mrads. The total dose values were used to calculate the experimental radiation yield (G scission values). G(x) values were calculated using the radiochemical yield equation of Saito, et.al. (Equation 6.8).[12]

$$G(x) = [[1/M_W - 1/ M_{W0}] \times [100 \times N_A]] / D \qquad \textit{(Eq. 6.8)}$$

The glass transition (Tg) measurements for all polystyrene samples in this study were obtained by differential scanning calorimetry (DSC) using a Perkin-Elmer Series 7 Thermal Analysis System. The Tg values were assessed by semi-automated determination of the half-step height temperature between the onset and peak of the heat flow curve (half vitrification). Powder samples (5 – 16 mg) from the standard and irradiated powders were weighed into open aluminum pans and analyzed by the following thermal profile. The samples were cooled from room temperature to 25^{o}C, heated from 25^{o}C to 150^{o}C at 10^{o}C/min., held at 150^{o}C for 5 min., then cooled from 150^{o}C to 25^{o}C at 10^{o}C/min. The samples were reheated from 25^{o}C to 150^{o}C at 10^{o}C/min. and any transitions were measured and recorded. The DSC instrument performance was confirmed through calibration using an indium standard.

All polystyrene spectra were obtained using a BIORAD FTS 40 FTIR spectrometer equipped with a mercury cadmium telluride detector and a SB-ATR reflectance microscope assembly. The co-added spectra were collected and averaged over 100 scans at a range of 4,000 – 750 cm^{-1} at 8 cm^{-1} resolution. There are specific bands of interest in the crosslinking reactions expected for polystyrene as well. Using FTIR Parkinson and Keyser followed the changes in polystyrene chemical structure observed following exposure to gamma irradiation. Even with significant total dose, the changes in the polystyrene spectrum

are nearly imperceptible. Parkinson's work[11] showed that irradiation of polystyrene led to degradation of the phenyl side chain with losses in peak intensity for the ring C-H bands at 3061 cm-1 to 3083 cm-1 and an increase in the peak at 825 cm-1 (Figure 3.3) that is attributed to crosslinking through the phenyl side chain (implying that the primary crosslinking mechanism occurred between the ring carbons of neighboring polystyrene chains).

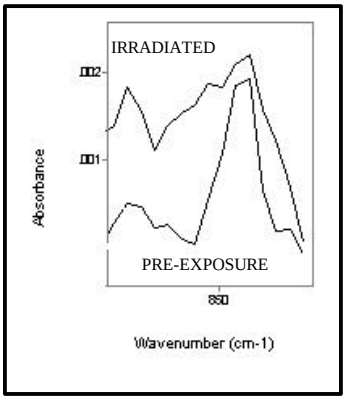

Figure 6.2. FTIR Absorbance Difference 800 to 920 cm^{-1} for Polystyrene Crosslinking.

Results and Discussion

Current modeling expressions[12-16] for changes to the molecular weight distribution of polymers for crosslinking in the absence of significant degradation by scission begin with evaluation of a single molecular weight uniformly comprised of chains with the same degree of polymerization (M_I). The basic formula for the predicted shift from pre-exposure, number average molecular weight (Mn_0) to the post-exposure Mn_d as a function of G(x) and dose is provided in Equation 6.9. A rate constant (k) emerges from the equation that is related to the yield value (G).

$$1/Mn_d - 1/Mn_0 = (G_d \times D)/(100 \times N) = kD \qquad (Eq.\ 6.9)$$

The current modeling expressions become more complex when the k value is inserted at each molecular weight for the determination of the unaffected fraction of chains at M_I, and for the determination of the

distribution of the resultant crosslinked chains to the remaining partitions of the molecular weight distribution.

The calculated results for Mw and PD are presented in Table 6.2. The increase in weight-average molecular weight supports crosslinking events that diminish in the extent of change as the Mw_0 decreases. The G(x) values are provided in Table 6.3.

PRE-EXP	Mw	2483	5802	10233	16270	42482	73253
	PD	1.06	1.06	1.05	1.05	1.05	1.05
POST-EXP	Mw	2517	6079	10592	16719	45001	78601
	PD	1.17	1.08	1.13	1.08	1.22	1.40

Table 6.2. Molecular weight and Polydispersity Data for the Polystyrene Standards.

The GPC chromatograms displayed in Figures 6.3 and 6.4, along with the PD values in Table 6.3, suggest that the higher molecular weight polystyrene samples have undergone significantly more change than the lower Mw samples. The higher G(x) values for the lower Mw polymers demonstrate that the lower molecular weight polystyrene samples are undergoing scission at a ten-fold rate. As discussed in previous studies, the number of ionization per molecule diminish with lower molecular weight at a specified G value and total absorbed dose.

Dose (rads - Si)	G(x)	Mn_x	Mn_0	N_a	D (eV)
0	0.000	2483	2483	6.02E+23	1
2.50E+08	0.021	2517	2483	6.02E+23	1.56E+22
0	0.000	5802	5802	6.02E+23	1
2.50E+08	0.030	6079	5802	6.02E+23	1.56E+22
0	0.000	10233	10233	6.02E+23	1
2.50E+08	0.013	10592	10233	6.02E+23	1.56E+22
0	0.000	16270	16270	6.02E+23	1
1.20E+08	0.013	16719	16270	6.02E+23	7.49E+21
0	0.000	42482	42482	6.02E+23	1
2.50E+08	0.005	45001	42482	6.02E+23	1.56E+22
0	0.000	73253	73253	6.02E+23	1
2.50E+08	0.004	78601	73253	6.02E+23	1.56E+22

Table 6.3. G values for Crosslinking Radiation Yield for Each Polystyrene Mw Sample.

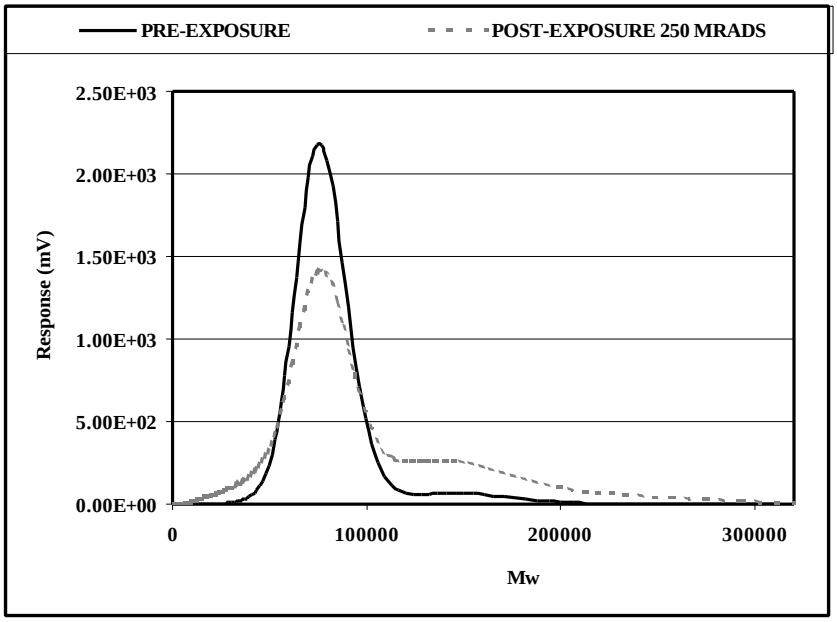

Figure 6.3. GPC Chromatograms for PS Mw 75,700 Illustrating the Extent of Crosslinking in Mw Distribution. [Pre- and Post- Exposure to 250 Mrads Total Dose]

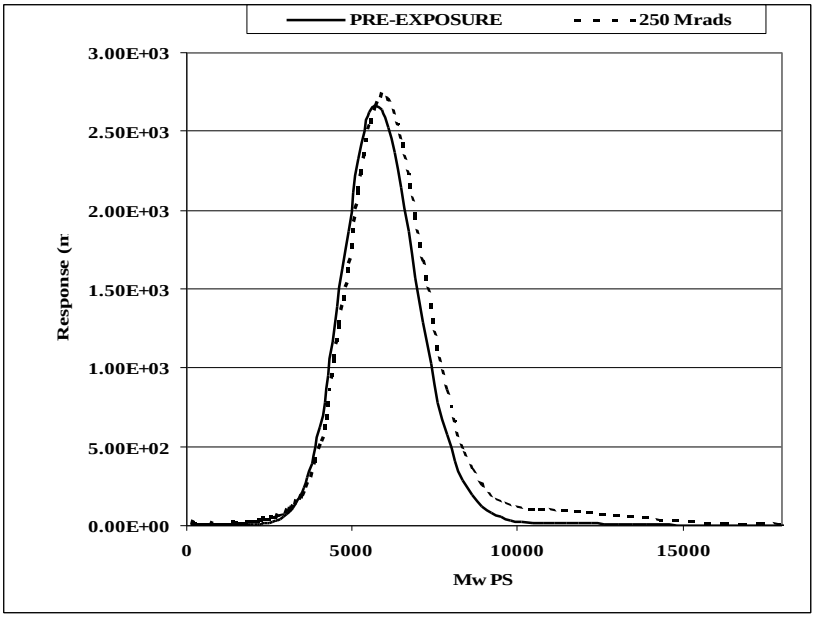

Figure 6.4. GPC Chromatograms for PS Mw 2,430 [Pre- and Post- Exposure to 250 Mrads Total Dose] Illustrating the Extent of Crosslinking in Mw Distribution.

The thermal analysis data is presented in Figure 6.5. All of the polystyrene standards displayed insignificant change in the Tg values. The linear range of the Fox-Flory function displayed by polystyrene suggests that the polystyrene damage is not sufficient to observe any significant effects from free volume.

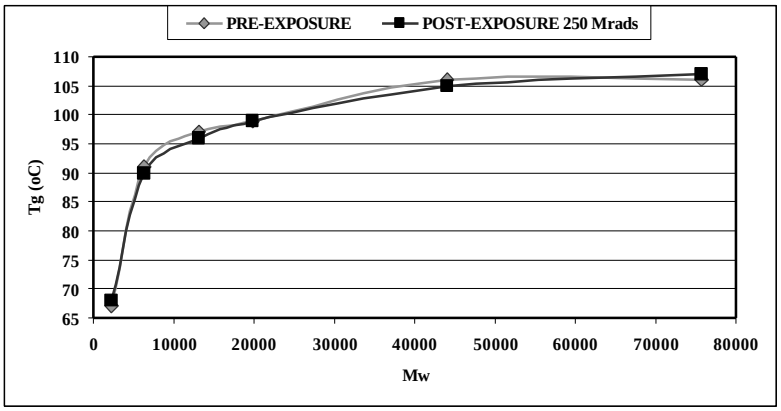

Figure 6.5. Pre- and Post Exposure Tg values for the Polystyrene Linear Series Following Irradiation with 250 Mrads Total Absorbed Dose.

The FTIR spectra for the irradiated samples did not differ significantly from the pre-exposure samples with the exception of the 2430 Mw polystyrene sample (Figure 6.6) which displayed an increase in the absorbance band for bonding between the ring carbons of neighboring polystyrene chains as described by Parkinson.[11] The limits of FTIR in detecting the subtle chemical bonds resulting from crosslinking reactions is limited by the low concentration of crosslinks in the structure. The low G(x) value of 0.004 obtained for the 75,700 Mw polystyrene sample yields about 0.08 crosslinks per chain based on random scission or 8% of the bulk polymer chains would be crosslinked at a single site on the chain (well below the limit of detection by FTIR.). The DSC and FTIR data displayed limited usefulness in understanding the change in radiation yield as a function of Mw.

Using established crosslink yield values derived from Eq. 6.9, and the GPC approach previously described for the scission model, an expression for predicting the final concentration of chains at M_I following exposure (m_{Ipost}) can be written (Equations 6.10, 6.11 and 6.12). Where m_I is the concentration of molecules at partition I, N_A is Avagadro's number, M_I is the molecular weight of the molecules at partition

I, and k_c is the dose dependent rate constant derived from G value for the crosslinking events per polystyrene chain at an absorbed dose of 250 Mrads (Figure 6.6).

$$m_{Ipost} = m_{Ir} + m_{CL\ Chains} \qquad (Eq.\ 6.10)$$

$$m_{Ir} = [[m_{I-} (m_I [k_c(N_A/M_I)^{-1.8848}])] \qquad (Eq.\ 6.11)$$

$$m_{Ir\ CL\ fragments} = S\ for\ j=m_{Ir}\ to\ m_{min}\ [(m_j [k_s(N_A/M_I)^{-1.8848}] /(P_j - P_0))]]\ x\ (P_{max}\text{-}P_j/P_{max}) \qquad (Eq.\ 6.12)$$

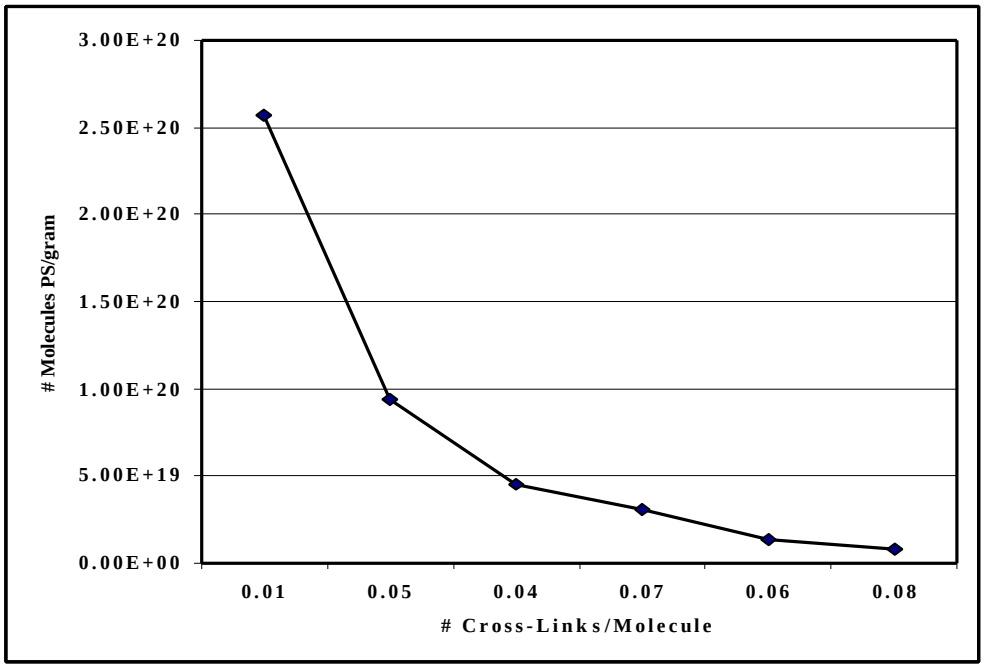

Figure 6.6. Predicted Crosslink Events/Molecule of PS for 250 Mrads Total Dose.

Compliance with the G-Based Model

The equation can now be applied to all partitions in the polystyrene sample molecular weight range using the rate constant for each individual contributing M_x band in the distribution. The equation was applied to the linear series polystyrene samples where the results demonstrate the suppression of scission for polystyrene polymers in the linear range of the Fox-Flory function (Figures 6.7 – 6.11). For the higher Mw polystyrene standards, the modeling predicted the pattern of degradation, but anticipated significantly more degradation, this deviation from the model may be attributable to the presence of diffused oxygen gas (air) saturating the polystyrene sample during irradiation.[17] The oxygen will quench reactive ion intermediates when formed during the exposure period, and thereby lead to oxidation products as a competing reaction pathway.

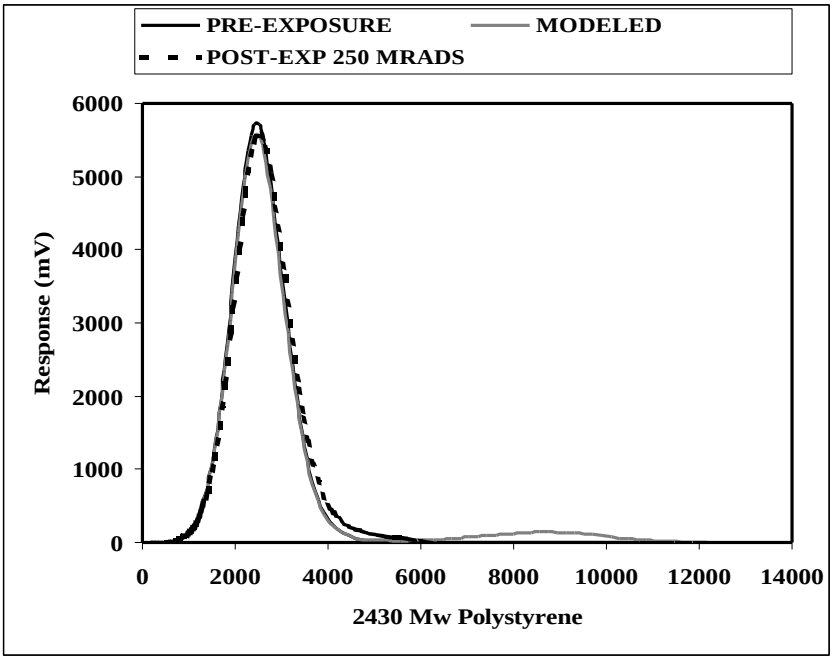

Figure 6.7. Predicted Crosslinking vs. Experimental Data for PS Mw 2,430 [250 Mrads].

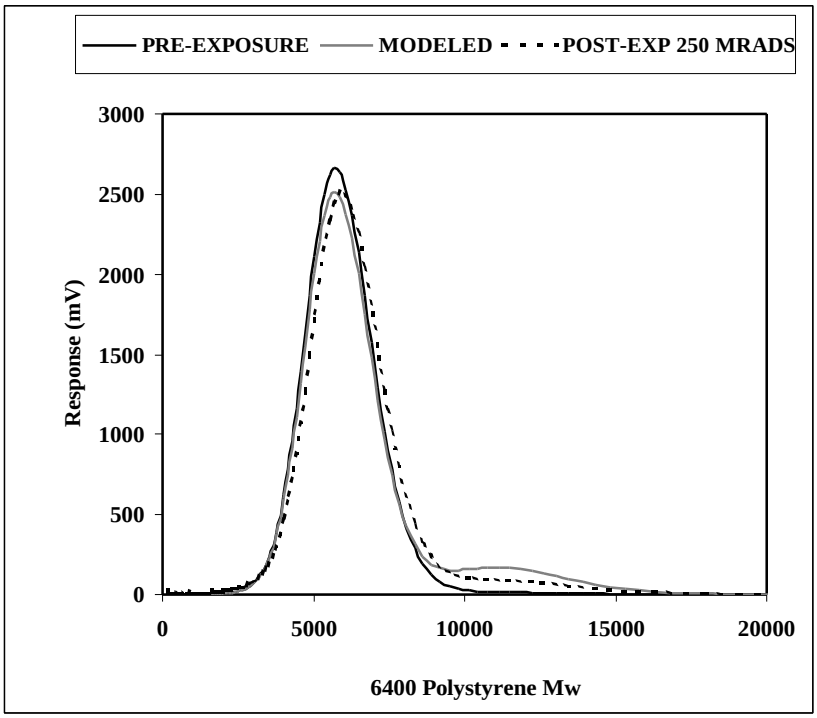

Figure 6.8. Predicted Crosslinking vs. Experimental Data for PS Mw 6,400 [250 Mrads].

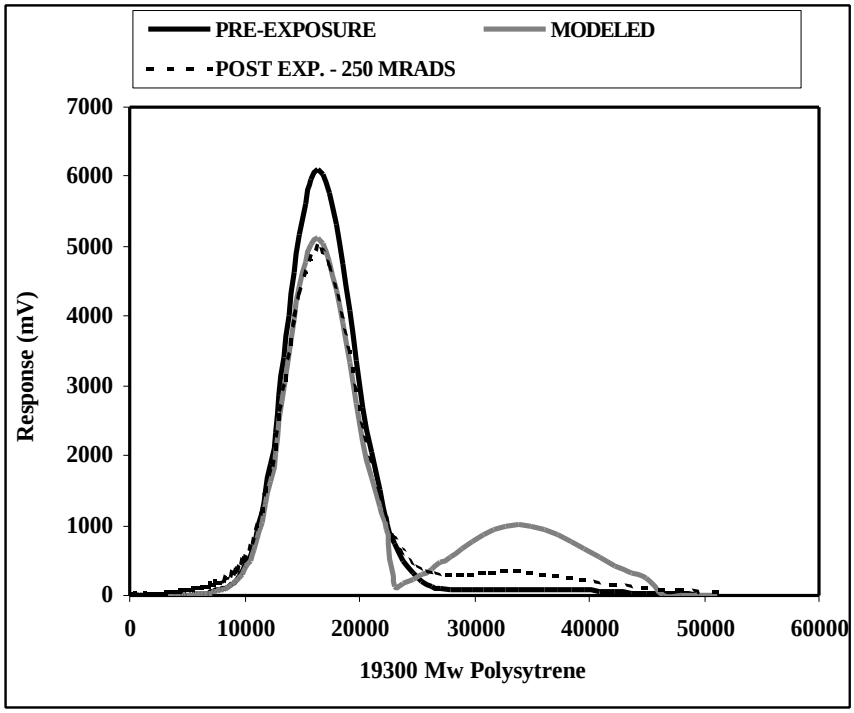

Figure 6.9. Predicted Crosslinking vs. Experimental Data for PS Mw 19,300 [250 Mrads].

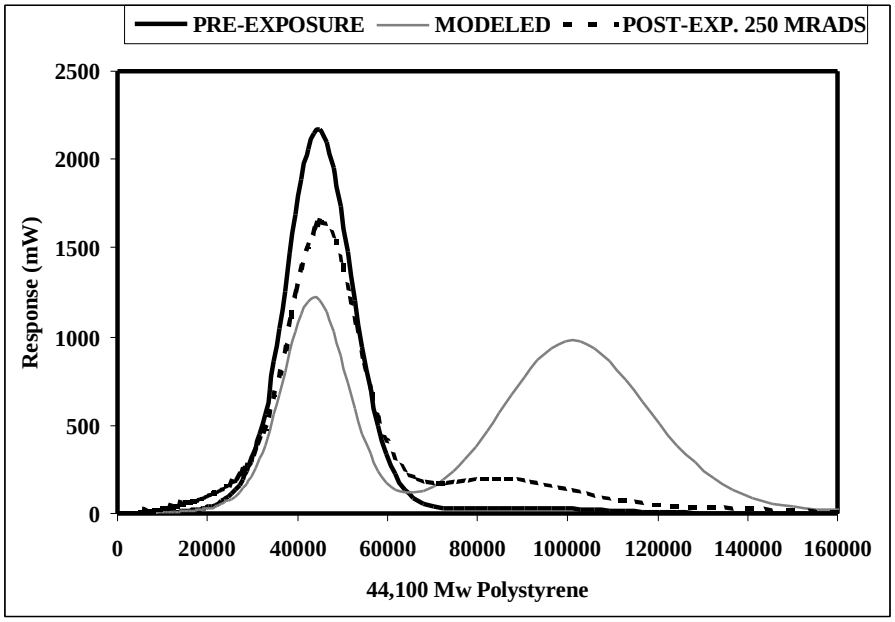

Figure 6.10. Predicted Crosslinking vs. Experimental Data for PS Mw 44,100 [250 Mrads].

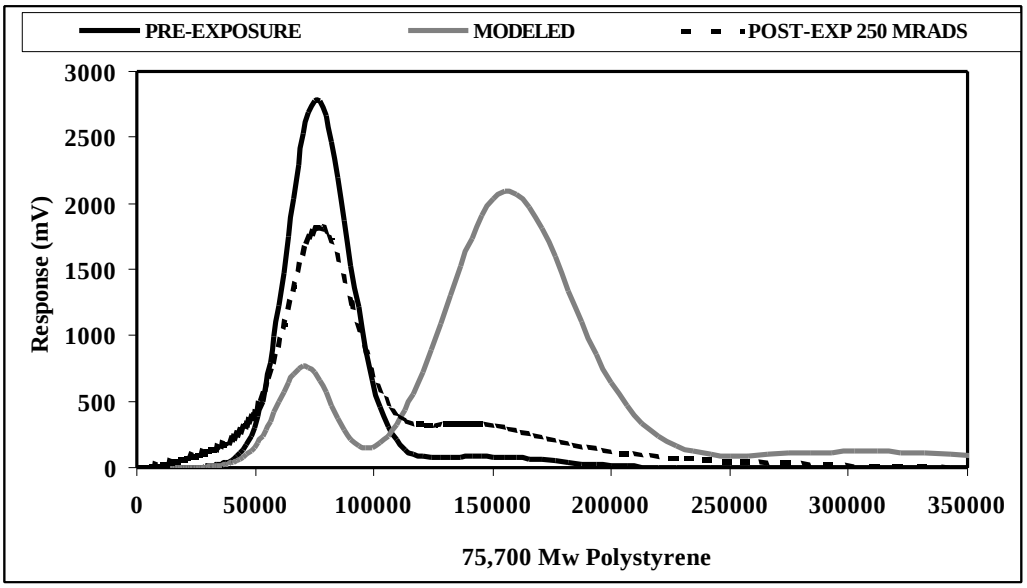

Figure 6.11. Predicted Crosslinking vs. Experimental Data for PS Mw 75,700 [250 Mrads].

Conclusions

The degradation behavior of polymers that degrade primarily by crosslinking reactions have been evaluated using modified modeling methods and analysis. Thc low G(s) values displayed by crosslinking polymers present a challenge to the investigator in clearly identifying the chemical mechanism and physical significance of degradation associated with total dose. Previous reports have discussed the rationale for the stability of crosslinking polymers by the tertiary chemical structure that limits rotational and translational motion of the main-chains. The structural features restrict the polymer form undergoing significant chemical change when absorbing high amounts of total dose ionizing energy.

The use of modeling and Mw partition analysis of the polymer has provided information on the extent of damage to the main-chain components. The methods permit evaluation and improvement in the use of radiation yield values, along with the importance of free volume. In the current study, the affect of free volume was not apparent by use of the glass transition temperature. A rapid change for the Tg in the linear region of the Fox-Flory function was observed in previous study for low molecular weight PMMA that degrades primarily through scission. The low molecular weight crosslinking polystyrene polymer did not display a higher radiation yield in the same thermal range. The effect of free volume in this thermal range will lead to a higher scission rate for the polystyrene, and thereby offset the crosslinking yield. The conclusion is supported by the broadened polydispersity of the lower molecular weight polystyrene sample.

The improved modeling approach for crosslinking yield permits facile comparison of modeling and experimental data on the Mw distribution . The model also permits introduction of other modifications to the present equations enabling simultaneous evaluation of scission, crosslinking, end-group effects and conformational energy, for example, temperature dependent activation energy (E_a).

References

1. Charlesby, A., et. al.; *Proceedings of the Royal Chemical Society of London, Series A, Mathematical and Physical Sciences*, 1954, *224*, 1156, p. 120.

2. Saito, O.; *Radiation Chemistry of Macromolecules Volume ;I* Dole, M., Ed.; Academic Press, New York, 1972.

3. O' Donnell, J. H., et. al.; *Macromolecules*, 1979, *12*, p. 113.

4. Wolf, B. A.; *Macromolecules*, 1981, *14*, p. 654.

5. Kashiwagi, T., Et. al.; *Macromolecules*, 1986, *19*, p. 2412.

6. Harmon, J. P. and Heffner, K. H.; *Forthcoming Publication*

7. Harmon, J. P. and Heffner, K. H.; *Forthcoming Publication*

8. *Chromatography of Polymers: Characterization by SEC and FFF, ACS Symposium Series 521* Provder, T. Ed., American Chemical Society, Washington, D.C., 1993.

9. Driscoll, K. and Amin Sanayai, R.; *Macromolecule: Communications to the Editor*, *24*, 15, 1991, p. 4479.

10. DiBenedetto, A. T.; *Journal of Polymer Science*, *25*, 1987, p. 1949.

11. Parkinson, W.W. and Keyser, R. M.; *Radiation Chemistry of Macromolecules Volume II*, Dole, M., Ed.; Academic Press, New York, 1973, p 57.

12. Saito, O.; *Radiation Chemistry of Macromolecules Volume I*; Dole, M., Ed.; Academic Press, New York, 1972.

13. Charlesby, A., et. al.; *Proceedings of the Royal Chemical Society of London, Series A, Mathematical and Physical Sciences*, 1954, *224*, 1156, p. 120.

14. O' Donnell, J. H., et. al.; *Macromolecules*, 1979, *12*, p. 113.
15. Wolf, B. A.; *Macromolecules*, 1981, *14*, p. 654.

16. Kashiwagi, T., Et. al.; *Macromolecules*, 1986, *19*, p. 2412.

17. Harmon, J. P., et. al.; *American Chemical Society Symposium Series 620*, Clough, R. L. and Shalaby, S. W., Eds.; American Chemical Society, Washington, D.C., 1996, p. 302.

Chapter Seven

Conclusions

This study has investigated the effects of free volume and molecular weight on the degradation chemistry induced by an ionizing radiation regime similar to the near earth space environment, The study has demonstrated how the total dose for the mission environment of a spacecraft is determined using the established modeling software codes such as: AE8, AP8, JPL-91, SHIELDOSE, SRIM and CASINO. This work has demonstrated how the equivalent ionizing energy can be simulated in a ground test at constant dose rate to a target material of interest using gamma photons emitted a cobalt 60 photon source. The manner for setting up and measuring total dose to establish an isodose field for irradiating the target polymers for this study has been defined. In doing so, the ionizing potential for a selected spaceflight radiation regime has been simulated, and thereby enabled the polymer research conducted for this study.

The research yielded results leading to the conclusion that the molecular weight and free volume are significant factors in the rate of scission and crosslink reactions for the molecular weight range of the polymer linear series evaluated by this study. The results demonstrated that the modeling methods used by previous investigators referenced in this study were validated using limited molecular weight ranges outside of the linear region of the Fox-Flory function, that is, the degree of fit to experimental re-distribution of the molecular weight of irradiated polymer was performed on linear polymers where the free volume approaches a consistent value in the asymptotic region of the Fox-Flory function (Tg approaches Tg_{∞}).

This results of this study addressed this need and introduced new expressions that maintained the baseline G-based modeling approach used by previous investigators, and applied a partitioning method for evaluating the damage to the polymer by narrow molecular weight bundles. This approach permits experimental verification and validation of the model by gel permeation chromatography from which the

partitioning approach derived. This model now accomplishes the unique ability to apply the effects of free volume using the activation energy at the Tg for each Mw bundle. The model further allows the incorporation of end-group effects as a function of the molecular weight partition. Where the rate of depolymerization is a function of the number of end-groups for a particular Mw partition. The flexibility of this modeling approach provides strength as a tool for evaluating, explaining and later predicting the chemical behavior of polymers following exposure to ionizing radiation.

The results of this study have provided the opportunity to further improve modeling methods for radiation-induced polymer degradation, and have provided new tools to understand the effects of free volume. The results of this study point to the importance of free volume in stabilizing polymer formulations while maintaining the properties required for polymer performance. For basic research, the study has led to the need for more focus on the interaction of the polymer chains, and the chemistry of the terminal ends of the polymer. For example, selection of end-cap moieties that restrict de-polymerization at the terminal ends of the polymer would allow for evaluation of main-chain scission in the Fox-Flory linear range. This would also permit a study of the effects conformation and tacticity.

Further studies are recommended that apply this modeling approach to other classes of polymers that degrade when subjected to ionizing radiation. The model assumes that each polymer is amenable to chromatography or other relative Mw distribution method (e.g. matrix-assisted laser desorption ionization-mass spectrometry: MALDI-MS) for validation and for baselining the initial pre-exposed condition of the polymer. This permits the introduction of strategic elemental or molecular changes to the polymer main-chain or side group for studies to further improve the model based on chemical structure of the polymer.

Ultimately the model will evolve to contain multiple modifications that can be incorporated into the baseline scission and crosslinking expressions on the basis of elemental composition and chemical structure. The advanced, radiation modeling expressions will have applicability to a wide range of academic and industrial uses for aviation, communications, medicine, and the exploration of space.

Appendix A

FTIR Charts (Atactic PMMA)

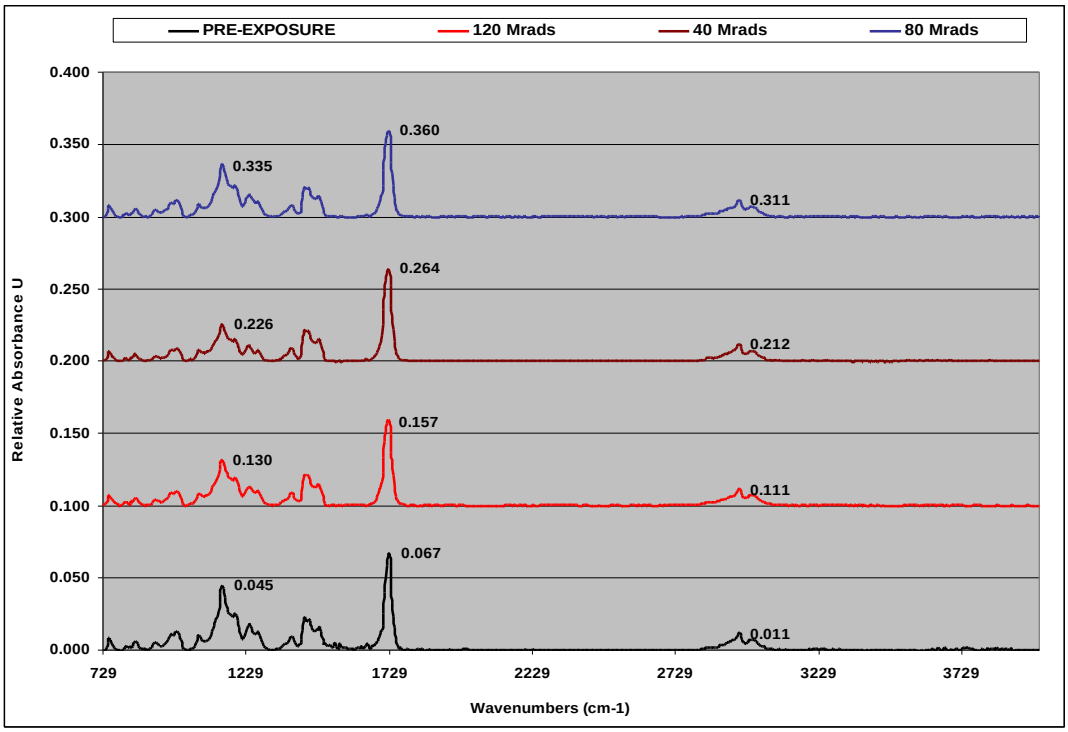

Figure A.1 FTIR ATR Spectra for PMMA 6,800 Unexposed and Exposed [40, 80 and 120 Mrads].

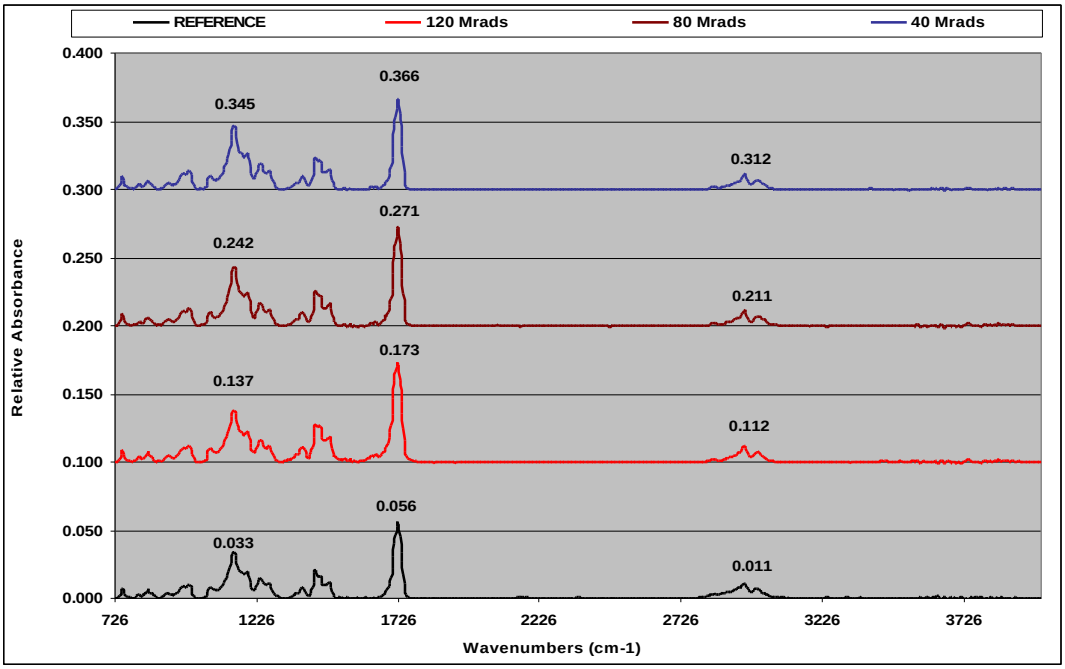

Figure A.2 FTIR ATR Spectra for PMMA 14,200 Unexposed and Exposed [40, 80 and 120 Mrads].

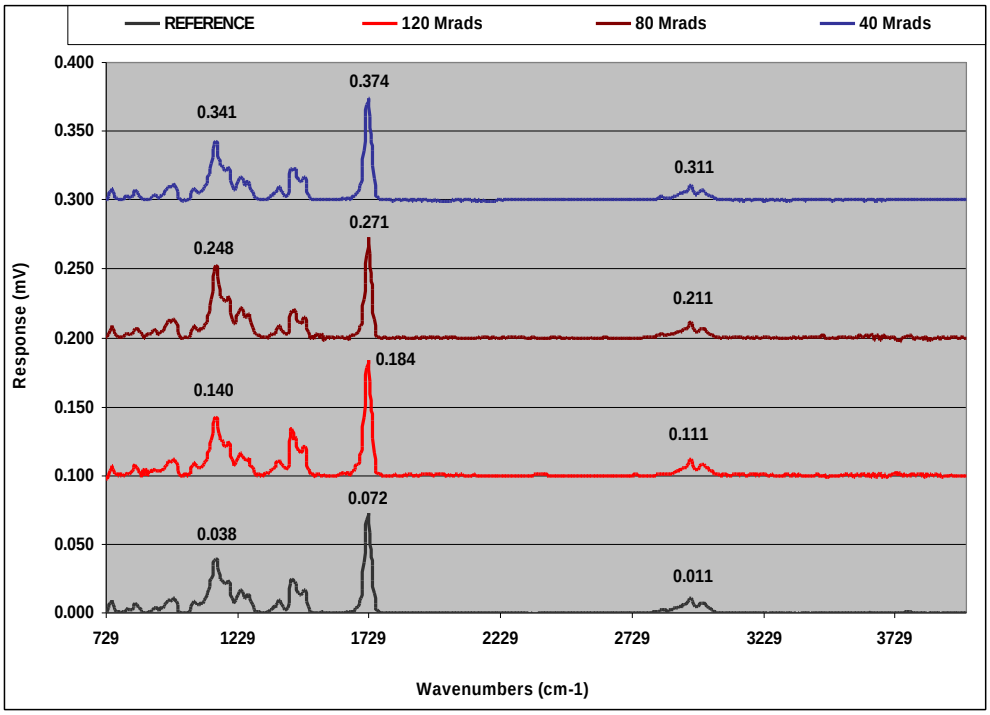

Figure A.3 FTIR ATR Spectra for PMMA 17,900 Unexposed and Exposed [40, 80 and 120 Mrads].

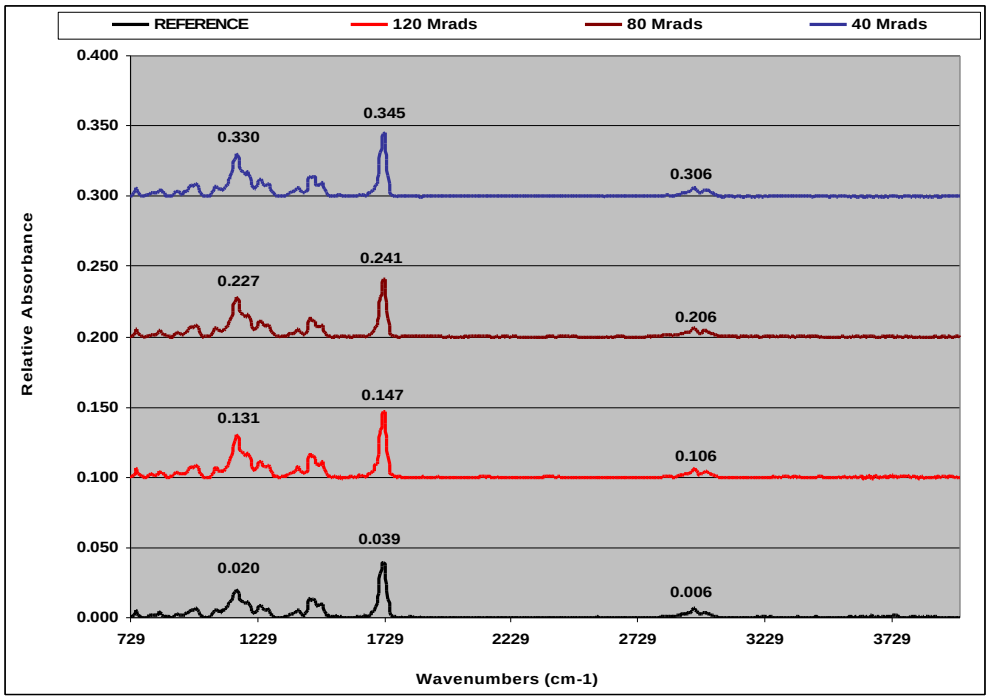

Figure A.4 FTIR ATR Spectra for PMMA 68,200 Unexposed and Exposed [40, 80 and 120 Mrads].

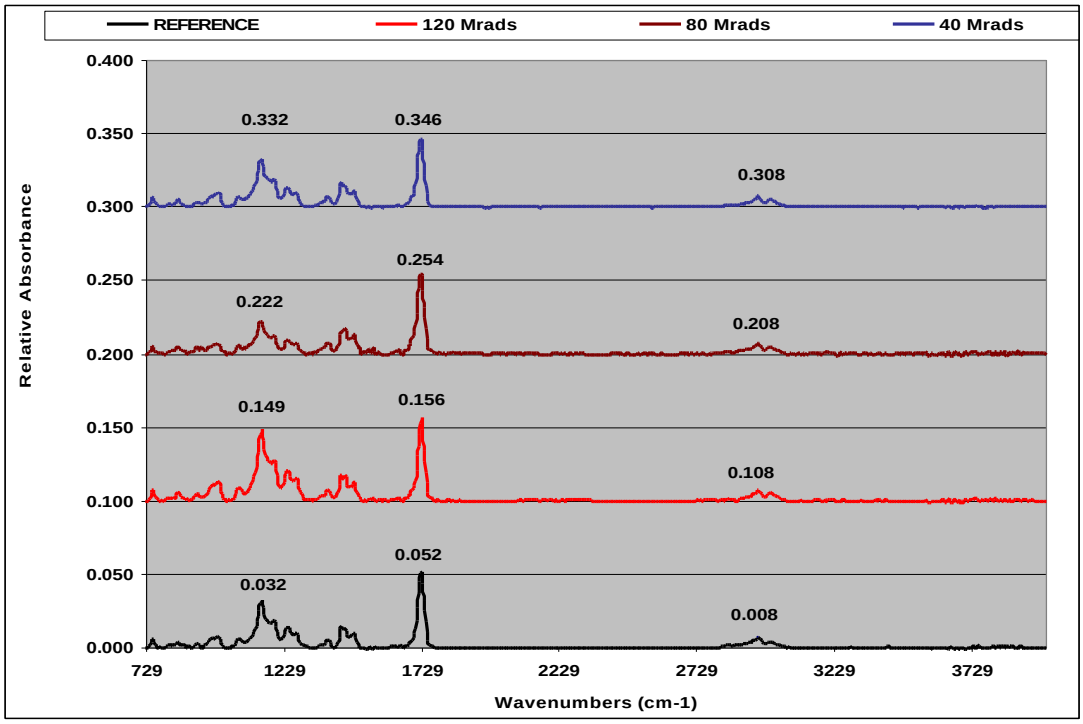

Figure A.5 FTIR ATR Spectra for PMMA 147,100 Unexposed and Exposed [40, 80 and 120 Mrads].

Appendix B

FTIR Charts (*iso*-PMMA)

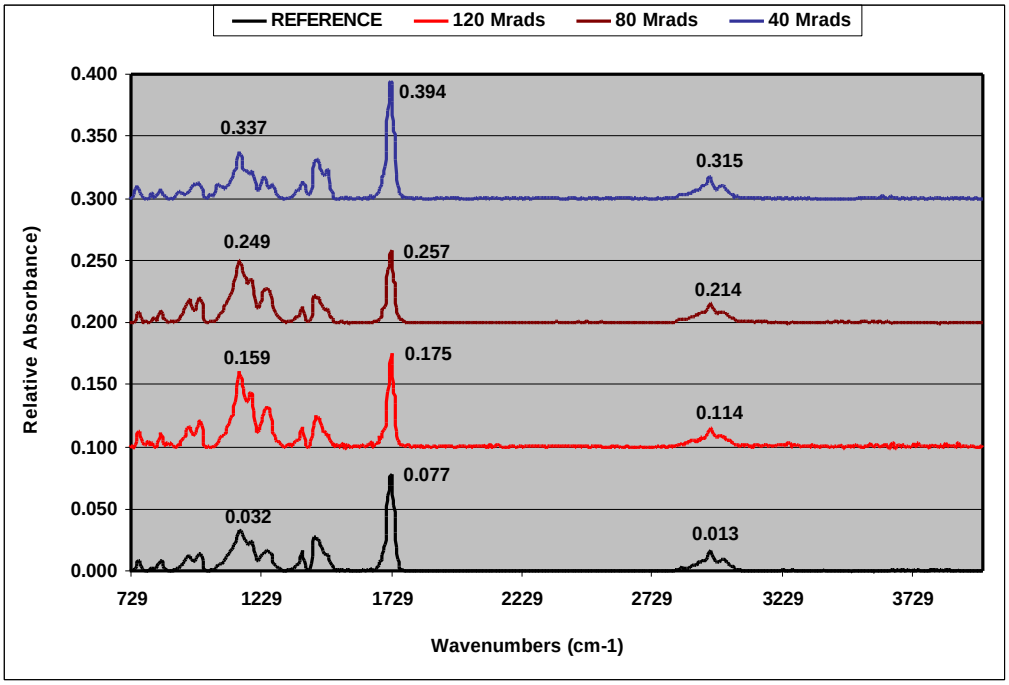

Figure B.1 FTIR ATR Spectra for PMMA 4,200 Unexposed and Exposed [40, 80 and 120 Mrads].

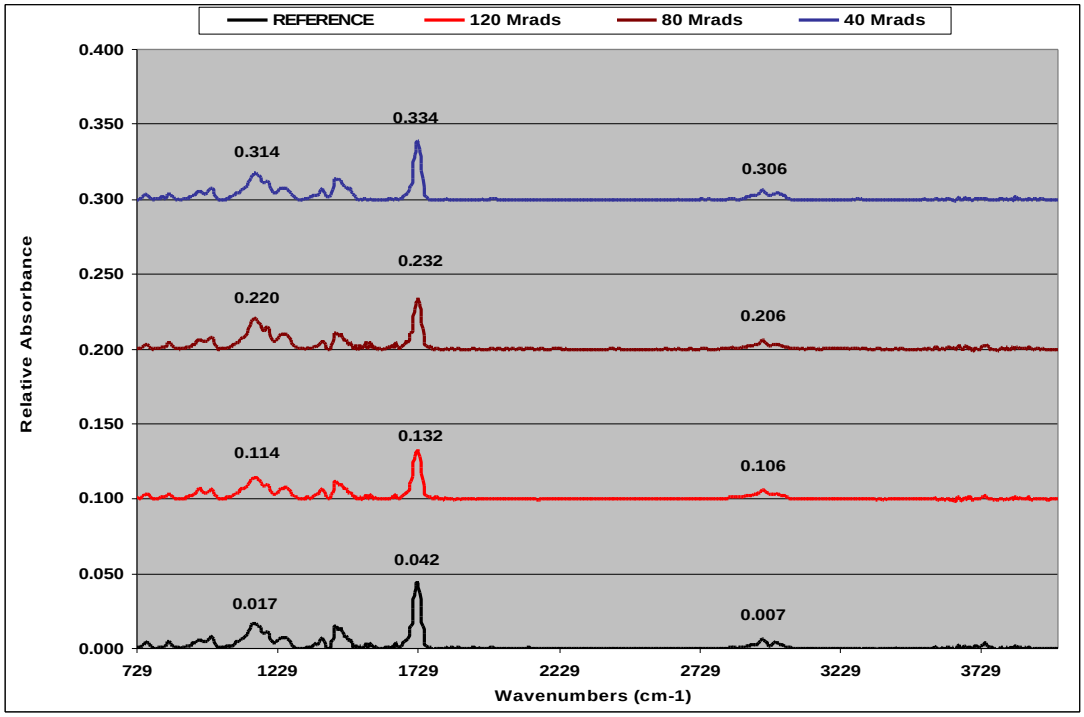

Figure B.2 FTIR ATR Spectra for PMMA 11,700 Unexposed and Exposed [40, 80 and 120 Mrads].

About the Author

Ken Heffner received a Bachelor's Degree in Chemistry in 1976 and a Master's Degree in Chemistry in 1987 each from the University of South Florida. While in the Ph.D. program at USF , he has held a position as Senior Staff Design Engineer for Honeywell International, Inc. - Defense and Space Electronics Systems Division in Clearwater, FL where he established the Specialty Coatings technology group performing $2 million/year in research and development for satellite materials technologies. In his career at Honeywell, Ken has been recognized with the Corporate Technical Achievement Award, Two Outstanding Engineer of the Year Awards, six international patents with three patent applications currently pending, Corporate Award for Outstanding Technical Paper, Six Sigma Certification and multiple On-Time Program Performance Awards. Honeywell will be releasing a new, trademarked technology for licensing developed by Ken Heffner for Honeywell. He has published eight technical papers presented at conferences for IPC, ASM and government-sponsored workshops. During this time, Ken has supported the humanities and education in the cultural arts for young students (K-12) through his service on the Board of Directors for several Not-for Profit youth organizations including Bravo Center for the Arts, Pinellas Youth Symphony and Blessed Sacrament School.